**This document is downloaded from DR-NTU (https://dr.ntu.edu.sg)**
**Nanyang Technological University, Singapore.**

# Structural study of ribosome : 1) structural basis of EF-G in translocation. 2) molecular mechanism of ribosome-dependent toxin YoeB in mRNA cleavage

Chen, Yun

2015

Chen, Y. (2015). Structural study of ribosome : 1) structural basis of EF-G in translocation. 2) molecular mechanism of ribosome-dependent toxin YoeB in mRNA cleavage. Doctoral thesis, Nanyang Technological University, Singapore.

https://hdl.handle.net/10356/65648

https://doi.org/10.32657/10356/65648

---

*Downloaded on 20 Mar 2024 16:33:34 SGT*

# Structural study of ribosome:
# 1) Structural basis of EF-G in translocation
# 2) Molecular mechanism of ribosome-dependent toxin YoeB in mRNA cleavage

Chen Yun

School of Biological Sciences
Nanyang Technological University

2015

# Structural study of ribosome:
# 1) Structural basis of EF-G in translocation
# 2) Molecular mechanism of ribosome-dependent toxin YoeB in mRNA cleavage

Chen Yun

School of Biological Sciences
Nanyang Technological University

A thesis submitted to the Nanyang Technological University
in partial fulfillment of the requirement for the degree of
Doctor of Philosophy

2015

# Acknowledgement

I would like to express my deepest gratitude to my Ph.D. supervisor Prof. Gao Yonggui for giving me this great opportunity working in his lab. I am grateful for his warm guidance and generous support the last four years, during which he has always been a great mentor as well as a good friend. It's not only his expertise but also his attitude towards science and enthusiasm for research that influenced me significantly.

I want to thank my Ph.D. Quality Examination panel members Prof. Julien Lescar, Prof. Liang Zhao-xun and Prof. Bhattacharyya Surajit for sacrificing their valuable time giving me precious advice on my Ph.D. study. Also, I would like to thank all the examiners for reviewing and commenting on this thesis.

I am grateful to Dr. Veeru who has been my working partner during the last two years. We collaborate closely on many of the projects. During this period I have learned a lot from him, particularly regarding molecular replacement, structure refinement and model building. I want to express my gratitude to our previous group member Dr. Fengshu as well, who initially started the EF-G project and selflessly shared much of her valued experience and knowledge with me. My thanks also go to all the other members of Gao's lab for their support and making GYG lab a place with such nice working environment.

I want to extend my thanks to the beamline scientists in SLS in Switzerland for their help with data collection in synchrotron. Their excellent work in developing powerful detectors, robots as well as the software, makes data collection and processing much easier for the novice users like me. I wish to thank Prof. Tang Kai for his acceptance of the collaboration in mass spectrometry experiment and all his lab members for their kind assistance.

I would present my special acknowledgement to NTU for supporting my Ph.D. and giving me the opportunity to study in such a wonderful country.

Last but not least, I feel sincerely grateful to my family and friends, who trust me and support me unconditionally, as they always do. Their love and concern is my best motivation.

# Table of contents

**Acknowledgement**

**Table of contents** ---------------------------------------------------------------------5

**Abstract** ---------------------------------------------------------------------------------9

**List of tables**------------------------------------------------------------------------------11

**List of figures** ---------------------------------------------------------------------------12

**List of abbreviations**-------------------------------------------------------------------14

## Chapter I: Structural basis of EF-G in translocation

**1. Introduction** --------------------------------------------------------------------------17

1.1 Bacterial ribosome and translation ------------------------------------------------17

1.1.1 Bacterial ribosome------------------------------------------------------------------17

1.1.2 Bacterial translation-----------------------------------------------------------------20

1.2 Elongation cycle and translocation---------------------------------------------------23

1.2.1 Elongation cycle ----------------------------------------------------------------------23

1.2.2 A-site occupation and peptidyl transfer-------------------------------------------24

1.2.3 Hybrid state ribosome and translocation ------------------------------------------24

1.3 Translational GTPases ---------------------------------------------------------------------26

1.3.1 Translational GTPases ----------------------------------------------------------------26

1.3.2 Structural studies of ribosome with bound GTPases -------------------------28

1.4 Structural studies of ribosome bound with EF-G-----------------------------------29

1.5 Aims and significance ---------------------------------------------------------------------32

**2 Materials and methods** ---------------------------------------------------------------**34**

2.1 Plasmids construction and protein purification -----------------------------------34

2.1.1 Purification kits for EF-G molecular cloning ---------------------------34

2.1.2 Construction of EF-G expression plasmid ------------------------------34

2.1.3 Purification of EF-G protein ---------------------------------------------35

2.2 Preparation of L9 mutant ribosome, tRNA and mRNA---------------------------36

2.2.1 L9 mutant ribosome purification ----------------------------------------36

2.2.2 tRNA and mRNA preparation --------------------------------------------38

2.3 Complex formation and binding assays --------------------------------------------38

2.3.1 Formation of the EF-G-ribosome complex ------------------------38

2.3.2 Assay of EF-G binding to ribosome --------------------------------------39

2.4 Crystallization trials ---------------------------------------------------------------39

2.5 Data collection and structure determination -------------------------------------40

**3. Results ------------------------------------------------------------------------------41**

3.1 EF-G purification, ribosome preparation and binding assay -------------------41

3.1.1 EF-G expression and purification ----------------------------------------41

3.1.2 L9 mutant ribosome purification ----------------------------------------43

3.1.3 EF-G binding assay------------------------------------------------------45

3.2 Crystallization of the EF-G-ribosome complex-------------------------------------46

3.3 Structure determination ---------------------------------------------------------48

3.4 Structural analysis-----------------------------------------------------------------51

3.4.1 Overall structure and small subunit rotation--------------------------51

3.4.2 Active site and switch I region of EF-G ----------------------------------58

3.4.3 Domain IV of EF-G and decoding center --------------------------------60

3.4.4 L1 stalk movement and hybrid P/E tRNA-------------------------------62

**4. Discussion --------------------------------------------------------------------------66**

4.1 GTPase activation and mechanism of GTP hydrolysis ---------------------------66

4.2 Hybrid P/E tRNA formation and L1 stalk movement ----------------------------73

4.3 Implication for translocation------------------------------------------------------------75

4.4 Personal perspective--------------------------------------------------------------------77

## Chapter II: Molecular mechanism of ribosome-dependent toxin YoeB in mRNA cleavage

**1. Introduction ---------------------------------------------------------------------------82**

1.1. Bacterial toxin-antitoxin systems------------------------------------------------------82

    1.1.1 Toxin-antitoxin systems ----------------------------------------------------82

    1.1.2 Classification of TA systems and type II TA systems-------------------83

1.2 Cellular targets and physiological functions of TA systems ---------------------85

    1.2.1 Cellular targets of TA systems ---------------------------------------------85

    1.2.2 Physiologic function of TA systems----------------------------------------87

1.3 Applications of TA systems ------------------------------------------------------------88

1.4 MazF and RelE systems-------------------------------------------------------------------89

1.5 YoeB and YefM ------------------------------------------------------------------------------90

1.6 Aims and significance ---------------------------------------------------------------------92

**2. Materials and methods -----------------------------------------------------------------94**

2.1 Plasmid construction and protein purification ------------------------------------94

2.2 Preparation of wild type ribosomes, tRNA and mRNA---------------------------94

2.3 Complex formation and crystallization ----------------------------------------------94

2.4 Data collection and structure determination --------------------------------------95

2.5 MALDI mass spectrometry --------------------------------------------------------------96

**3. Results -------------------------------------------------------------------------------------97**

3.1 Ribosome-YoeB crystallization --------------------------------------------------------97

3.2 Structure determination -----------------------------------------------------------------98

3.3 Structural analysis -----------------------------------------------------------------------100

3.3.1 Overall structure of the ribosome-YoeB complex--------------------100

3.3.2. Interactions between YoeB and ribosome----------------------------102

3.3.3 Active site interactions---------------------------------------------------103

3.4 YoeB cleaves mRNA following the second position of the A-site codon -----105

**4. Discussion ---------------------------------------------------------------------------106**

4.1 Comparison of RelE and YoeB bound ribosome structures --------------------106

4.2 Mechanism of YoeB dependent mRNA cleavage---------------------------------108

4.3 Personal perspective-----------------------------------------------------------------111

**Reference ----------------------------------------------------------------------------------113**

**Publication and author contribution -------------------------------------------- 122**

## Abstract

During bacterial protein synthesis, elongation factor G (EF-G) facilitates the forward movement of the tRNA–mRNA by one codon, which is coupled to the ratchet-like movement of the ribosome and triggered by EF-G–mediated GTP hydrolysis. This process, known as translocation, is the most conserved part between prokaryotic and eukaryotic translation. Despite its significance and decades of studies, the detailed mechanism of translocation still largely remains elusive. In current thesis, we present the structure of the *Thermus thermophilus* ribosome in complex with EF-G trapped by a GTP analogue. Binding with the ribosome and the GTP analogue facilitate the stabilization of EF-G switch I region, resulting in an ordered model of the active site. The positioning of the catalytic His87 into the active site is coupled to the hydrophobic-gate opening and involves the ribosomal 23S rRNA sarcin-ricin loop as well as domain III of EF-G. These findings provide a structural basis for the GTPase activation of EF-G, based on which, a substrate-promoted mechanism is proposed. The structure also reveals that the entire L1 stalk adopts a completely closed conformation by shifting toward the 50S body, thereby forming extensive contacts with the hybrid P/E tRNA. Together with the newly established interactions of the P/E tRNA with ribosomal proteins S13 and S19, these findings shed light on how the formation and stabilization of the hybrid tRNA is coupled to the head swiveling and body rotation of the 30S subunit, as well as to the closure of the L1 stalk of the 50S subunit.

Toxin-antitoxin (TA) modules, composed of a stable toxin and its cognate liable antitoxin, are common in prokaryotes. YoeB, a typical endoribonuclease, belongs to the YoeB-YefM TA module and mediates cellular adaptation in diverse bacteria by degrading mRNAs upon its activation. While the catalytic core of YoeB is thought to be identical to other well-studied nucleases, this enzyme specifically targets mRNA substrates that are associated with ribosomes *in vivo*. However, the molecular mechanism of mRNA recognition and cleavage by YoeB, and the requirement of ribosome for its optimal activity, largely remain elusive. Here, we present the structure of YoeB bound to the 70S ribosome in a pre-cleavage state, revealing that both 30S and 50S subunits participate in YoeB

binding. The mRNA substrate is recognized by the catalytic core of YoeB. The general base/acid (Glu46/His83) are within hydrogen-bonding distance to their reaction atoms, demonstrating an active conformation of YoeB on ribosome. Moreover, the orientation of mRNA involves the universally conserved A1493 and G530 of 16S rRNA. In addition, mass spectrometry data indicated that YoeB cleaves mRNA following the second position at the A-site codon, resulting in a final product with a 3′–phosphate at the newly formed 3′ end. Our results demonstrate a classical acid-base catalysis for YoeB–mediated RNA hydrolysis and provide an insight into how the ribosome is essential for its specific activity.

## List of tables

Table 1. List of purification kits

Table 2. Components and final concentration of the EF-G-ribosome complex

Table 3. Statistics of data collection and structure refinement of EF-G-ribosome complex

Table 4. Rearrangement of inter-subunit bridges

Table 5. Five (currently) known TA system types

Table 6. Components and final concentration of YoeB bound ribosome complex

Table 7. Statistics of data collection and refinement of YoeB bound ribosome complex

## List of figures

Figure 1. Advances in our knowledge of the ribosome structure

Figure 2. Overview of bacterial translation

Figure 3. Overview of bacterial elongation cycle

Figure 4. Hybrid state ribosome and small subunit rotation

Figure 5. Domain arrangement of overall structure of EF-G and EF-4 (LepA)

Figure 6. Crystal packing analysis and new crystal form of L9 mutant ribosome

Figure 7. Crystal structure of post-translocational ribosome in complex with EF-G and fusidic acid binding site

Figure 8. EF-G expression construct

Figure 9. EF-G purification

Figure 10. L9 mutant ribosome purification

Figure 11. EF-G binding assay

Figure 12. Crystallization of the EF-G-ribosome complex

Figure 13. Overall structure and conformational change of the ribosome upon EF-G binding

Figure 14. Inter-subunit bridge comparison between pre- and post-translocational complexes

Figure 15. Interactions at the active site of EF-G

Figure 16. Domain IV positioning and conformational change of EF-G

Figure 17. Rearrangement of the decoding center

Figure 18. P/E tRNA and its interaction with the ribosome

Figure 19. L1 stalk movement and its interaction with P/E tRNA

Figure 20. EF-G domain III rearrangement and its interaction with switch I and SRL

Figure 21. “Hydrophobic gate” opening upon GTPase activation

Figure 22. EF-G G’ domain rearrangement

Figure 23. Active and inactive orientations of the catalytic residue His92

Figure 24. P/E tRNA trajectory

Figure 25. A790 gate opening

Figure 26. EF-G conformation comparison

Figure 27. Toxin-antitoxin systems in *E. coli* K-12 strain

Figure 28. Action mode of type II toxin-antitoxin systems

Figure 29. Cellular targets of TA systems

Figure 30. Example applications of TA systems in virus control

Figure 31. Crystal structure of the YoeB-YefM complex

Figure 32. Crystals of YoeB-ribosome complex

Figure 33. Structure of YoeB bound to the 70S ribosome

Figure 34. Interactions between YoeB and ribosome

Figure 35. Interactions at the mRNA cleavage site

Figure 36. MS analysis of YoeB cleaved mRNA fragments

Figure 37. Differences between RelE and YoeB bound ribosomes

Figure 38. Amino acid sequence alignment of YoeB homologues and the proposed catalytic mechanism

## List of abbreviations

| | |
|---|---|
| ASL | Anticodon stem loop |
| ATP | Adenosine triphosphate |
| CBB | Coomassie brilliant blue |
| DC | Decoding center |
| DDAO | N,N-Dimethyldecylamine-N-oxide |
| DOBC | Deoxy Big Chap |
| DTT | Dithiothreitol |
| *E. coli* | *Escherichia coli* |
| EDTA | Ethylenediaminetetraacetic acid |
| EF-G | Elongation factor G |
| EF-Tu | Elongation factor Tu |
| GTP | Guanosine triphosphate |
| GDPCP | 5'-guanosyl-methylene-triphosphate |
| HEGA-9 | D-Glucitol,1-deoxy-1-[(2-hydroxyethyl)(1-oxononyl)amino]- |
| HEPES | 4-(2-hydroxyethyl)-1-piperazineethanesulfonic acid |
| HIV | Human immunodeficiency virus |
| HPC | Herpes C virus |
| IF | Initiation factor |
| IPTG | Isopropyl β-D-1-thiogalactopyranoside |
| LB | Luria-Bertani |
| MALDI | Matrix-assisted laser desorption/ionization |
| MES | 2-(N-morpholino)ethanesulfonic acid |
| MME | Monomethyl ether |
| mRNA | messenger RNA |

| | |
|---|---|
| MS | Mass spectrometry |
| MW | Molecular weight |
| OD | Optical density |
| PCR | Polymerase Chain Reaction |
| PDB | Protein data bank |
| PEG | Poly ethylene glycol |
| Pi | Phosphate |
| PMSF | Phenyl-methyl-sulfonyl fluoride |
| PoTC | Post terminal complex |
| PTC | Peptidyl transfer center |
| RF | Release factor |
| RRF | Ribosome recycling factor |
| SD | Shine-Dalgarno |
| SDS-PAGE | Sodium dodecyl sulphate polyacrylamide gelelectrophoresis |
| SRL | Sarcin ricin loop |
| *T.Th.* | Thermus thermophillus |
| TA module | Toxin-antitoxin module |
| TEV | Tobacco Etch Virus |
| tRNA | transfer RNA |
| UV | Ultraviolet |

# Chapter I:

# Structural basis of EF-G in translocation

# 1. Introduction

## 1.1 Bacterial ribosome and translation

### 1.1.1 Bacterial ribosome

At the heart of protein synthesis lies the ribosome, one of the most complicated and sophisticated macromolecules in all living organisms. Although ribosomes from bacteria, archaea and eukaryotes (the three domains of life) differ in size, sequence and structure, they all perform similar function during translation. In addition, ribosomes are also found in chloroplasts and mitochondria of eukaryotes. These organelles are believed to be the descendants of bacteria since their ribosomes are similar to those of bacteria (1).

The bacterial ribosome (70S) is a cytoplasmic nucleoprotein particle with a mass of ~2.5 MDa and comprising of two subunits denoted 30S (small subunit) and 50S (large subunit). The small subunit consists of the 16S ribosomal RNA (rRNA, ~1500 nucleotides) and 21 proteins (S1-S21), while the large subunit is composed of two ribosomal RNAs, namely 5S rRNA (~ 120 nucleotides) and 23S rRNA (~2900 nucleotides), as well as 33 proteins (L1-L33) (2).

Initially it was thought that the ribosomal proteins were responsible for the ribosome's various functions, while the RNA acted as a scaffold (3). Later, however, it became evident that the rRNAs are the major catalytic molecules during the different states in protein synthesis (4). For example, decoding of the mRNA involves the 16S rRNA of the small subunit (5, 6) and peptide synthesis depends on the 23S rRNA of the large subunit (7). The ribosomal elements that catalyze these reactions are known as the decoding center (DC) and the peptidyl transfer center (PTC), respectively. Thus, the ribosome is known as one of the best examples of a ribozyme. Nonetheless, the ribosomal proteins are required for maintaining the overall architectures of the rRNAs in the ribosome (8). In addition, they also function in ribosome biogenesis and assist in many significant ribosomal activities such as mRNA decoding, peptide transfer (9) and mRNA helicase activity (10).

Although the important biological functions of the ribosome were well established forty years ago, the understanding of ribosome structure was extremely limited as demonstrated in Figure 1A (11). The best available model of the ribosome was based on negative stain cryo-EM and revealed a two-subunit structure resembling a palm (13).

Structural studies of ribosome have gained vast popularity ever since then. However, our understanding of ribosome structure progressed slowly due to its vast size and complexity. Most information came from low-resolution cryo-EM reconstructions (12). Although people had managed to obtain ribosome crystals, either the poor diffraction or the challenge to solve phase problem for this huge complex, hindered the determination of the high-resolution structure of ribosome (13). Thanks to the development of synchrotron X-ray sources, detectors and computing methods, complete atomic resolution structures of both the small and the large subunit of bacterial ribosome were elucidated at the beginning of the 21-st century after decades of effort (14-16). Venki Ramakrishnan, Thomas Steitz and Ada Yonath shared Nobel Prize in Chemistry in 2009 for this great achievement. Their work had greatly expanded our knowledge towards understanding the architecture of the bacterial ribosome. Many more detailed features have been characterized and visualized (Figure 1C). For example, the existence of the exit tunnel on the large subunit through which the nascent polypeptide chain is exported has been observed and confirmed (7, 14). In addition to the conventionally known aminoacyl site (A-site) and peptidy site (P-site), a third tRNA binding site was visualized and denoted as the exit site (E-site) (17, 18).

Ever since then, high-resolution structures of the entire 70S ribosome in many different functional states with all kinds of bound ligands have been determined (19-21), enabling a better understanding of many aspects of ribosome functioning, for example mRNA decoding, peptide transfer, as well as the action modes of different antibiotics and translational factors (22). Moreover, in 2011, crystal structures of the entire eukaryotic 80S (yeast) ribosome (23) as well as the separate 40S (24) and 60S (25) subunits were determined, further expanding our knowledge of ribosome. More recently, with the rapid development of cryo-EM single-particle analysis/reconstruction, particularly due to the availability of more advanced detectors and improved image processing techniques/software (26), the near-atomic resolution structures of yeast as well as human mitochondrial ribosome (27-31) and even human 80S ribosome (32) have become available (Figure 1B).

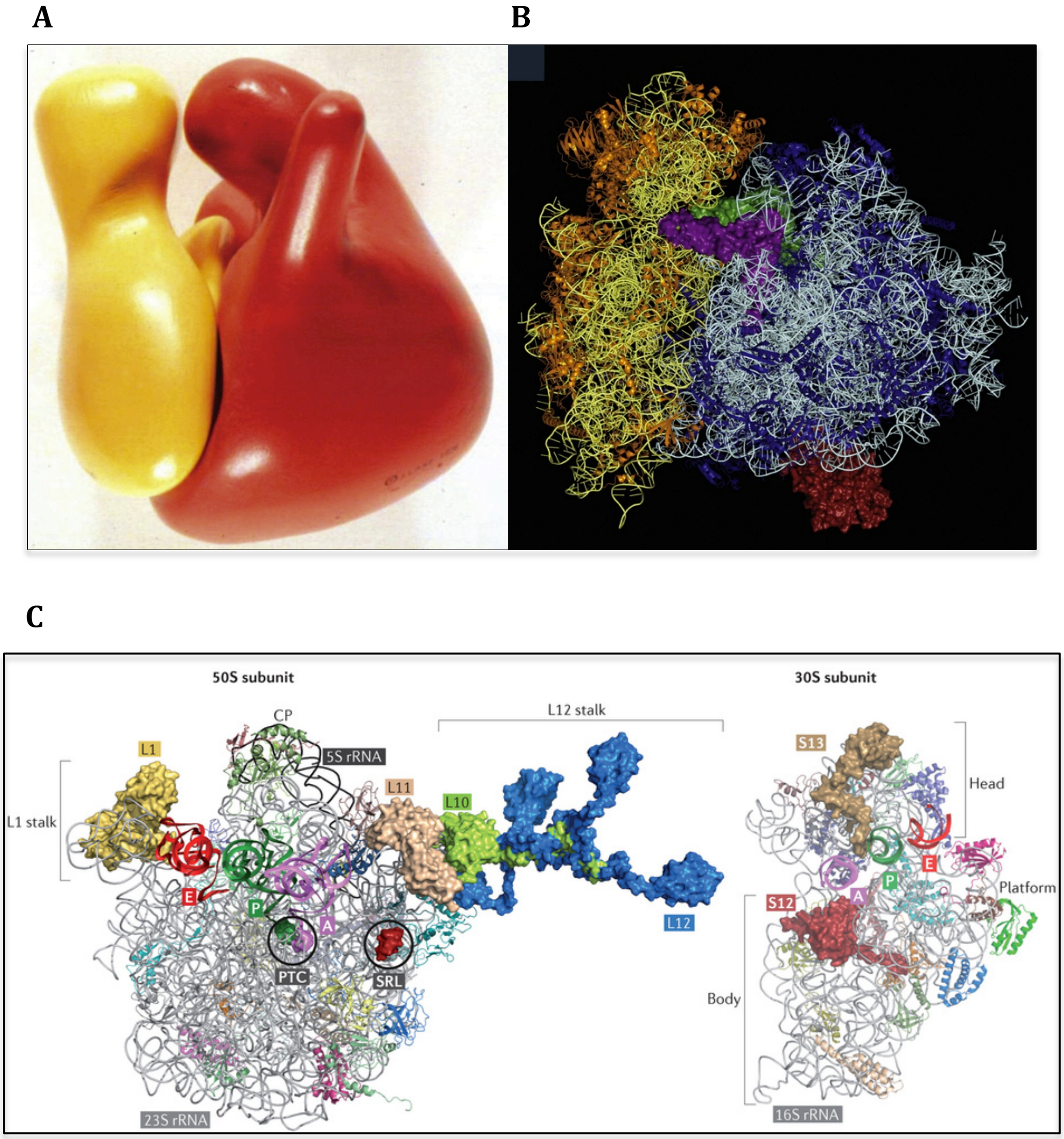
A
B
C
50S subunit
30S subunit
CP
L1
5S rRNA
L12 stalk
L11
L10
L1 stalk
E
P
A
PTC
SRL
L12
23S rRNA
S13
Head
E
P
A
S12
Platform
Body
16S rRNA

**Figure 1. Advances in our knowledge of the ribosome structure. (A)** Gross model of *E. coli* ribosome based on negative stain electron microscopy (11). Small and large subunits are shown in yellow and red, respectively. **(B)** High-resolution (3.4 Å) structure of the translating mammalian ribosome as revealed by single particle cryo-EM reconstruction (33). Small and large subunits are shown in yellow and blue respectively. (Adapted from V. Ramakrishnan, 2014) **(C)** Overall architecture of both subunits of bacterial ribosome. Critical structure features such as L1 stalk, peptide transfer center are indicated. The A-site, P-site and E-site tRNAs are also shown. (Adapted from Hiroshi Yamamoto *et al,* 2013)

### 1.1.2 Bacterial translation

In bacteria, the protein synthesis catalyzed by ribosome can be divided into three stages: initiation, elongation and termination (which can be further divided into peptide release and ribosome recycling), involving many different translational factors. The overall process is depicted in Figure 2.

Briefly, initiation of translation requires the placement of the specific initiator tRNA (tRNA$^{fMet}$) and the mRNA start codon in the peptidy site (P-site) on the ribosome. This process is assisted by three translation factors: initiation factors (IFs) 1, 2 and 3. The exact mechanism of how these factors promote initiation still remains elusive. It is proposed that IF3 binds to the 30S subunit first and removes the leftover mRNA and tRNA from the last round of translation (34). Then IF1 and IF2 assist in the binding of new mRNA according to the Shine-Dalgarno (SD) sequence and the initiator tRNA$^{fMet}$. IF2 promotes the association of the 50S subunit and the release of IF3 in a guanosine triphosphate (GTP) hydrolysis dependent manner (35, 36). After IF2 GTP hydrolysis, tRNA$^{fMet}$ is placed in the correct position while IF1 and IF2 are released from the ribosome (37). The complex is thus ready for elongation.

During the elongation cycle, the elongation factor Tu (EF-Tu) first delivers the amino-acyl tRNA to the amino acyl site (A-site) on the ribosome and then a new peptide bond is formed in the ribosome peptidyl transfer center (PTC) on the large subunit. After which, the elongation factor G (EF-G) binds to the ribosome and promotes the forward movement of the tRNA–mRNA by one codon, thereby moving the tRNAs from A- and P- sites to P- and E- sites, respectively. After the release of the deacylated-tRNA from the E-site, EF-Tu brings a new amino-acyl tRNA to the ribosome and the cycle continues until a stop codon is detected. (Figure 2)

Class I release factors (RF1 and RF2) recognize different stop codons through their specific tripeptide motifs (PXT in RF1 and SPF in RF2) (38) and catalyze the hydrolysis of the nascent polypeptide through the universally conserved GGQ motif (39, 40). Class II release factor (RF3) facilitates the dissociation of class I release factors (41) and the ribosome remains in complex with mRNA and a deacylated tRNA at P-site (known as the post termination complex PoTC). Ribosome recycling factor (RRF) and EF-G bind together to PoTC and split the ribosome into two subunits that can be reused for the next round of translation (42).

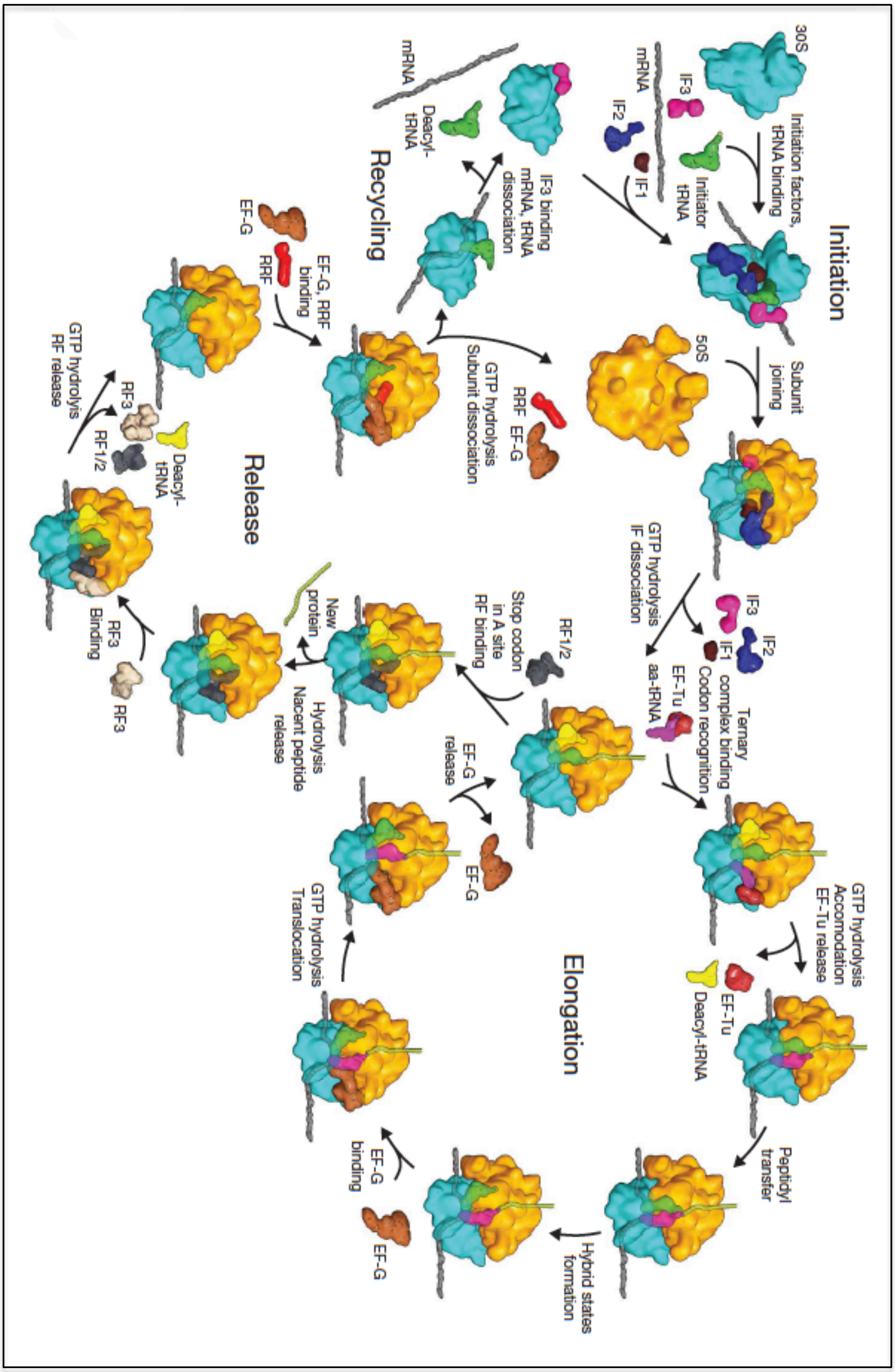
Initiation
30S
Initiation factors, tRNA binding
mRNA
IF3
IF2
IF1
Initiator tRNA
Subunit joining
50S
GTP hydrolysis
IF dissociation
IF3
IF2
IF1
Ternary complex binding
Codon recognition
EF-Tu
aa-tRNA
GTP hydrolysis
Accomodation
EF-Tu release
EF-Tu
Deacyl-tRNA
Elongation
Peptidyl transfer
Hybrid states formation
EF-G
EF-G binding
GTP hydrolysis
Translocation
EF-G release
EF-G
RF1/2
Stop codon in A site
RF binding
New protein
Hydrolysis
Nacent peptide release
RF3 Binding
RF3
Release
Deacyl-tRNA
RF3
RF1/2
GTP hydrolysis
RF release
EF-G, RRF binding
EF-G
RRF
Recycling
RRF
EF-G
GTP hydrolysis
Subunit dissociation
IF3 binding
mRNA, tRNA dissociation
Deacyl-tRNA
mRNA

**Figure 2. Overview of bacterial translation.** For simplicity, not all intermediate states are shown. aa-tRNA, aminoacyl-tRNA; IF, initiation factor; EF, elongation factor; RF, release factor. (Figure adapted from T.M. Schmeing *et al*, 2009)

## 1.2 Elongation cycle and translocation

### 1.2.1 Elongation cycle

Among the three stages of translation, elongation is the most conserved process between bacteria and eukaryotes. It is catalyzed by two universally conserved translational factors EF-Tu and EF-G (eEF1 and eEF2 in eukaryotes, respectively). Since these factors are present in all three domains of life, they likely emerged before the domain separation occurred around 3 billion years ago (43). Elongation cycle can be further divided into three phases: A-site occupation, peptidyl transfer and translocation (Figure 3)(44).

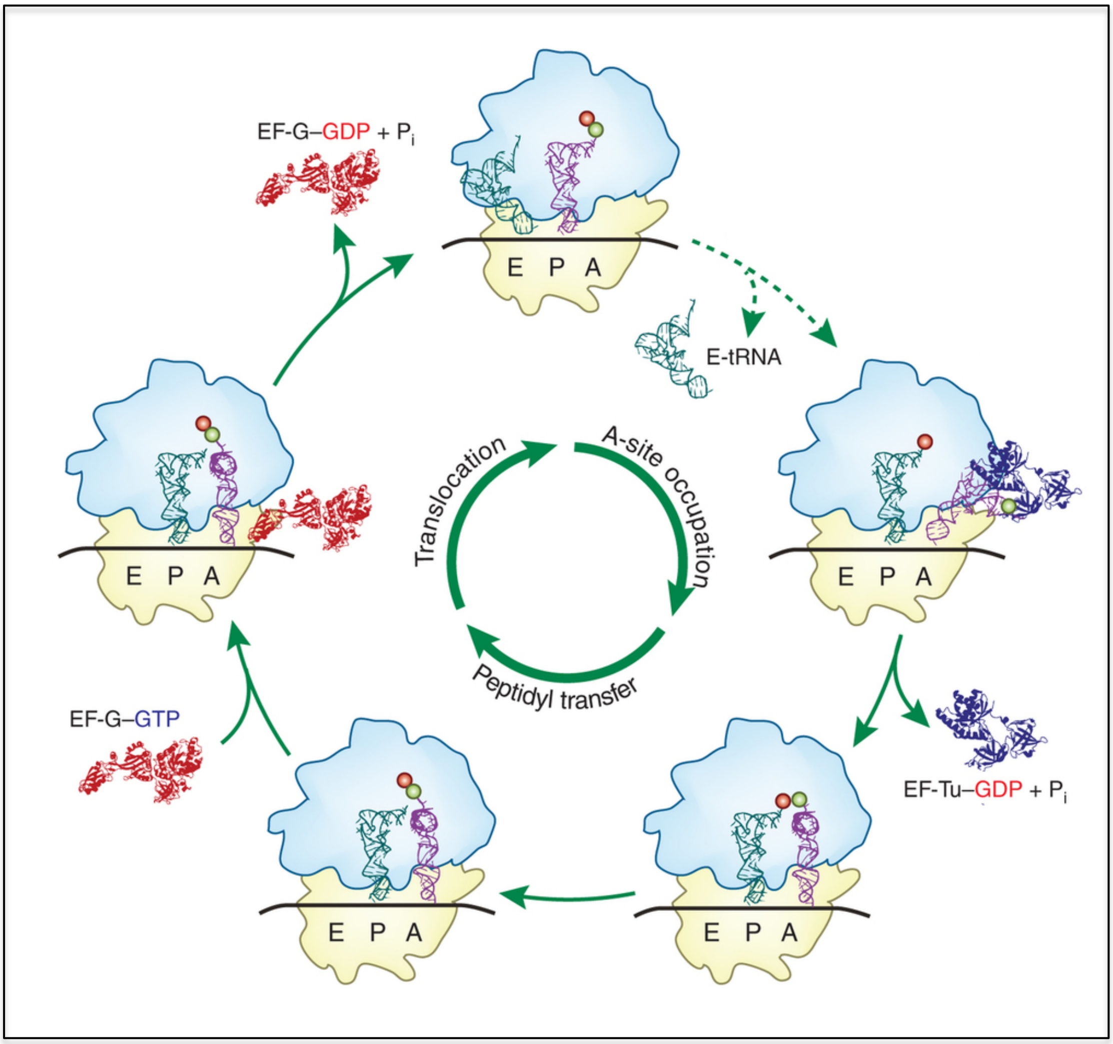

**Figure 3. Overview of bacterial elongation cycle.** Amino acyl tRNA is delivered to ribosome A-site by EF-Tu as a ternary complex with GTP. Peptide transfer is catalyzed at PTC with the nascent peptide chain moving from P- to A-site. EF-G then catalyzes the translocation of A- and P- site tRNAs to P- and E- site respectively, along with the mRNA. (Adapted from John Achenbach *et al*, 2013)

### 1.2.2 A-site occupation and peptidyl transfer

The first step of elongation is A-site occupation. After translation initiation, the ribosome contains the initiator $\mathrm{tRNA}^{\mathrm{fMet}}$ at the P-site and an empty A-site. The amino-acyl tRNA is delivered to the A-site by the EF-Tu as a ternary complex (aminoacyl-tRNA-EF-Tu-GTP). The selection of correct amino-acyl tRNA depends on the codon anticodon base-pairing interaction at the decoding center on the small subunit. Upon successful decoding, GTP on EF-Tu will be hydrolyzed leading to conformational changes and the release of EF-Tu-GDP complex from the ribosome. The aminoacyl-tRNA is free to fully accommodate into the A-site with its amino-acyl end positioned in the PTC on the large subunit (45-47), where peptide transfer is catalyzed. This process of decoding and aminoacyl-tRNA accommodation is collectively known as A-site occupation. At the CCA end of the A-site tRNA, new peptide bond is formed by transferring the peptidyl residue from the peptidyl-tRNA at P-site to the aminoacyl-tRNA at the A-site, thereby elongating the nascent peptide chain by one amino acid. At this stage, the ribosome bears a deacylated tRNA at P-site and an elongated tRNA at A-site, which represents a pre-translocational state of ribosome.

### 1.2.3 Hybrid state ribosome and translocation

The pre-translocational ribosome spontaneously forms a hybrid state with tRNAs in A/P and P/E hybrid sites, meaning that the amino-acyl ends of the tRNAs move forward to P- and E-sites on the large subunits while the anticodon stem loops (ASL) remain fixed in A- and P-sites, respectively (Figure 4C) (48). This hybrid state was initially discovered by cryo-EM analysis and is coupled to small subunit rotation relatively the large subunit (Figure 4A) and L1 stalk movement forming a “closed” configuration (49, 50). The L1 stalk moves inwards towards the P-site of ribosome, establishing new interactions with the P/E hybrid state tRNA. Later on, a rotation within the small subunit itself was also observed by cryo-EM (51). Namely, the 30S head swivels relatively to the 30S body to different degree indicating different intermediate states of the ribosome. (Figure 4B)

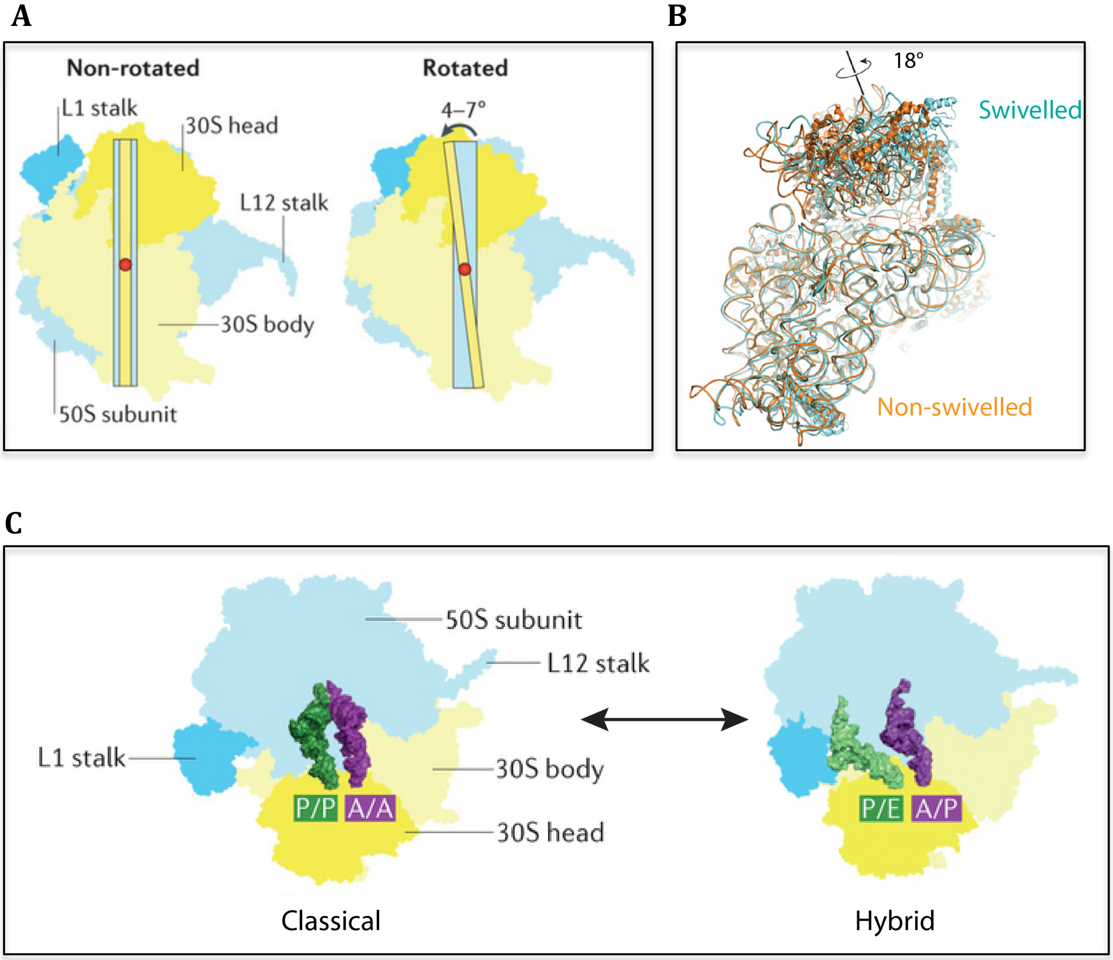
A
Non-rotated
Rotated
L1 stalk
30S head
L12 stalk
4–7°
30S body
50S subunit
B
18°
Swivelled
Non-swivelled
C
50S subunit
L12 stalk
L1 stalk
30S body
P/P
A/A
30S head
P/E
A/P
Classical
Hybrid

**Figure 4. Hybrid state ribosome and small subunit rotation. (A)** Hybrid ribosome 30S subunit is compared with that of classical ribosome by aligning the 50S subunits. Arrows and numbers indicate the direction and degree of body rotation. **(B)** Head swiveling of the small subunit head. Arrow and number indicate the direction and degree of body rotation. **(C)** Formation of the hybrid state ribosome characterized by hybrid A/P, P/E tRNAs and L1 "closed" configuration. (Adapted from Hiroshi Yamamoto *et al,* 2013)

While the pre-translocational ribosome equilibrates between the classical state and the hybrid state (52, 53), EF-G-GTP binds preferentially to the hybrid state ribosome thereby stabilizing this state. EF-G promotes forward movement of the tRNA-mRNA by exactly one codon, resulting in a classical state ribosome with two tRNAs at P- and E- sites, respectively, known as a post-translocational state ribosome. This process is referred to as translocation and accompanied by GTP hydrolysis on the EF-G, which significantly increases the reaction rate, although the exact mechanism is still not clear (54). The ribosome is thus ready for the next round of elongation with the de-aminoacylated tRNA ejected from the E-site. This release of E-site tRNA is believed to take place either after translocation (55, 56) or on occupation of the A-site with the following aminoacyl-tRNA (57, 58). Elongation cycle continues and the polypeptide chain is consecutively synthesized until a stop codon is detected at the A-site and the ribosome goes to the translation termination stage.

Translocation comprises the movement of two tRNAs from A- and P-sites to P- and E-sites on the ribosome accompanied by the movement of mRNA through codon anticodon base-pairing interactions in the two sites. It is one of the most complex processes during translation. Understanding the detailed mechanism of translocation is not only a fundamental issue in life science, but also relevant to understanding the action mode of a number of antibiotics, such as fusidic acids, (59).

## 1.3 Translational GTPases

### 1.3.1 Translational GTPases

GTPases are called molecular switches for their ability to interconvert between guanosine 5'-diphosphate (GDP)- and guanosine 5'-triphosphate (GTP)-bound states. Cycling between these states facilitates periodic interactions with their cognate binding partners (60). In case of translational GTPases, this partner is the ribosome.

Translational GTPases are translational factors, which utilize GTP hydrolysis induced conformational changes to enable their respective functions in translation. There are four classical translational GTPases involved in bacterial translation, IF2, EF-Tu, EF-G and RF3, which have different roles in different stages of translation. In addition, several additional GTPase factors, including RelA, EF-4 (LepA) and BipA, have been revealed to be associated with ribosomes under stress conditions (61). Although the sequences and functions of translational GTPase vary, they all share a G domain structurally similar to the small Ras-like G proteins (Figure 5). Thus, the translational GTPases belong to the superfamily of P-loop GTPases (62). This G domain forms the catalytic core in all the translational GTPases and is responsible for coupling the nucleotide binding and hydrolysis to the specific function of each individual GTPase (63). Similar to other G proteins, translational GTPases also exchange the nucleotide (GDP *vs*. GTP), which is accompanied by conformational changes in two conserved dynamic regions known as switch I and switch II. When GTP is bound, translational GTPase is in its active form interacting with the ribosome and the switch regions interacting with GTP-γ-phosphate. After GTP hydrolysis and Pi (pyrophosphate) release, however, the protein convers to GDP bound state and the switch regions lose the contacts, relaxing back to inactive form. Thus, only in its active (GTP) state has a translational GTPase a high affinity to the ribosome and exerting its biological function, while the inactive (GDP) state after GTP hydrolysis will be released from the ribosome (64).

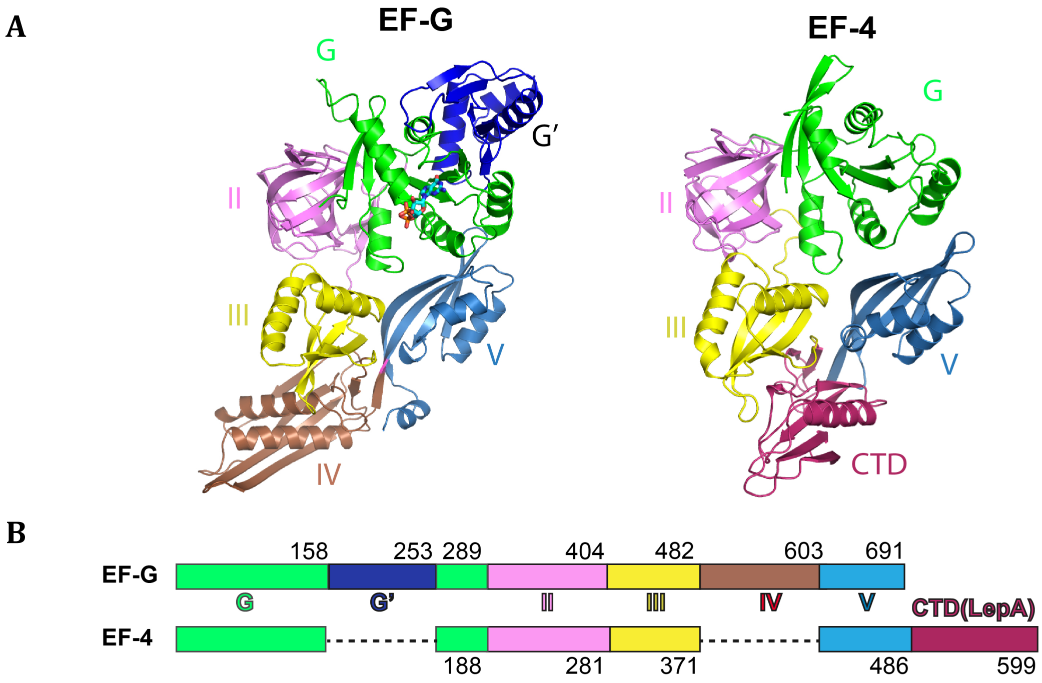

**Figure 5. Domain arrangement and overall structure of EF-G and EF-4 (LepA). (A)** Structures of isolated EF-G and EF-4 are obtained from Protein Data Bank (PDB ID: 2BM0 and 3CB4, respectively). Domain I (green), a.k.a. the G domainn, is the nucleotide-binding region. G' domain insertion (dark blue) in it is a characteristic feature of the EF-G protein. EF-G has a unique domain IV (brown), whereas EF-4 has unique C-terminal domains (warm pink). **(B)** Schematic diagram depicting the domain arrangement of EF-G and EF-4.

### 1.3.2 Structural studies of ribosome with bound GTPases

Despite the importance of the translational GTPases, insight into their functioning at atomic level has emerged only recently. While low-resolution structural information of the interactions between ribosome and these GTPases were obtained from cyo-EM studies (45, 46)(65), crystallization of ribosome with these factors proved to be a big challenge due to the fact that the binding sites of the translational GTPases are occupied by the L9 protein form the neighboring molecule in the crystal packing (Figure 6), depriving them from the opportunity to bind during the crystallization process (66). It was not until 2009 that a new crystal form was obtained by deleting the N terminal part of the L9 protein resulting in the determination of high-resolution structures of ribosome bound with EF-Tu and EF-G (47)(67). These structures shed light on many aspects of the interaction between GTPase and the ribosome, particularly during mRNA decoding and translocation. Shortly after, two structures of RF3 bound ribosome were solved using the same strategy of L9 mutation (68). Since then, L9 mutant ribosome crystallization has been a commonly used tool in studying the structure of ribosome complexes with GTPases.

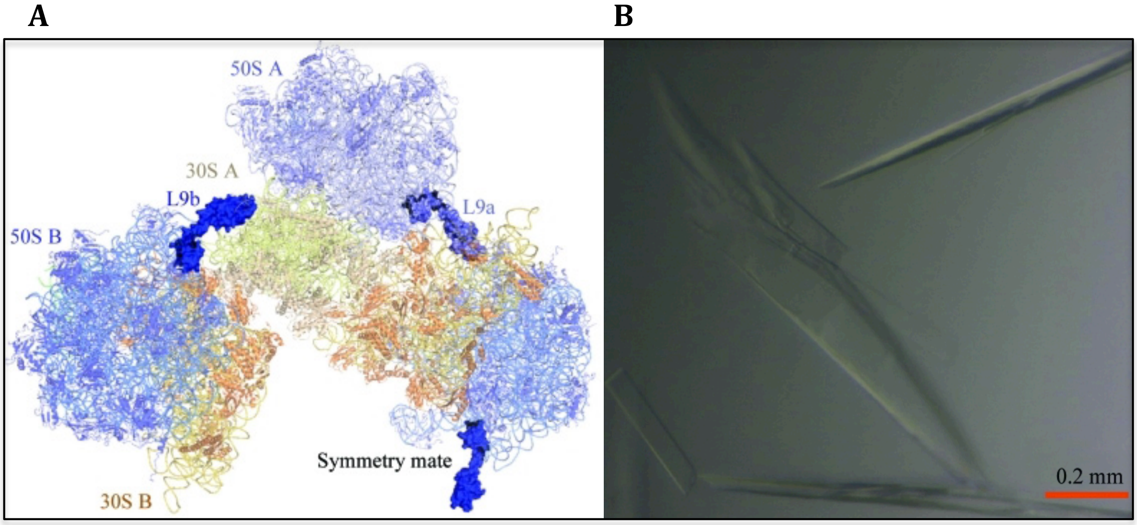

**Figure 6. Crystal packing analysis and new crystal form of L9 mutant ribosome. (A)** Crystal packing analysis using the structure of *T. Th.* 70S ribosome in complex with mRNA and tRNA (Selmer *et al.* 2012). In crystal packing, ribosomal protein L9 (dark blue) from one ribosome projects into the factor binding site of the neighboring ribosome. 30S proteins and rRNA are shown in yellow, 50S proteins and rRNA are shown in blue. **(B)** Example of L9 mutant ribosome crystals. Red bar is shown for size reference. (Figure adapted from Selmer *et al*, 2012)

## 1.4 Structural studies of ribosome bound with EF-G

The universally conserved mechanism of translocation catalyzed by EF-G (eEF2 in eukaryotes) involves a sequence of intermediate states. Structural studies on ribosome with EF-G and eEF2 at low-to-intermediate resolution provided a wealth of information about ribosome ratcheting and translocation (48, 49, 65). However, understanding of GTPase activation and translocation processes at the atomic level requires high-resolution structure.

As EF-G belongs to the translational GTPases, crystallization study of ribosome bound with EF-G had been impossible until 2009, when the crystal structure of EF-G bound to L9 mutant ribosome (discussed above) trapped with the antibiotic fusidic acid was published (67) (Figure 7). Fusidic acid is one of the most commonly used antibiotics in clinical, it functions as an inhibitor of translocation, allowing the GTP hydrolysis but preventing the release of EF-G (69). Thus, it is not surprising that this structure represents the post-translocational state with a deacylated tRNAs at P- and E- sites. (Figure 7A)

The conformational changes of the ribosome upon EF-G binding were clearly visualized and detailed interactions between the ribosome and EF-G were elucidated. In particular, domain IV of EF-G projects deep into the decoding center of A-site and makes extensive contacts with P-site tRNA and mRNA, implying its critical role in translocation. In this structure, EF-G adopts a new conformation that is very different from that observed in crystal structure of isolated EF-G, which displays a more "compact" structure (70, 71). In addition, the electron density map clearly shows the location and conformation of fusidic acid (Figure 7B), which was visualized for the first time because of its low affinity for the isolated EF-G. The fusidic acid binding-site is comprised of G domain (switch II region), domain II and domain III (Figure 7B), indicating that the main effect of fusidic acid appears to be the locking of domain II and thus preventing the conformational change transmission required for EF-G release. More over, upon EF-G binding, the L12 stalk was bent towards EF-G and one copy of the CTD of L12 was observed to interact with both L11 and G' domain of EF-G, rationalizing its significance in GTPase activity (72, 73).

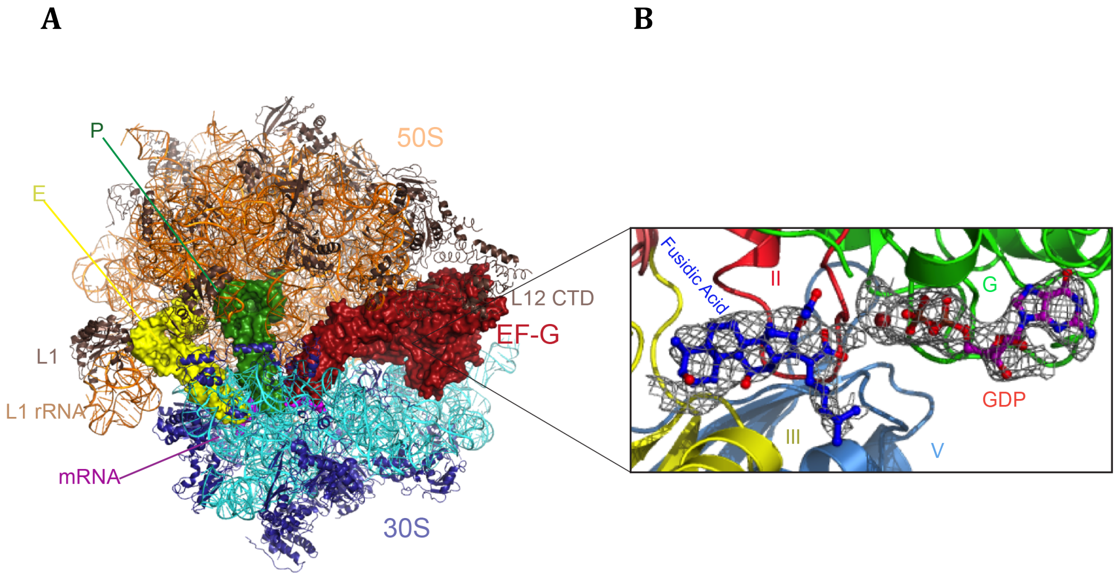

**Figure 7. Crystal structure of post-translocational state ribosome in complex with EF-G and fusidic acid binding site. (A)** Crystal structure of post-translocational state ribosome in complex with EF-G. EF-G is shown in red, 50S subunit is shown in orange, the 30S subunit is shown in cyan, P-site tRNA in green, E-site tRNA in yellow and mRNA in purple. Structural features like decoding center (DC) and L1 stalk are denoted. **(B)** Close-up view of fusidic acid binding site. EF-G is shown as cartoon. Domain G, II, III and V of EF-G are colored green, red, yellow and sky blue respectively. Fusidic acid and GDP are shown as sticks with unbiased difference Fourier electron density map respectively. (Adapted from Gao *et al,* 2009)

Despite the structural insight obtained from the EF-G bound to the ribosome, much still remains unknown concerning the bacterial ribosome translocation. First and foremost, the above-mentioned structure represents a classic state post-translocational ribosome where no small subunit rotation or swiveling is observed. However, the structure of EF-G bound to the ratcheted ribosome, which is the authentic substrate of EF-G-GTP, is crucial for elucidating the mechanism of translocation.

Secondly, the mechanism of GTP hydrolysis by the translational GTPase factors has been a long-standing mystery, however, the EF-G in the reported structure was in a GDP-state, limiting its usefulness in elucidation of the GTP hydrolysis mechanism. Recent structural studies have provided initial information about this fundamental process (45, 46, 65, 68, 74). In particular, the structure of ribosome bound to EF-Tu in a ternary complex with GDPCP, (an non-hydrolysable analogue of GTP) and aminoacyl-tRNA, reveals the structural basis for GTPase activation of by EF-Tu (74) though the exact mechanism of GTP hydrolysis requires additional validation. However, EF-Tu only binds to ribosome in the classical state and GTP hydrolysis is triggered by the conformational change of switch I in response to codon-anticodon recognition at the decoding site. In contrast, other translational GTPase factors including EF-G require ribosome in a ratcheted state for binding and GTPase activation. The structure of RF3 in GTP form bound to the ratcheted ribosome has recently become available (68, 75), yet, the disorder of the switch region and the long distance between the proposed catalytic His92 and the γ-phosphate of the nucleotide, suggest an inactive form. Thus, these structures were also limited in further rationalization of the mechanism of activation of GTPase activity.

Thirdly, the dynamic L1 stalk, comprising L1 rRNA (helices 76-78 of 23S rRNA) and L1 protein, is of significant importance in assisting the release of E-site tRNA and directing the tRNA/mRNA movement during translocation (76). Coupled to ribosome rotation, the L1 stalk adopts a fully closed conformation by undergoing a large movement toward the 50S body and interacting with the hybrid P/E tRNA (49). Interestingly, tRNA in the hybrid state is a prerequisite for the optimal EF-G catalyzed translocation of the mRNA/tRNA complex on the ribosome. Moreover, it appears that there is an allosteric collaboration between EF-G and the L1 stalk during translocation (77). The atomic interaction of the entire L1 stalk with P/E tRNA, as well as the detailed positioning of L1 stalk and P/E tRNA with respect to EF-G on the ribosome, are essential aspects to reveal the structural basis for how these components are coordinated in promoting translocation, but all are largely unknown.

Last but not least, EF-G together with ribosome recycling factor (RRF) is necessary for ribosome dissociation into two subunits upon completion of the polypeptide. This occurs through an EF-G mediated GTP-dependent conformational switch positioning RRF to clash with the 30S subunit. It has been reported that the action modes of EF-G in translocation and ribosome recycling are different (78), but without a high-resolution structure of ribosome bound EF-

G in a GTP state, it would be difficult to understand the underlying structural differences between EF-G dependent translocation and recycling.

In summary, in order to better understand the molecular mechanism of translocation, a high-resolution structure of ribosome in a pre-translocational state bound with EF-G is of utmost importance.

## 1.5 Aims and significance

During the bacterial protein synthesis, movement of tRNA-mRNA complex is catalyzed by the elongation factor G (EF-G), which belongs to the translational GTPases. This movement, known as translocation, involves the spontaneous formation of ratcheting state ribosome, which is characterized by the small subunit body rotation and head swiveling. Coupled to this ratcheting state formation, the aminoacyl ends of two tRNAs move from A- and P- sites to P- and E- sites on the 50S subunit, respectively, while the anticodon stem loop remain fixed on A- and P- sites, creating the hybrid state A/P and P/E tRNAs. EF-G binds to the ratcheting ribosome and facilitates the motion of two tRNAs to the classical P- and E- sites, together with the advancement of mRNA one codon forward in an GTP hydrolysis dependent manner. Translocation is one of the most complex processes in translation and the mechanism of translocation remains one of the most fundamental unsolved issues in life science. Structural studies have provided initial attempts studying the ribosome complex bound with EF-G, using either cryo-EM or X-ray crystallography. In particular, the high-resolution structure of ribosome bound with EF-G in a post-translocational state has revealed much perspective on this important biological process.

However, much information is still lacking, preventing us from having a better understanding of translocation. Particularly, the long-standing mystery of GTP hydrolysis mechanism, the dynamic interaction of the entire L1 stalk with P/E hybrid tRNA, and the different action modes of EF-G during translocation and ribosome recycling, largely remain unknown. Determining the high-resolution structure of EF-G bound to ribosome in the pre-translocational state is a prerequisite to address these issues.

Hence, in this study, we aimed to determine the crystal structure of ribosome in a pre-translocational state in complex with EF-G by using a non-hydrolysable GTP analogue. This structure will shed light on many aspects of ribosomal translocation, as well as the universal mechanism of GTP hydrolysis by translational GTPases.

# 2. Materials and methods

## 2.1 Plasmids construction and protein purification

### 2.1.1 Purification kits for EF-G molecular cloning

Commercial kits used in generating the EF-G expression constructs are listed in Table1.

**Table 1. List of purification kits**

| Method | Kit name | Company |
|---|---|---|
| Genomic DNA extraction | DNeasy Tissue Kit | QIAGEN |
| Gel extraction | QIAquick Gel Extraction Kit | QIAGEN |
| PCR purification | QIAquick PCR Purification Kit | QIAGEN |
| Miniprep/Plasmid DNA extraction | QIAprep Spin Miniprep Kit | QIAGEN |

### 2.1.2 Construction of EF-G expression plasmid

Plasmid for the over-expression of EF-G was constructed by previous lab members as described earlier (67). Briefly, the gene encoding EF-G was amplified by PCR from *T. thermophilus* genomic DNA. PCR product was subjected to double digestion with restriction enzymes Nde I and EcoR I (NEB) at 37 °C for 3 hours. Vector pDBHT-2-Tev (modified from the commercial pET28a in our lab) was treated with the same enzyme to obtain the linearized vector. Ligation of the vector and the insert was performed with T4 DNA ligase (NEB) at 22 °C for 30 minutes, after which the ligation mixture was transformed into the *E. coli* DH5α competent cell and grown overnight in the presence of kanamycin for selection. Positive colony was selected by colony PCR and construct verification was done by DNA sequencing (1st Base). The constructed plasmid contains a six-histidine (His) tag followed by the cleavage site of Tobacco Etch Virus (TEV) nuclear-inclusion-a endopeptidase at the N-terminus of the (Figure 8), allowing the removal of the affinity tag from the final product.

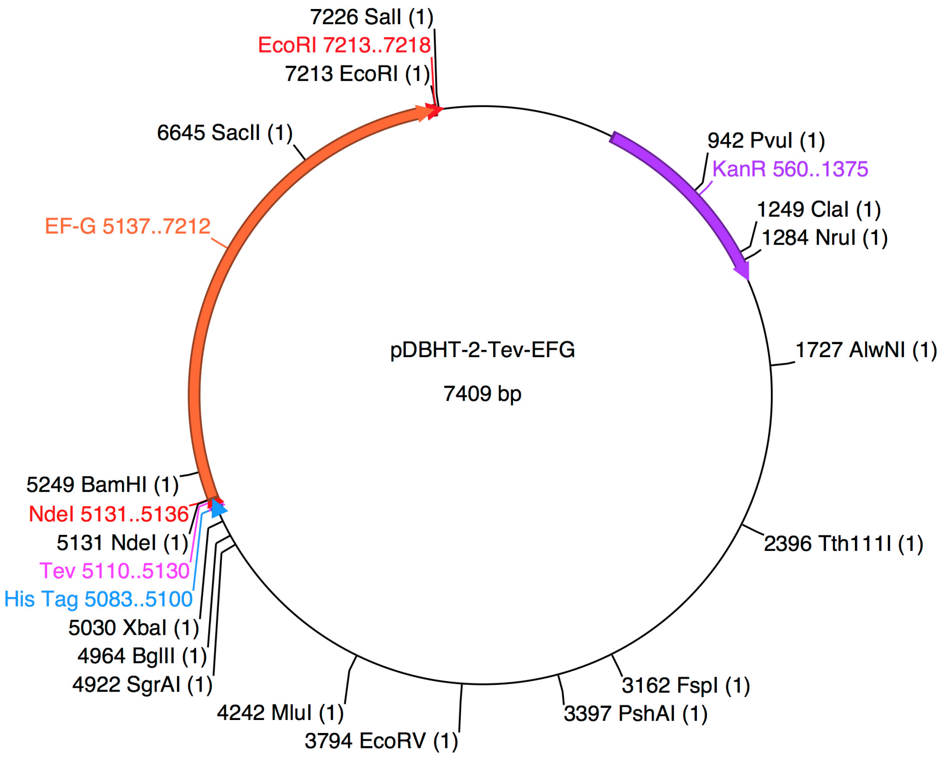
7226 SalI (1)
EcoRI 7213..7218
7213 EcoRI (1)
6645 SacII (1)
EF-G 5137..7212
942 PvuI (1)
KanR 560..1375
1249 ClaI (1)
1284 NruI (1)
pDBHT-2-Tev-EFG
7409 bp
1727 AlwNI (1)
5249 BamHI (1)
NdeI 5131..5136
5131 NdeI (1)
Tev 5110..5130
His Tag 5083..5100
5030 XbaI (1)
4964 BglII (1)
4922 SgrAI (1)
2396 Tth111I (1)
3162 FspI (1)
3397 PshAI (1)
4242 MluI (1)
3794 EcoRV (1)

**Figure 8. EF-G expression construct.** The gene encoding EF-G in *T. Th.* was cloned into the expression vector pDBHT-2-Tev introducing an N-terminal His tag and Tev protease cleavage site. His tag, Tev cleavage site, EF-G gene, kanamycin resistance cassette and two restriction enzymes are indicated.

### 2.1.3 Purification of EF-G protein

EF-G was expressed and purified as described earlier (67). Briefly, the constructed plasmid was transformed into *E. coli* BL21 (DE3) competent cells by heat shock. The overnight culture was obtained by inoculating 100 ml Luria-Bertani (LB) media containing appropriate antibiotics (50 ug/ml kanamycin and 34 ug/ml chloramphenicol) with a single colony from the agar plate. Subsequently, 50 ml overnight culture was inoculated into 5 L of LB-media (supplemented with same antibiotics) and cells were grown at 37 °C with constant agitation (200 rpm). When $OD_{600}$ reached 0.8, isopropyl β-D-1-thiogalactopyranoside (IPTG) was added to a final concentration of 0.5 mM to induce protein expression. Cells were cultured at 16 °C with continuous agitation (150 rpm) for ~20 hours. Cells were harvested by centrifugation at 5000 rpm (Beckman JLA8.1) for 30 min. and flash frozen with liquid nitrogen. Cell pellets were stored at -80 °C for future use.

For protein purification, cell pellets from -80 °C stock were re-suspended in lysis buffer (10 ml per 10 g of cells) consisting of 50 mM sodium phosphate (pH 8.0), 300 mM NaCl, 5 mM β-mercaptoethanol. Cells were then disrupted by using PANDA (GEA Process Engineering) cell homogenizer at 4 °C (600 bar), and the lysate was clarified by centrifuge at 20 000 rpm (Beckman rotor JA25.5) at 4 °C for 30 min. Supernatant was incubated in 65 °C water bath for 30 min and centrifuged again to remove the debris (denatured host proteins). The resulting supernatant was filtered through a 0.45 μm filter prior to loading onto the 5 ml HisTrap HP column (GE Healthcare) (equilibrated with lysis buffer). Target protein was eluted with a linear gradient of buffer B (50 mM sodium phosphate pH 8.0, 300 mM NaCl, 500 mM imidazole and 5 mM β-mercaptoethanol) and the EF-G containing fractions were pooled after SDS-PAGE confirmation. Collected sample was digested with TEV protease (sample protease ratio1:70) overnight at 4 °C to cleave the His tag and concentrated to less than 5 ml before loading onto the Hiload 26/60 Superdex 200 column (GE Healthcare), which was pre-equilibrated with GF buffer (50 mM sodium phosphate pH 8.0, 50 mM NaCl, 5 mM β-mercaptoethanol). Target peak was pooled and loaded onto HisTrap HP QP column (GE Healthcare) (equilibrated with GF buffer). Proteins were eluted with a linear gradient of salt (NaCl 50 mM to 1 M). The protein fractions were collected and buffer was exchanged to buffer G (50 mM KCl, 10 mM $NH_4Cl$, 10 mM MgOAc, 5 mM HEPES-KOH pH 7.5) with Amicon Ultra-15 centrifugal filter unit (Millipore). EF-G protein was concentrated to a final concentration of 500 μM/ml. All used buffers, except for His tag affinity purification, were prepared with RNase free chemicals. The final protein sample was tested with RNase Alert Lab Test Kit (Ambion) to confirm the absence of RNase contamination. EF-G protein was then flash frozen in liquid nitrogen and stored at -80 °C for further use.

## 2.2 Preparation of L9 mutant ribosome, tRNA and mRNA

### 2.2.1 L9 mutant ribosome purification

*T. Th.* strain HB8 was used to construct the HB8-MRCMSAW1 mutant strain, in which the portion of the L9 gene coding from residue 56 to the C terminus was deleted by replacement with a kanamycin resistance gene by homologous recombination as described (67).

L9 mutant ribosome was purified as previously described (21). Briefly, *T. Th.* HB8-MRCMSAW1 cells were re-suspended in buffer A (100 mM $NH_4Cl$, 10.5 mM Mg-acetate, 0.5 mM EDTA, 20 mM K-Hepes, pH 7.5) according to the ratio of 1.5 ml buffer per 1 g of cells. After the addition of DNAse I (Roche) (8 µg per 1 g of cells), the cells were disrupted in a cell homogenizer PANDA (GEA Process Engineering). The resulting cell lysate was centrifuged at 30 000 rpm (Beckman 45Ti rotor) for 1 hour. Supernatant was carefully collected, with care not to disturb the pellet consisting of the cell debris, and loaded onto the 1.1 M sucrose cushion in buffer B (0.5 M KCl, 10.5 mM Mg-acetate, 0.5 mM EDTA, 20 mM HEPES, pH 7.5). Crude ribosome pellets were obtained by centrifugation at 45 000 rpm (Beckman 45 Ti rotor) for 17.5 hours and washed with buffer C (1.5 M ammonium sulfate, 10 mM Mg-acetate, 400 mM KCl, 20 mM Tris-HCl, pH 7.5). After re-suspension in buffer C and filtration through a 0.45 µm filter, the sample was then applied to a Toyopearl butyl 650S column (GE healthcare) pre-equilibrated with the same buffer. 70S ribosome was eluted with a reverse gradient of ammonium sulfate by using buffer D (10 mM Mg-acetate, 400 mM KCl, 20 mM Tris-Cl, pH 7.5). The ribosome fractions, which should now be free of a contaminating endogenous ribonucleases, were collected and diluted 2-fold with buffer E (50 mM KCl, 10 mM $NH_4Cl$, 10.25 mM Mg-acetate, 0.25 mM EDTA, 10 mM HEPES, pH 7.5). Ribosomes were pelleted overnight by centrifugation at 43 000 rpm (45Ti rotor). Pellet was re-suspended in buffer E containing 5% sucrose and layered onto 10–40% sucrose gradient in buffer E and centrifuged at 28 000 rpm for 19 hours using Beckman Ti 15 zonal rotor. Absorbance was measured at 260 nm, fractions corresponding to 70S ribosome were pooled and diluted with buffer E. Ribosome pellets were obtained by overnight centrifugation (43 000 rpm for more than 16 hours) and re-suspended in buffer G (50 mM KCl, 10 mM $NH_4Cl$, 10 mM Mg-acetate, 5 mM HEPES, pH 7.5) to a final concentration of approximately 350 $A_{260}$ units/ml. All buffers were supplemented with 6 mM 2-mercaptoethanol, 0.1 mM benzamidine and 0.5 mM phenyl-methyl-sulfonyl fluoride (PMSF) just before use. All procedures were performed at 0-4 °C. The ribosome was flash frozen in liquid nitrogen, aliquotted and stored at -80 °C for further use.

### 2.2.2 tRNA and mRNA preparation

Both *E. coli* tRNA$^{fMet}$ and tRNA$^{Phe}$ were purchased from Sigma. The Z4CO2 mRNA with sequence 5' GGCAAGGAGGUAAAA**AUGUUC**AAAA 3', in which AUG and UUC represent the P- and A- site codons corresponding to the tRNA$^{fMet}$ and tRNA$^{Phe}$ , respectively, was obtained from Dharmacon.

## 2.3 Complex formation and binding assay

### 2.3.1 Formation of the EF-G-ribosome complex

Complex of 70S ribosome with mRNA (Z4CO2), tRNA$^{fMet}$, tRNA$^{Phe}$ and EF-G in a GDPCP state was assembled according to Table 2, using a similar procedure as previously described (67). Briefly, ribosomes (4 µM) and mRNA (8 µM) were initially incubated at 55 °C for 6 min, then tRNA$^{fMet}$ (8 µM) was added and incubated for another 30 min at 55 °C. Subsequently, tRNA$^{Phe}$ (8 µM) was added for a further 30 min incubation before the mixture was cooled down to 37 °C. Meanwhile, EF-G (20 µM) and GDPCP (100 µM) were mixed and incubated at room temperature for 30 min before adding to the ribosome mixture. The complex was finally incubated for 30 min at 37 °C and kept at room temperature for 30 min.

**Table 2. Components and final concentration of the pre-tranlocation complex**

| Component | Final concentration |
|---|---|
| Buffer G | 1x |
| L9 mutant 70S ribosome | 4 μM |
| Z4C02 mRNA | 8 μM |
| $\text{tRNA}^{\text{fMet}}$ | 8 μM |
| $\text{tRNA}^{\text{Phe}}$ | 8 μM |
| EF-G | 20 μM |
| GDPCP | 100 μM |

### 2.3.2 Assay of EF-G binding to the ribosome

The EF-G-ribosome complex was loaded onto 1.1M sucrose cushion (in buffer G) containing 100 μM GDPCP and ultra-centrifuged at 100 000 rpm at 4 °C for more than 3 hours (Beckman MLA130 rotor). Supernatant was removed, and after being washed with buffer G (containing 100 μM GDPCP) for three times, the pellet was re-suspended and diluted with buffer G to a final concentration of 4 μM. "Empty" ribosomes and EF-G were also diluted with buffer G to the same concentration and used as controls. All three samples were analyzed by SDS-PAGE. Protein bands were visualized by staining with either Coomassie Brilliant Blue (CBB) or SYPRO Ruby (Sigma). EF-G binding efficiency was assessed by comparing the protein band intensities of different samples.

## 2.4 Crystallization trials

Sitting-drop vapor diffusion method was used to set up crystallization trials. Initial attempts to crystallize the complex were conducted by using either the detergent deoxy big CHAP (DOBC) or D-Glucitol,1-deoxy-1-[(2-hydroxyethyl)(1-oxononyl)amino]- (HEGA-9) as reported (67) (79). However, crystals were difficult to grow and proved to diffract poorly. To improve the crystal quality, detergent and additive screening were carried out using commercial screening kits (Detergent Screen HT and Additive Screen HT, Hampton Research). The detergent N,N-Dimethyldecylamine-N-oxide (DDAO) was selected for following crystallization experiments because it could enhance the complex crystallization as the crystal grew bigger with nicer morphology.

Crystals were grown by mixing 2.5 µl reservoir solution (0.1 M MES pH 6.5, 5.8-6.8% PEG20K, 30-120 mM KCl, 0.8-2.5% glycerol) and 2.5 µl complex (final concentration 3.2 µM). Crystals obtained their final size within two weeks and were transferred stepwise to a final solution containing crystallization buffer and 28% PEG550MME as cryo-protectant. All crystals were then flash frozen by plunging into liquid nitrogen.

### 2.5 Data collection and structure determination

Data collection was carried out on beamline PX I of the Swiss Light Source (SLS) on a Pilatus 6M (Dectris) detector at 100K. All data were processed with XDS software package (80). Empty 70S ribosome structure (21) was used to obtain an initial model and further refined was carried out with CNS (81). All model building was done using COOT (82) and all electron density maps were generated with CNS or CCP4 suite (83). All figures were made with PyMOL (DeLano Scientific).

# 3. Results

## 3.1 EF-G purification, ribosome preparation and binding assay

### 3.1.1 EF-G expression and purification

The constructed plasmid for expressing EF-G with N-terminal TEV protease cleavable His tag was verified by DNA sequencing. Plasmid was then transformed into *E. coli* BL21 (DE3) strain to over-express the recombinant protein. EF-G exhibited high level of expression and solubility as previously reported (67) and no anomalous growth of *E.coli* was observed. After a four-step purification strategy including nickel (Ni) affinity chromatography, TEV protease cleavage, gel filtration chromatography and ion exchange chromatography, the purity EF-G was confirmed by SDS-PAGE (Figure 9B). SDS-PAGE result in combination with the gel filtration elution profile (Figure 9A) indicated a highly pure and homogenous sample eligible for crystallization studies. The RNase alert test was used to confirm that there was no RNase contamination. The cleavable fluorescent-labeled substrate provided in the kit would be digested in the presence of RNase so that the fluorescence could be detected by short-wave UV illumination. The absence of fluorescence (Figure 9C) with purified EF-G sample confirmed that it is suitable for ribosome related work, while the positive control sample (commercial RNase A) had very strong fluorescence. After purification, the yield from 5 L cell culture for EF-G was ~50 mg.

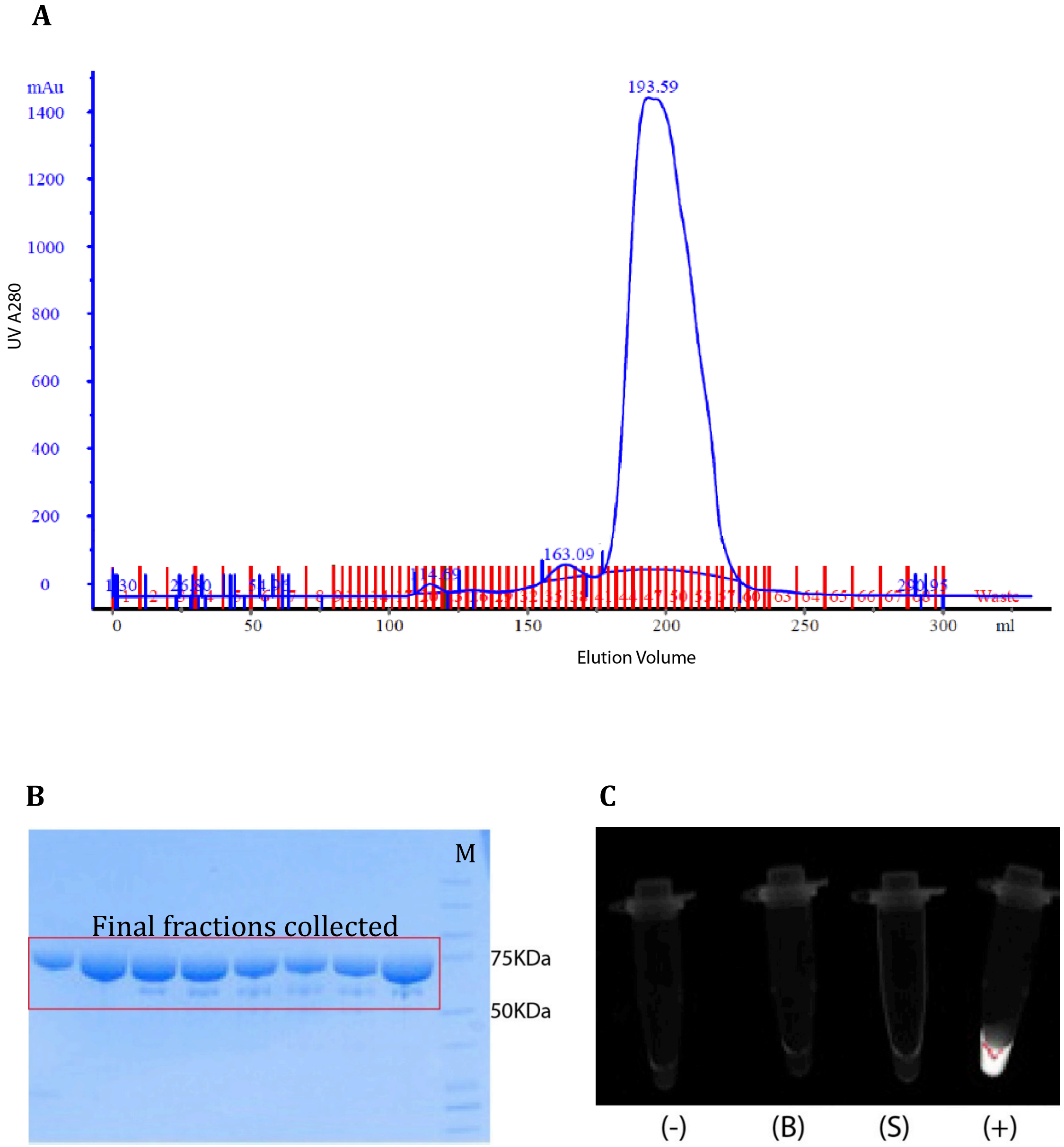

**Figure 9. EF-G purification. (A)** Gel filtration chromatography profile of EF-G using a Superdex 200 26/60 column. **(B)** SDS-PAGE gel analysis of EF-G after ion-exchange chromatography. M: protein marker. **(C)** RNase alert test of final EF-G protein. (-) RNase free water as negative control, (B) buffer used to store EF-G, (S) EF-G protein sample at working concentration, (+) RNase A as positive control.

### 3.1.2 L9 mutant ribosome purification

Ribosome was purified as previously described (21). Succinctly, crude ribosomes were obtained by pelleting through sucrose cushion and endogenous ribonuclease was removed by passing through the hydrophobic Toyopearl butyl 650S column (Figure 10A). Ribosome was eluted with a reverse gradient of ammonium sulfate. Elution profile showed a clear separation of 70S ribosome peak from other contaminant although it was not sure if 50S or 30S subunits still exist at this stage. Ribosome was further purified by 10-40% sucrose gradient centrifugation using a Ti 15 zonal rotor followed by fractionation. When $A_{260}$ of fractions was measured and plotted (Figure 10B), a major peak corresponding to the 70S (fraction 26-30) and a minor peak of 50S subunit (fraction 20-25) was visible. 70S portion was collected, pelleted, re-suspended and concentrated to approximately 350 $A_{260}$ units/ml. Ribosome quality was inspected by 1% agarose gel electrophoresis (Figure 10C). Two clear bands corresponding to 23S and 16S rRNA indicated a lack of degradation and therefore a high sample quality suitable for future experiment. For each round of ribosome purification, 250 g of cell pellet was used and 5-6 ml sample (about 2000 $A_{260}$ units in total) was obtained.

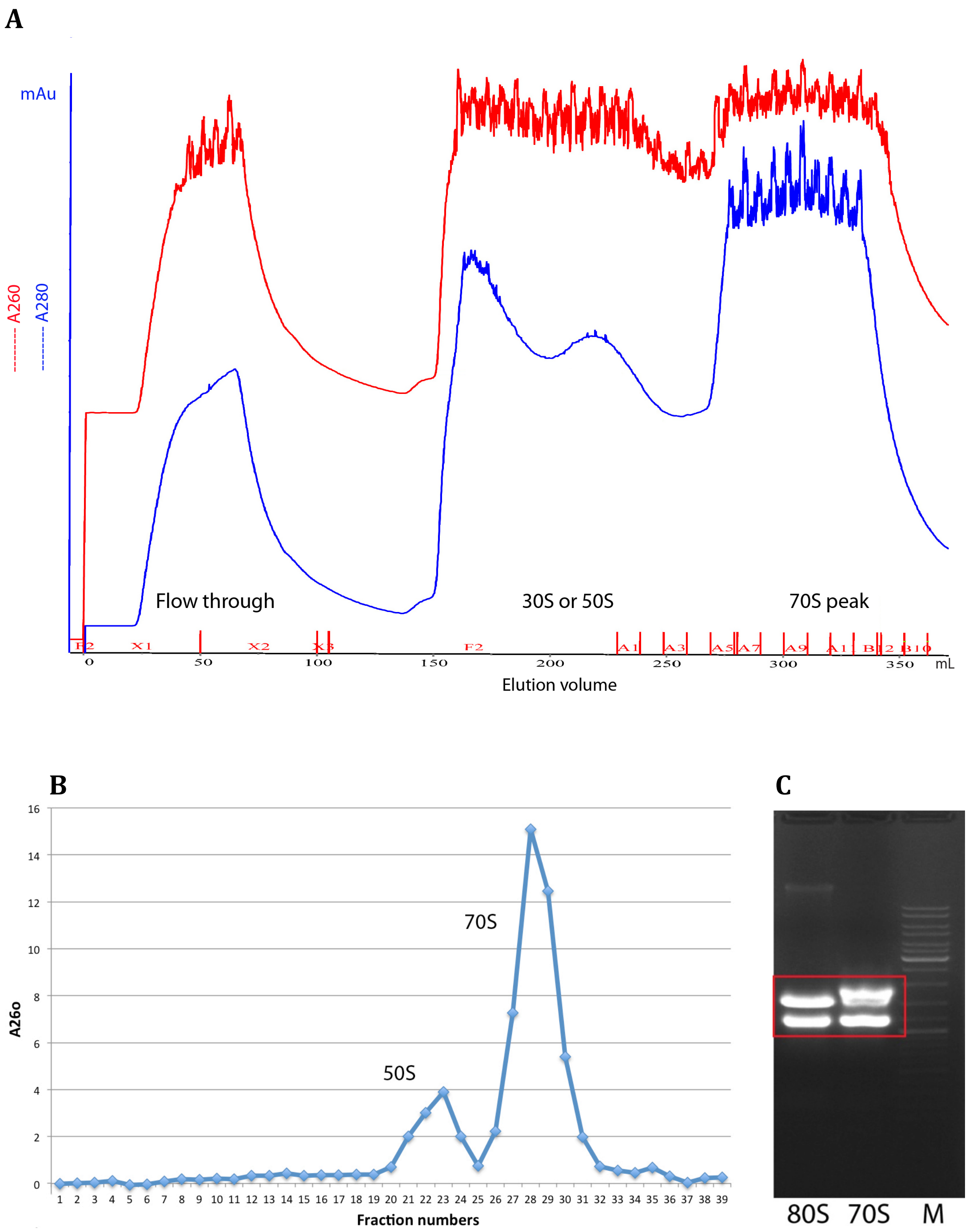

**Figure 10. L9 mutant ribosome purification. (A)** Elution profile of Toyopearl butyl 650S column purification. Fractions corresponding to flow-through, 30S or 50S subunits and 70S ribosomes are indicated. **(B)** Ribosome profile of sucrose gradient purification. 50S and 70S peaks are labeled. **(C)** Agarose gel electrophoresis of purified 70S ribosome, Bands corresponding to 23S and 16S rRNAs are indicated. Yeast 80S ribosome purified by other lab members was used as a control, M: marker.

### 3.1.3 EF-G binding assay

To confirm the binding of EF-G with ribosome, the assembled EF-G-ribosome complex was loaded onto 1.1 M sucrose cushion and centrifuged at 100 000 rpm for more than 3 hours to pellet the ribosomes and remove the unbound ligands (mRNA, tRNA and EF-G). In order to maintain the EF-G in the GDPCP state, the sucrose solution was supplemented with 100 μM GDPCP. Ribosome pellets were re-suspended and analyzed by SDS-PAGE.

Compared with control (“empty”) ribosomes, a band corresponding to EF-G was clearly detected from the complex of ribosome (Figure 11A), suggesting a stable binding of EF-G in GDPCP form with ribosome that is maintained throughout sucrose cushion centrifugation. The stable binding of EF-G renders the complex recovered from sucrose cushion an ideal sample for crystallization trials. In fact, the complex is more homogeneous since extra ligands are removed during pelleting. The stoichiometry ratio of EF-G was evaluated to be roughly 1 to 1 in the complex according to the quantification of band intensities on the SDS-PAGE gel stained by SYPRO Ruby.

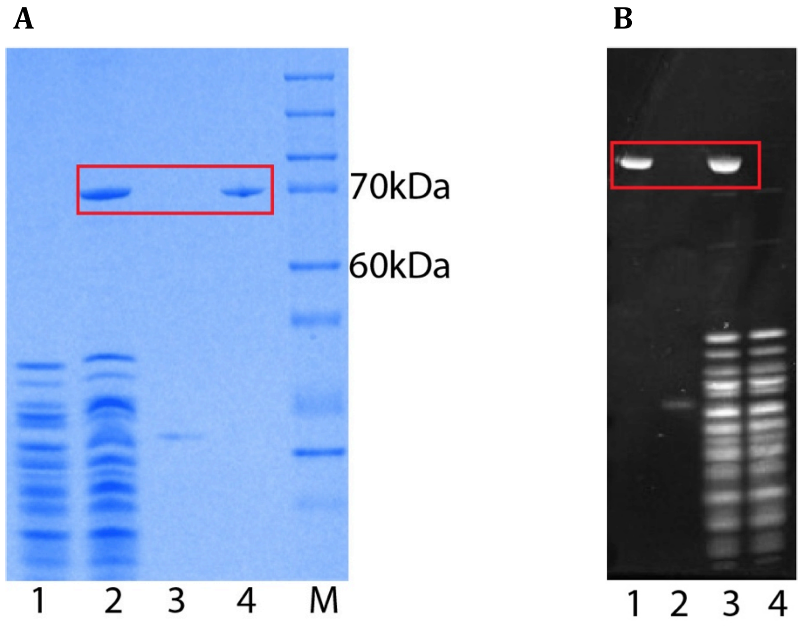

**Figure 11. EF-G binding assay.** **(A)** SDS-PAGE check stained by CBB. Lane 1, “empty” ribosome as a control; lane 2, EF-G ribosome complex sample recovered from sucrose cushion; lane 3, ribosome recycling factor (RRF) not relevant to this study; lane 4, isolated EF-G protein as control; M, protein size marker. **(B)** SDS-PAGE check stained by SYRO Ruby. Lane 1, isolated EF-G as a control; lane 2, RRF not relevant to this study; lane 3, EF-G-ribosome complex sample recovered from sucrose cushion; lane 4, empty ribosome as control.

### 3.2 Crystallization of the EF-G-ribosome complex

Initial crystallization trials were carried out according to the method previous reported (67). By varying the concentration of PEG 20K, needle-shaped crystals were obtained (Figure 12A), which usually appeared as a cluster of needles. HEGA-9 facilitated the crystal formation compared with DOBC, which is not unexpected as HEGA-9 is usually chosen for crystallization of L9 mutant ribosome. After several rounds of optimization by varing the PEG concentration, plate-shaped crystals were obtained (Figure 12B) and over a hundred crystals were picked and sent to synchrotron (SLS, Switzerland) to test diffraction. However, it proved difficult to obtain good diffraction data from these crystals as the best resolution was ~10 Å while most were more than 20 Å. In addition, anisotropy remains a major obstacle because the crystals were thin, two dimensional and diffracted extremely poor from one specific direction.

This motivated us to seek for new crystallization conditions and both additive and detergent screening were performed using commercial kits from Hampton Research. DDAO was selected as a detergent in following experiments as it improved both the crystal size and morphology compared with HEGA-9 and DOBC (Figure 12C). KCl, sucrose and glycerol were frequently used additives when trying to crystallize L9 mutant ribosome as they feature in many other reported reservoir conditions of ribosome crystallization. This was in accordance with our additive screening results and although some other additives also yielded crystals, the crystals were poorly formed. By screening different combinations and concentrations of these three reagents, we finally succeeded in increasing the thickness of the crystals (Figure 12D) resulting in significant improvement of diffraction (beyond 3 Å).

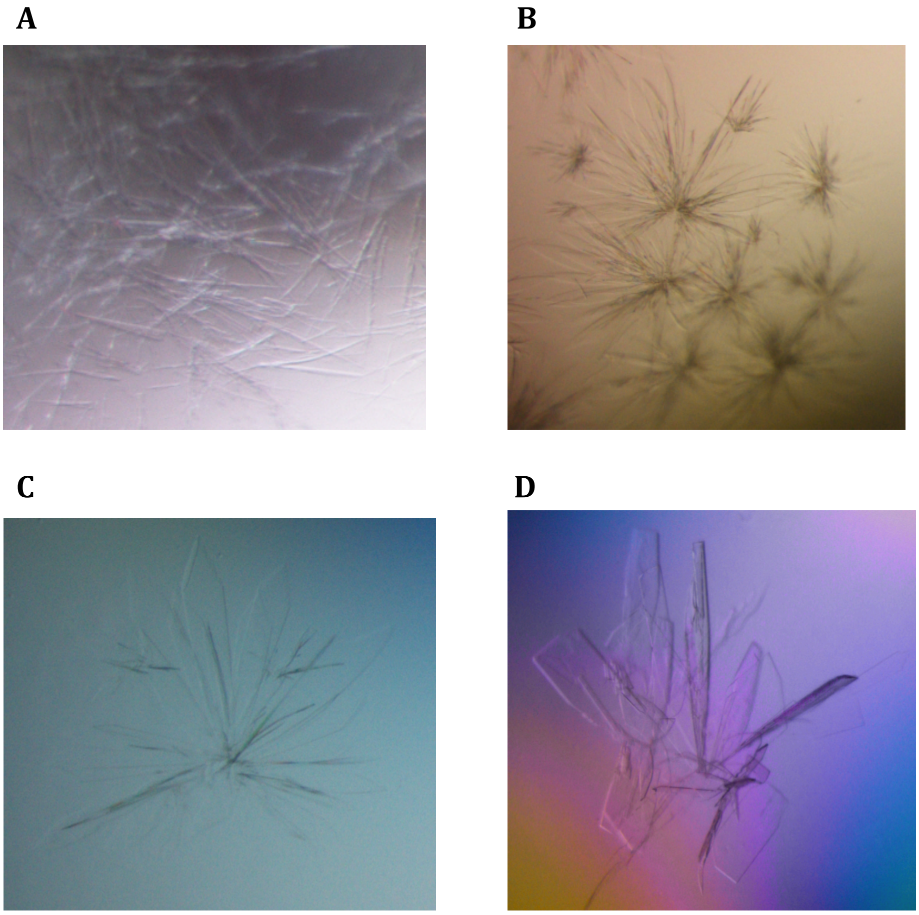

**Figure 12. Crystallization of the EF-G ribosome complex. (A)** Initial crystal hints obtained from reported conditions using HEGA-9 as detergent. **(B)** Crystals optimized based on the reported conditions using HEGA-9 as detergent. **(C)** Initial crystal hints obtained from detergent screening with DDAO as detergent. **(D)** Well-diffracting crystals optimized based on DDAO conditions and with different combination of additives.

### 3.3 Structure determination

A full dataset for the EF-G ribosome complex was collected at beamline PX I of the Swiss Light Source (SLS) on a Pilatus 6M (Dectris) detector at 100K. Data was processed with XDS and the statistics of data collection is summarized in Table 3. The complex crystallized in the space group $P2_1$, similar to the post-translocational complex reported previously (67), which was not unexpected because the conformational change within the ribosome should not influence crystal packing.

Empty 70S ribosome structure (21) was used to obtain an initial model, which was further refined with CNS (81). The difference density map clearly revealed the presence of the mRNA, P-site tRNA, EF-G and GDPCP. The model was then manually built using COOT (82). The final structure was refined to 2.95 Å resolution (I/ σ(I)=1.6), with a final R/$R_{free}$ of 0.210/0.244. Statistics of structure refinement is summarized in Table 3. The coordinates and structure factors have been deposited in Protein Data Bank (PDB) with accession code 4BTC and 4BTD for small subunit and large subunit, respectively.

## Table 3. Statistics of data collection and structure refinement of the EF-G-ribosome complex

| | |
|---|---|
| **Data collection** | |
| Space group | $P2_1$ |
| Unit cell dimentions: | |
| a,b,c (Å) | a=202.9, b=242.6, c=309.3 |
| $\alpha,\beta,\gamma$ (°) | $\alpha=\gamma=90$, $\beta=91.6$ |
| Resolution (Å) | 50-2.95 (3.05-2.95) |
| $R_{sym}$ (%) | 26.4 (115.6) |
| $I/\sigma I$ | 8.0 (1.6) |
| Completeness (%) | 100.0 (100.0) |
| Redundancy | 7.2 (6.3) |
| **Refinement** | |
| Resolution (Å) | 50-2.95 |
| No. of unique reflections | 4452517 |
| Rwork/Rfree | 21.0 /24.4 |
| No. of atoms | |
| RNA | 99250 |
| Protein | 54037 |
| Ions | 488 |
| Others | 32 |
| Average B factor | |
| RNA | 54.2 |
| Protein | 64.3 |
| Ions | 64.5 |
| Others | 60.2 |
| Rmsd from idealty | |
| Bond length (Å) | 0.006 |
| Bond angle (°) | 1.22 |

* Numbers in parenthesis refers to outer resolution shell
† I/s = 2.0 at 3.0 Å

## 3.4 Structural analysis

### 3.4.1 Overall structure and small subunit rotation

The structure of EF-G bound to ribosome, trapped in the state prior to GTP hydrolysis, reveals a fully rotated complex (Figure 13A). Compared with the previously published structure of EF-G bound to the ribosome (67), which was trapped by fusidic acid in the post-translocational state, the present structure demonstrates a counter-clockwise rotation of the 30S subunit relative to the 50S subunit by 7.4°, and a swiveling of the 30S head by 9.0° toward the L1 stalk (Figure 13B). The binding of EF-G in GTP form also induces conformational change in both L7/L12 and L1 stalks, whereas the 50S body remains rigid (Figure 13C). One copy of the C-terminal domain (CTD) of protein L12 interacts with domain G' of EF-G (Figure 13C). Additionally, the stalk base comprising L11 rRNA and L11 protein (Figure 13C) shifts toward the 50S body by ~5 Å when measured at the tip of H43. As for the L1 stalk, it moves toward the 50S body by ~26 Å at the distal end, thereby establishing extensive contacts with the P/E tRNA (Figure 13C) and resulting in a completely "closed" conformation.

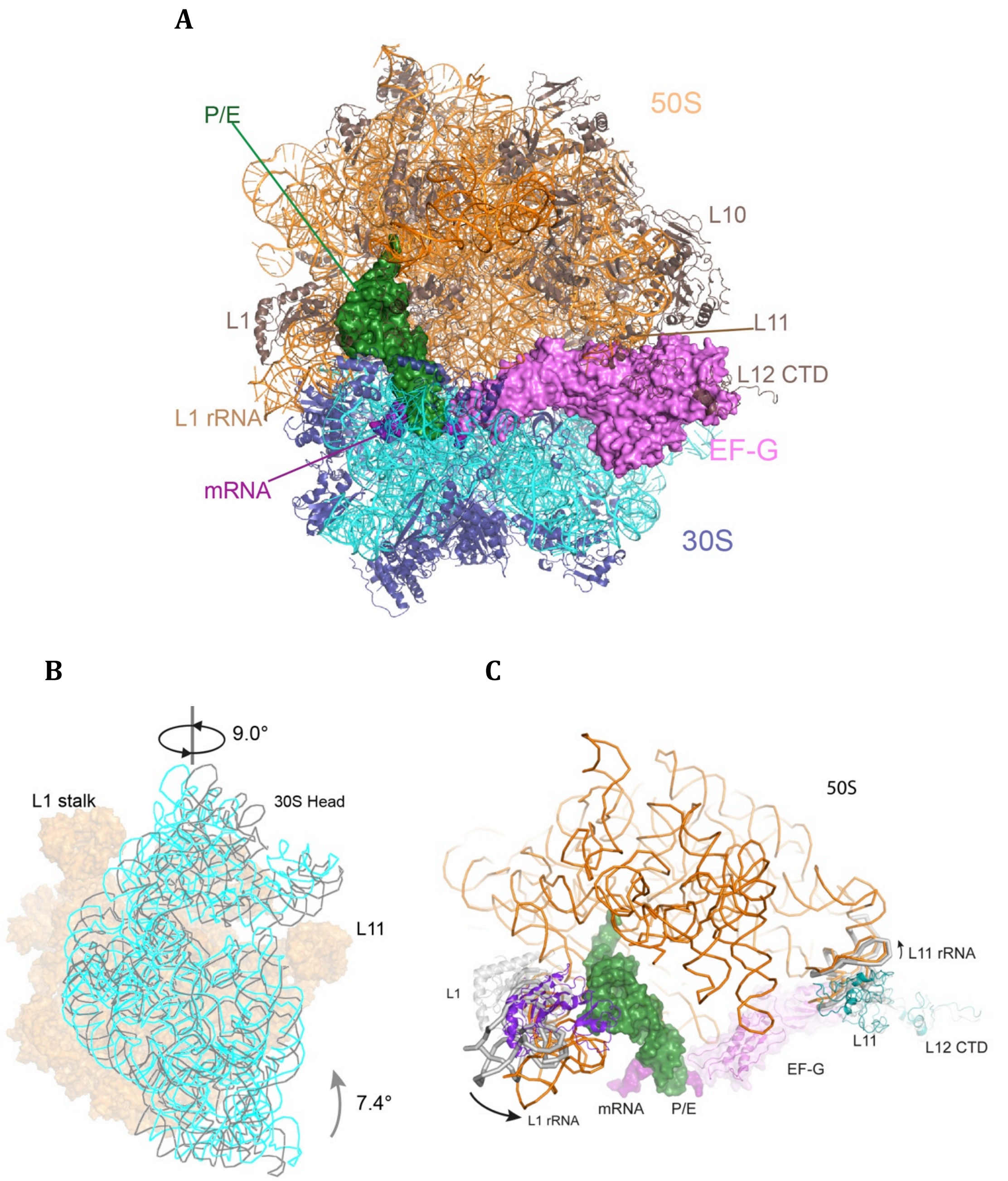
A
P/E
50S
L10
L1
L11
L12 CTD
L1 rRNA
EF-G
mRNA
30S
B
9.0°
L1 stalk
30S Head
L11
7.4°
C
50S
L11 rRNA
L1
L11
L12 CTD
EF-G
mRNA
P/E
L1 rRNA

**Figure 13. Overall structure and conformational change of the ribosome upon EF-G binding. (A)** Overall view of the EF-G ribosome complex. EF-G, hybrid P/E tRNA and mRNA are shown in surfaces. The 50S and 30S subunits are shown as cartoon in orange and blue, respectively. **(B)** Body rotation and head swiveling of 16S rRNA (cyan) in the 30S subunit relative to the 50S subunit, compared with 16S rRNA (gray) in the post-translocational complex. **(C)** Global changes of the stalks in the 50S subunit. The L1 stalk (L1 rRNA and L1 protein) and L11 rRNA in the post-translocational complex are colored gray and conformational changes are indicated with arrows. The L11 region (L11 protein and L11 rRNA) is an important component of the ribosome GTPase associated center, the rearrangement of EF-G positioning on the ribosome thereby appears to induce its conformational change.

Inter-subunit motion is necessary for the function of ribosome. Coupled to ribosome rotation, large rearrangements take place in inter-subunit bridges. A comparison of currently EF-G-ribosome and post-translocational complexes shows that the central inter-subunit bridges are rather conserved, but the peripheral bridges can undergo a significant change, including disruption of a number of bridges, as well as the formation of new connections. Inter-subunit bridge rearrangements are depicted in Figure 14 and summarized in Table 4.

A comparison of the current structure with the recently published structures of the ribosome in various states of rotation demonstrates a conformational similarity of the central bridges, implying a common feature in ribosome ratcheting during the process of translation. However, the central bridge B2a, located at the decoding site, was found to have a quite unique conformation in our complex, probably due to EF-G binding. The peripheral bridge B1b, which connects the head of 30S and the central protuberance of 50S, involves ribosomal proteins L5, L31, S13, and S19. L31 was previously observed to be involved in subunit bridges (84), but has not been clearly observed. Notably, we could build an entire model of L31, revealing that its C-terminal tail forms a number of contacts with S19 and 16S rRNA in the 30S head, participating in the formation of bridge B1b (Figure 14 and Table 4). In contrast, L5 shifts away from S13 and S19, completely abolishing its contact with S19, as well as weakening the interaction with S13.

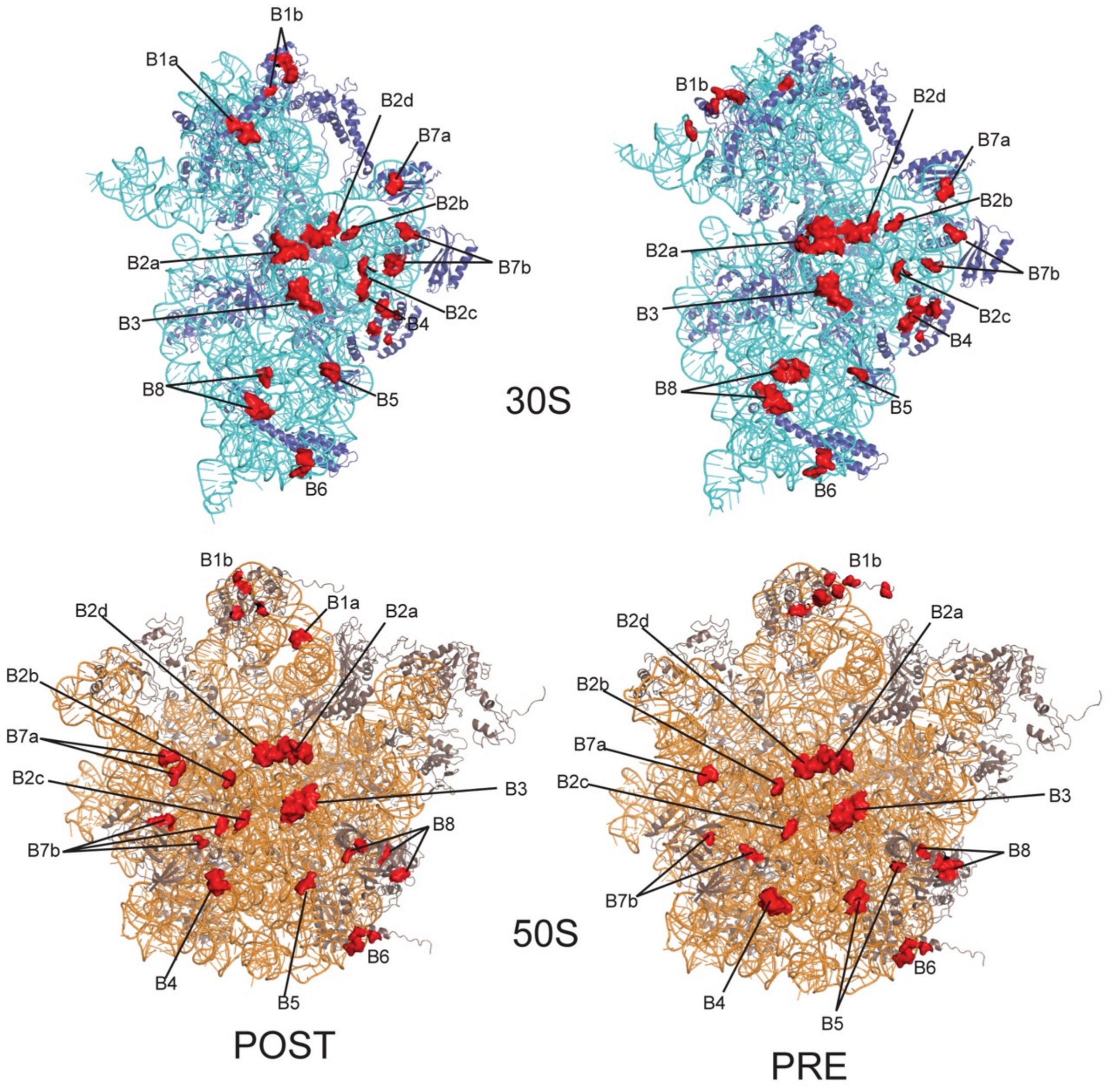
B1b
B1a
B2d
B7a
B2b
B2a
B7b
B3
B2c
B4
B8
B5
30S
B6
B1b
B2d
B7a
B2b
B2a
B7b
B3
B2c
B4
B8
B5
B6
B1b
B2d
B1a
B2a
B2b
B7a
B2c
B3
B8
B7b
B6
50S
B4
B5
POST
B1b
B2d
B2a
B2b
B7a
B2c
B3
B8
B7b
B6
B4
B5
PRE

**Figure 14. Inter-subunit bridge comparison between pre- and post-translocational complexes.** The inter-subunit contacts are highlighted as surface in red for both 30S and 50S subunits. The upper panel represents 30S while the lower panel represents the 50S, accordingly. Bridge numbering is according to the previous report by Yusupov and coworkers (85).

Table 4. Rearrangement of inter-subunit bridges[a]

| Bridge | Post-translocation[b] | | EF-G-ribosome[c] | | Change |
|---|---|---|---|---|---|
| | 30S | 50S | 30S | 50S | |
| B1a | S13 M82,D83, R93 | H38 C888 | - | - | Disrupted |
| B1b | S13 V7,G68<br>S13 L56,R57,R3 | L5 D116,L139<br>L31 G17,E34 | - | - | Disrupted |
| | | | S13 A72<br>S19 D13,L16,P42, E43, E64,V67<br>h33 P1012 | L5 R115<br>L31 R48,V50,T52, A56,F59,R61<br>L31 K69 | New |
| B2a | h44 r1407 | H69 A1912 | NC | NC | |
| | h44 r1408 | H69 A1916 | NC | NC | |
| | h44 r1409 | H69 P1914 | h44 r1409 | H69 C1914 | |
| | - | - | h44 A1492 | H69 A1913 | New |
| | h44 r1494 | H69 r1912 | NC | NC | |
| | h44 r1494…Mg… | H69 P1913 | - | - | Mg lost |
| | - | - | h44 r1495 | H69 r1919 | New |
| | h45 rG1517 | H69 r1919 | NC | NC | |
| B2b | h24 r783 | H68 P1836 | - | - | Disrupted |
| | - | - | h24 P784 | H68 P1836 | New |
| B2c | h24 r770...Mg... | H67 P1832 | NC | NC | Mg retained |
| | h27 r899 | H67 P1832 | - | - | Disrupted |
| B2d | h24 U793...Mg... | H69 P1920 | NC | NC | |
| | h45 P1517…Mg… | H69 P1920 | NC | NC | |
| B3 | h44 A1418 | H71 GC1948-58 | NC | NC | |
| | h44 A1483 | H71 | NC | NC | |

| | | | | | |
|---|---|---|---|---|---|
| | | CG1947-59 | | | |
| | h44 r1484 | H71 r1960 | NC | NC | |
| B4 | S15 S40,H53,L56 | h34 G715, | S15 S40,H53,L56, V60 | NC | Similar |
| | S15 R64,G89 | h34 P715,P716 | NC | h34 P714,P715,P716 | Similar |
| | - | - | S15, K44 | r716 | New |
| B5 | h44 r1429 | H62 r1703 | NC | NC | |
| | h44 r1428 | H62 r1703 | - | - | Disrupted |
| | - | - | h44 r1429 | H62 P1704 | New |
| B6 | h44 G1443 | H101 P2864 | NC | NC | |
| | h44 r1443,r1446 | L19 R118,D122 | NC | NC | |
| B7a | h23 A702 | H68 G1846 | - | - | Disrupted |
| | h23 A702 | H68 A1848 | - | - | Disrupted |
| | - | - | h23 A702 | H68 P1847 | New |
| B7b | h23 P713 | L2 Q166,R176 | - | - | Disrupted |
| | h24 P774 | L2 K202 | NC | NC | |
| | h24 P773…Mg.. | H66 P1793 | - | - | Disrupted |
| | - | - | h23 r712 | L2 Q164 | New |
| | - | - | h24 P774 | L2 K202 N203 | New |
| B8 | h14 P345,P346 | L19 R41 | h14 P345,P346 | L19 E36,K35 | |
| | h14 P339 | L14 E9,N13 | NC | NC | |
| | h14 C345…Mg… | L14 S116,A118 | h14 C345…Mg… | L14 V115,S116 | |
| | - | - | h14 U343…Mg… | L14 S116 | New |
| | - | - | h14 P338 | L14 E9 | New |
| | - | - | h14 P340 | L14 T96 | New |
| | - | - | h14 r345 | L14 R107 | New |
| | - | - | h14 P346 | L14 R104,R107 | New |

[a] Abbreviations: NC, no change (indicated interactions are maintained between post-translocational and current states); -, interaction absent; h and H indicate

rRNA helices (h for 16S rRNA, H for 23S rRNA); r, ribose 2'-OH interaction; P, phosphate non-bridging oxygen interaction; ...Mg..., interaction mediated by a magnesium bridge (75).

[b] The post-translocation structure refers to the *T. thermophilus* 70S ribosome bound with EF-G trapped in a post-translocation state (67).

[c] The EF-G-ribosome structure refers to the *T. thermophilus* 70S ribosome bound with EF-G in a GDPCP state presented in this thesis.

### 3.4.2 Active site and the switch I region of EF-G

The unbiased difference map clearly shows the bound nucleotide GDPCP, proposed catalytic residue His87, and the switch regions of EF-G (Figure 15A). An $Mg^{2+}$ ion, coordinated with GDPCP, and the side chains of EF-G residues Thr26 and Thr64 are clearly visualized (Figure 15A and B). GDPCP binds to the same pocket in domain G as previously observed for GDP or GTP. In addition to the G motifs (G1, G4, and G5) known to be involved in guanine-nucleotide recognition (74), a significant finding involves the observation of nucleotide binding by the other two G motifs, namely G2 and G3. G2 is part of the switch I, and G3 is located in the switch II region of EF-G and comprises the proposed catalytic residue His87 (His92 in *E. coli*). The side chain hydroxyl of Thr64 in G2 forms bilateral interactions with both the $\gamma$-phosphate oxygen of GDPCP and the $Mg^{2+}$ ion (Figure 15B). The catalytic residue His87 is located only 3.0 Å away from the $\gamma$-phosphate oxygen of GDPCP, suggesting an activated conformation of EF-G.

The highly conserved SRL (a.k.a. the 2660 loop) of 23S rRNA helix H95 is the longest universally conserved RNA stretch (12 nucleotides in a row) (86, 87). H95 of 23S rRNAs inserts into the cleft formed by domains G, III, and V of EF-G, and is involved in formation of the nucleotide-binding pocket by partially occluding the entrance (Figure 15A). The phosphate oxygen atom of A2662 in the SRL is within hydrogen-bonding distance of His87 (Figure 15A) and this interaction is proposed to be crucial for the activation of His87 in a similar manner as previously observed for EF-Tu (74). Together, these results explain why the toxin $\alpha$-sarcin that cleaves the 23S rRNA between G2661 and A2662 causes ribosome inactivation through abolishing GTPase activation of translational GTPases (71). Additionally, it appears that one $Mg^{2+}$ ion conducts a network of interaction between the SRL (2662-2664) and Asp22 in G1.

In the immediate vicinity of the active site, a network of interactions involving the SRL (G2661 and A2660), EF-G (Glu456, Arg660, Ser661 and Gln664), and L6 (Lys175) is formed, with A2660 being the central residue (Figure 15C). Particularly, the base of A2660 stacks with Arg660 of domain V of EF-G, which in turn interacts with Asp89 and Val88 right next to the catalytic His87, thereby likely engaging in the repositioning of His87 into its active conformation. This observation allows us to rationalize previous biochemical data indicating that depurination of A2660 by ricin affected EF-G activity (87), and that nucleobase of A2660 is critical for EF-G GTPase activation (88, 89).

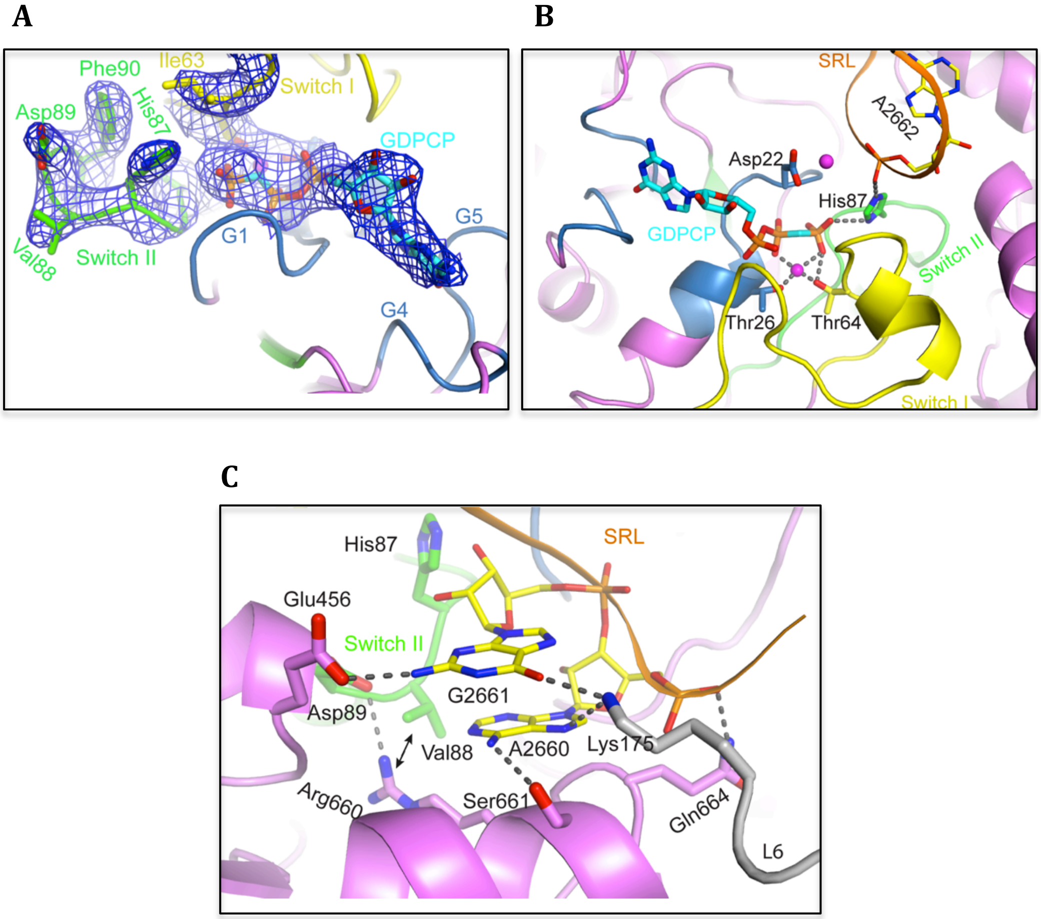
A
B
C
Phe90
Ile63
Switch I
Asp89
His87
GDPCP
G1
G5
Val88
Switch II
G4
SRL
A2662
Asp22
His87
GDPCP
Switch II
Thr26
Thr64
Switch I
His87
SRL
Glu456
Switch II
G2661
Asp89
Val88
A2660
Lys175
Arg660
Ser661
Gln664
L6

**Figure 15. Interactions at the active site of EF-G. (A)** Unbiased difference Fourier electron density map with refined GDPCP, $Mg^{2+}$ ion and EF-G. GDPCP (cyan) is shown in sticks, with carbon, oxygen, nitrogen and phosphate atoms colored green, blue and orange, respectively. $Mg^{2+}$ ion is shown as sphere in violet. Switch loops I (yellow) and II (green) of EF-G are also shown in sticks. EF-G G1, G4 and G5 motifs (blue) are denoted as well. **(B)** Newly established interactions in the GDPCP binding site. Sarcin-ricin loop of 23S rRNA is shown in orange, nucleotides involved in the interaction with EF-G are shown in sticks. Coloring as in panel A. Hydrogen bonds are shown as dashed line. **(C)** Interactions in the immediate vicinity of the active site. Gray, ribosomal protein L6; double-headed arrow, van der Waals interaction between Arg660 and Val88.

### 3.4.3 Domain IV of EF-G and decoding center

Domain IV of EF-G occupies the A-site of the 30S subunit in a similar fashion as in the post-translocational complex. However, in the post-translocational complex, the domain IV makes extensive contacts with mRNA and P-site tRNA, whereas we observed no such interactions. Domain IV forms contact mainly with inter-subunit bridge B2a instead. Domain IV is shifted towards the inter-subunit bridge B2a by approximately 4.7 and 3 Å at the domain tip (Gly502) and the helix αB4 (facing bridge B2a), respectively (Figure 16A). At the tip of domain IV, Arg504 forms hydrogen-bonding interaction with G1494 in 16S rRNA (Figure 16B). Additionally, the side chain of Arg499 inserts into the minor groove between 23S and 16S rRNAs where bridge B2a is formed, and the guanidinium group of Arg499 makes bidentate hydrogen bonds with G1495 of 16S rRNA and A1913 of 23S rRNA. The base of A1493 in 16S rRNA points outward, contacts the side chain of Met580, and forms a hydrogen bond with Ser578. Domain IV interacts with bridge B2a rather than with mRNA and P-site tRNA as seen in the post-translocational complex, and appears to stabilize this region of B2a, thereby facilitating ribosome ratcheting.

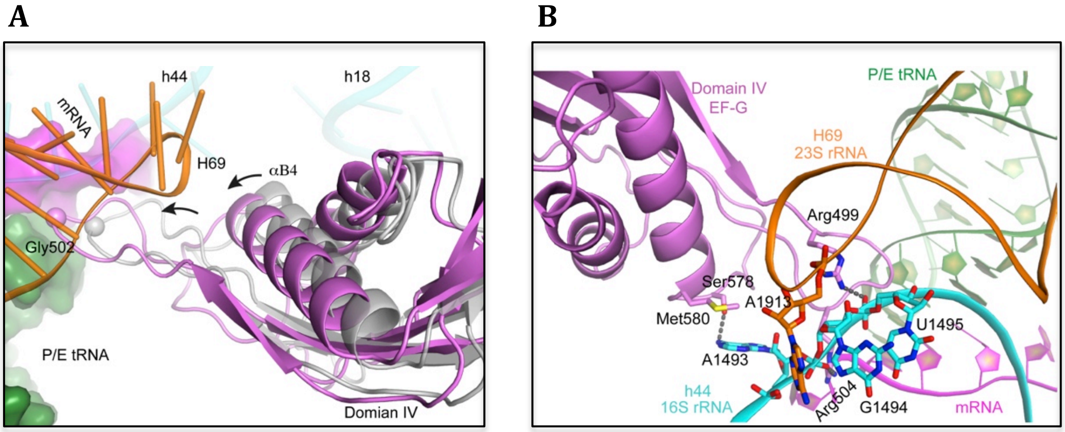

**Figure 16. EF-G Domain IV positioning and conformational change. (A)** The change of the positioning of domain IV (violet) of EF-G compared with post-translocational complex (gray). Gly520 is presented as spheres (green). 23S rRNA H69 is shown in orange cartoon. **(B)** Detailed interactions of domain IV of EF-G with 23S rRNA (orange) and 16S rRNA (cyan). The P/E tRNA (green) and mRNA (hot pink) are shown as cartoons with ribose and base indicated. Interactions, made after the tip of EF-G shifts toward the inter-subunit bridge, are shown. Ser578 and Met580, located at the tip of domain IV, form interactions with A1493 of 16 sRNA, as indicated.

Interestingly, the universally conserved A1913 of 23S rRNA as well as A1492 and A1493 of 16S rRNA adopt different conformations with EF-G bound to the current EF-G-ribosome and post-translocational complexes (Figure 17A and B). For the current EF-G-ribosome complex, A1913 (located at the tip of H69) inserts into h44 of 16S RNA to form a π-π stacking interaction with A1492 and only the A1493 base sticks out of h44. In contrast, all three bases rotate out, away from the central axis of h44, and point toward EF-G in the post-translocational complex. Notably, the inter-subunit interaction at bridge B2a involving these three nucleotides is different from that in previously published rotated ribosomes, in which A1492 and A1493 remain stacked in helix 44, and A1913 interacts with A1492 via a hydrogen bond (68, 90). The presented conformation of these conserved nucleotides represents a transition state formed upon EF-G binding in order to promote translocation, and appears to establish a rigid link at the decoding center between the neck region of the 30S subunit and the 50S subunit, which is presumably relevant to the coordination of ribosome rotation.

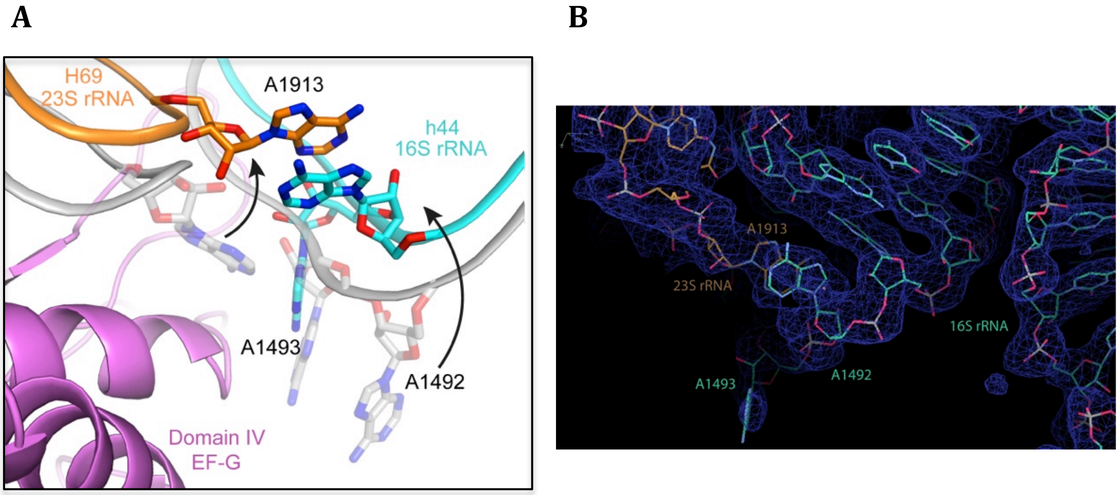

**Figure 17. Rearrangement of the decoding center. (A)** Conformational change at the decoding site involving the inter-subunit bridge B2a. Coupled to ribosome rotation, the tip of H69 in 23S rRNA and the h44 of the 16S rRNA move away from EF-G as shown. The universally conserved A1913 in 23S rRNA inserts into h44 of the 16S rRNA to establish stacking with A1492, which has also rotated into h44. The post-translocational complex is colored gray. **(B)** Electron density map corresponding to the three nucleotides depicted in panel A.

### 3.4.4 L1 stalk movement and hybrid P/E tRNA

#### 3.4.4.1 Hybrid P/E tRNA

The $\text{tRNA}^{\text{fMet}}$ in the present complex is in a hybrid state (P/E tRNA) (Figure 13A and Figure 18). As expected, its ASL remains in the P-site of 30S, where codon-anticodon interactions are made, whereas the 3'-CCA end occupies the position of the canonical E-site of 50S, in a similar way as observed for the RF3–ribosome complex (68). Coupled to inter-subunit rotation, the ASL of the P/E tRNA advances by 8.1 Å toward E-site, and G1338-A1339 of h42 in 16S rRNA interact with C41-C40 of P/E tRNA (Figure 18B and C), similar to the situation observed in the post-translocational complex. Although the overall structure of tRNA, including the dramatic distortion, is similar to that presented in either the RRF– or RF3–ribosome complex (68, 90), the TΨC and D loops have different conformations in our structure, probably due to their interactions with the L1 stalk. The positioning of the P/E tRNA places its elbow region suitably to form extensive contacts with both L1 rRNA and L1 protein (Figure 18A). It is not surprising that our complex represents the state similar to pre-translocational ribosome in which the L1 stalk is proposed to participate in the formation of hybrid tRNA (76).

In an elongation complex, proteins S13 and S19 are connected by an inter-subunit bridge involving protein L31, and their flexible C-terminal tails approach P- and A- site tRNAs, respectively (91). In contrast, the tails of proteins S13 and S19 make direct interactions with the ASL of the P/E tRNA in our complex (Figure 18C). Such a conformational change is likely relevant to ribosome ratcheting and EF-G binding. Simultaneously, Ala118 in S13 protein interacts with Glu86 in S19. In addition to the S13 tail interacting with the ASL of P/E tRNA, Arg114 is within hydrogen-bonding distance to the ribose O2 of A43. This newly established interaction appears to be critical for the formation of the distorted P/E tRNA in which a dramatic bend starting from the base pair A43-U27 was found in the present complex as well as in RF3 bound to ribosome. As for S19, its C-terminal tail extends toward the decoding center, forming an interaction interface with the ASL of P/E tRNA, h30 of 16S rRNA, and domain IV of EF-G.

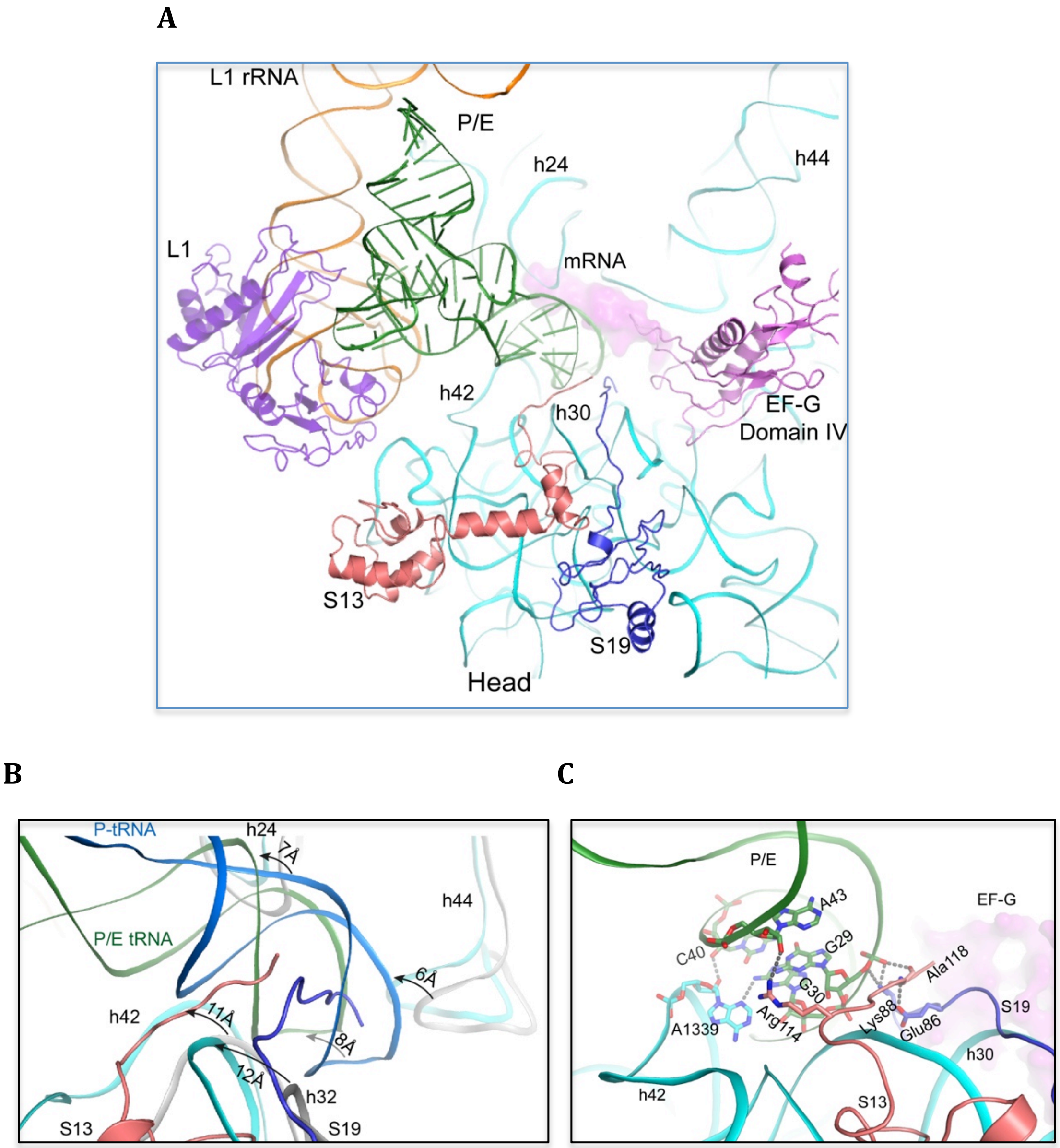
A
L1 rRNA
P/E
h24
h44
L1
mRNA
h42
h30
EF-G
Domain IV
S13
S19
Head
B
P-tRNA
h24
7Å
h44
P/E tRNA
6Å
h42
11Å
8Å
12Å
h32
S13
S19
C
P/E
EF-G
A43
C40
G29
G30
Ala118
A1339
Arg114
Lys88
Glu86
S19
h30
h42
S13

**Figure 18. P/E tRNA and its interaction with the ribosome. (A)** Overall structure of P/E tRNA and its positioning on the ribosome. The ribosomal protein L1, S13 and S19 are shown as cartoons colored purple, deep salmon and blue, respectively. EF-G, tRNA, 23S and 16S are colored violet, green, orange and cyan, respectively. **(B)** A close-up view of the ASL binding pocket. Coupled to ribosome ratcheting, the ASL of the P/E tRNA advances by 8.1 Å, whereas 16S rRNA in the 30S head moves by 11-12 Å, and 16S rRNA neck region moves by 6-7 Å. Such unequal bilateral displacement of the P-tRNA into P/E positioning causes tRNA deformation. **(C)** Interactions of the P/E tRNA with the 30S head (S13, S19 and G1338-A1339 in 16S rRNA).

### 3.4.4.2 L1 stalk and its interactions with P/E tRNA

EF-G binding to the ratcheted ribosome likely facilitates the stabilization of the dynamic L1 stalk, allowing us to obtain a model of the entire L1 stalk interacting with the hybrid P/E tRNA. The L1 stalk is in a conformation more closed toward the E-site and the 50S body when compared with that presented in the RRF- or RF3-ribosome complexes (68, 90). Structural comparison with the post-translocational complex also shows a tremendous movement of the L1 stalk toward 50S body, with the distal part of L1 rRNA (for example G2127 in H78) shifting by approximately 24 Å in distance and 26° in angle (Figure 19A). Such a conformational change displaces the canonical E-site tRNA by 15 Å.

Whether a P/E tRNA or an elongation E-site tRNA is bound to the ribosome, the structural comparison reveals a similar interaction interface between the tRNA and the L1 stalk (67, 79). The elbow region of tRNA, H77 and its linked loop in L1 rRNA wedge into a cleft created by the two domains of L1 protein, where extensive contacts between tRNA and the L1 stalk are formed (Figure 18A and Figure 19B). Notably, the interaction appears to become stronger upon P/E tRNA binding. The tip of the TΨC loop of P/E tRNA projects deep into the cleft of L1 protein, so that U55 and C56 can establish extensive contacts with Arg60, Asn140, Lys142, and Arg160 (Figure 19B), whereas they are too far apart to form these interactions in the post-translocational complex. Although a network of interaction involving Arg130 in L1 protein, G19 in P/E tRNA, and A2169 in 23S rRNA was observed in both pre- and post-translocational complexes, here Arg130 forms cation-π rather than hydrogen-bonding interaction with G19. Moreover, the stacking interaction between Pro134 of L1 protein and C56 of P/E tRNA is newly established. These interactions can facilitate the stabilization of the distorted P/E tRNA, rationalizing the role of the L1 stalk in hybrid state formation. In contrast, the relatively loose binding of elongation tRNA to the L1 stalk would be beneficial for its release. Despite the dramatic distortion of P/E tRNA, the interaction interface between tRNA and the L1 stalk seems constant during the process of translocation, from the current state (similar to pre-translocational with hybrid tRNA) to the post-translocational (with elongation tRNA) complex. Thus, it presumably requires a consistent shape of the elbow region in tRNA for retaining such interaction interface, which could be ascribed to the conserved base pairs 18-55 and 19-56. Consistent with these nucleotides (G19, U55, and C56) interacting with P/E tRNA, their mutations decrease the translocation rate (92).

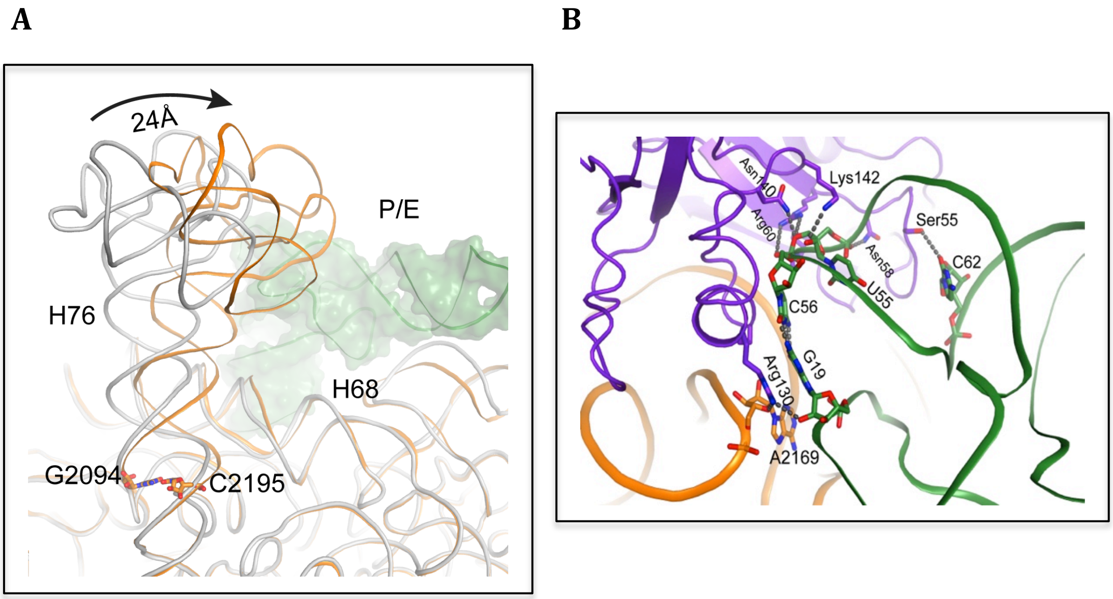
A
B
24Å
P/E
H76
H68
G2094
C2195
Asn140
Lys142
Arg60
Ser55
Asn58
C62
U55
C56
G19
Arg130
A2169

**Figure 19. L1 stalk movement and its interaction with P/E tRNA. (A)** A close-up view of the conformational change of the L1 rRNA (orange). Compared with the post-translocational complex (gray), H76 starts to diverge at/after the 23S rRNA base pair G2094:C2195 shown as stick model. **(B)** Detailed interactions of the P/E tRNA with the L1 stalk. The P/E tRNA in the current EF-G-ribosome complex makes numerous interactions with both L1 rRNA (orange) and L1 protein (purple).

# 4. Discussion

## 4.1 GTPase activation and mechanism of GTP hydrolysis

GTP hydrolysis of EF-G can accelerate the translocation; translocation mediated with EF-G-GTP is four-fold faster than that mediated by EF-G-GDPNP, which is a non-hydrolyzable analogue of GTP (54, 93, 94). Although the mechanism of this acceleration is unclear, it is considered to be moderate, compared with the effect of EF-G in accelerating the spontaneous translocation. The reaction rate of EF-G catalyzed translocation (with our without GTP hydrolysis) is at least four orders of magnitude faster than that of the spontaneous translocation (95). Thus, although it was initially reported that GTP hydrolysis promotes translocation by coupling the energy of hydrolysis to translocation (54), it was the same group who later showed that GTP hydrolysis and Pi release is not strictly coupled to translocation (96). The main effect of GTP hydrolysis seems to be ensuring that EF-G is released form the ribosome rapidly and efficiently (43).

GTP hydrolysis of translational GTPases takes place in all stages during bacterial translation and the mechanism is considered to be conserved. However, despite decades of study, this mechanism still remains elusive. Here, we discuss the implication obtained from current structure.

The switch I region of EF-G, essential for coupling GTP hydrolysis to conformational rearrangement, had never been modeled before our structure was reported. Domain III of EF-G contacts both the 30S (S12 and h5 of 16S rRNA) and the 50S (the SRL) subunits (Figure 20A). Interestingly, a number of contacts between the switch I and helix B3 in domain III, including Glu56-Arg468, Gln57-Asp464, and Arg61-Glu460, are newly established in the present complex (Figure 20B). In particular, the Arg61 forms bidentate hydrogen bonds with both Glu460 and phosphate oxygen of G2663 in the SRL. Apparently, these interactions (including that with γ-phosphate of GDPCP) facilitate stabilization of the switch I, thereby resulting in an ordered structure. Structural comparison of the pre- and post-translocational complexes reveals that the movement of the shoulder of the 30S subunit (S12 and h5) presumably causes the rearrangement of the entire domain III, as the movement of domain III is in the same direction as the movement of the 30S subunit (Figure 20A). By contacting switch I and both subunits of the ribosome, this strategic positioning of domain III likely provides the structural basis for the observation that EF-G lacking domain III exhibits a significantly decreased GTPase activity (97). Indeed, the tip of the SRL deviates by 1.3 Å (based on phosphate backbone) from that observed in the post-translocational complex. It appears that such a conformational change of the SRL was caused by the interactions between the SRL and EF-G (mainly involving domain III) in response to the precise ratcheting of ribosome, thereby achieving an active state of the SRL and the GTPase reaction of EF-G.

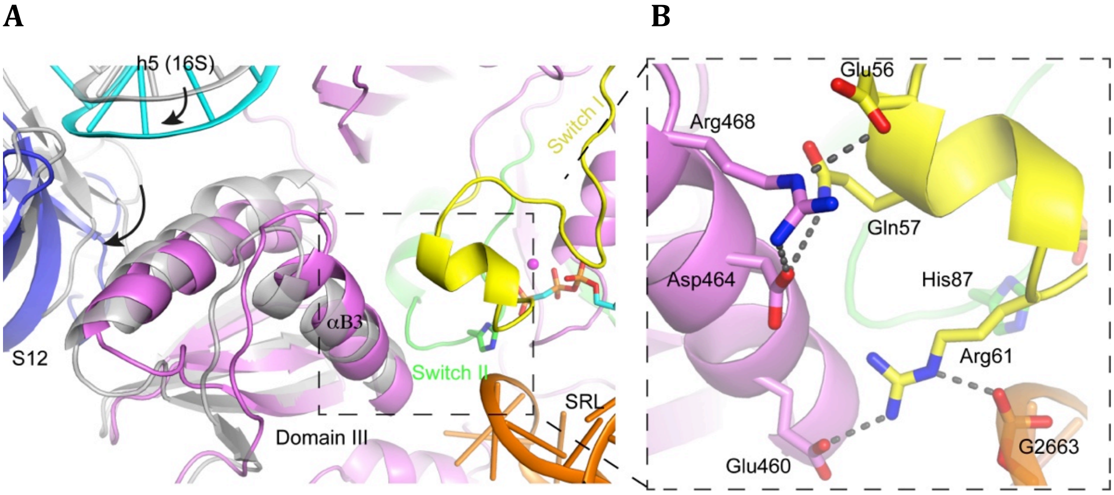

**Figure 20. EF-G domain III rearrangement and its interactions with switch I and SRL. (A)** The positioning of domain III and its rearrangement. Positioning of domain III in EF-G bound to the ribosome in ratcheted state is shown. Domain III contacts both subunits (h5 of 16S rRNA, S12 in the 30S and the SRL of 23S rRNA in the 50S subunit). For comparison, domain III of EF-G, 16S rRNA and S12 in the post-translocational complex are shown in gray. **(B)** Close-up view of the interactions amidst domain III, switch I, and the SRL (G2663).

SRL is highly conserved and rigid, compromising of 12 nucleotides in helix H95. Multiple reports, including mutation studies, have indicated its critical role in mediating EF-Tu and EF-G binding during the various processes of translation (98, 99). In particular, the A2660 nucleotide has been revealed to be essential for GTP hydrolysis (100). In the current structure, the phosphate oxygen atom of A2662 in the SRL is within hydrogen-bonding distance of His87 (Figure 15A), and this interaction is proposed to be crucial for the activation of His87, in a similar manner as previously observed for EF-Tu (74). In addition, A2660 and G2661 are involved in a network of interactions with EF-G and L6 as previously described, which rationalize previous biochemical data (87).

Two hydrophobic residues, Ile21 and Ile63, located in the P-loop and the switch I, respectively, regulate the access of catalytic His87 (His92 in *E. coli*) to the active site and are therefore referred to as the "hydrophobic gate" (101). Notably, His20 in the P-loop forms bidentate interactions with G2661 and A2660 in the SRL, and Asp22 is involved in a network of interaction with the SRL as well. These interactions likely cause the movement of the in-between (gatekeeper) Ile21 away from the GTP analog by over 2 Å when compared to the structure of isolated EF-G in GTP form (Figure 21), thereby opening the gate to accommodate the active conformation of His87. The importance of both His20 and Asp22 is in line with their universal conservation among all ribosomal GTPase factors (102). The lack of an ordered switch I in previous EF-G structures prevents us from determining how the conformational change of Ile63 is relevant to the "open" state. However, given the remarkable importance in EF-G GTPase activity, its conformational change between the pre- and post-translocational states, as well as its interaction with both subunits (Figure 20A), it is possible that the domain III of EF-G may function as a signal probe to sense the precise extent of ribosome ratcheting. Its rearrangement in response to ratcheting may in turn "open" Ile63 in coordination with the SRL. The highly conserved Arg61, located close to Ile63, appears to be the key to controlling the conformational transition of Ile63 by connecting both the SRL and domain III of EF-G.

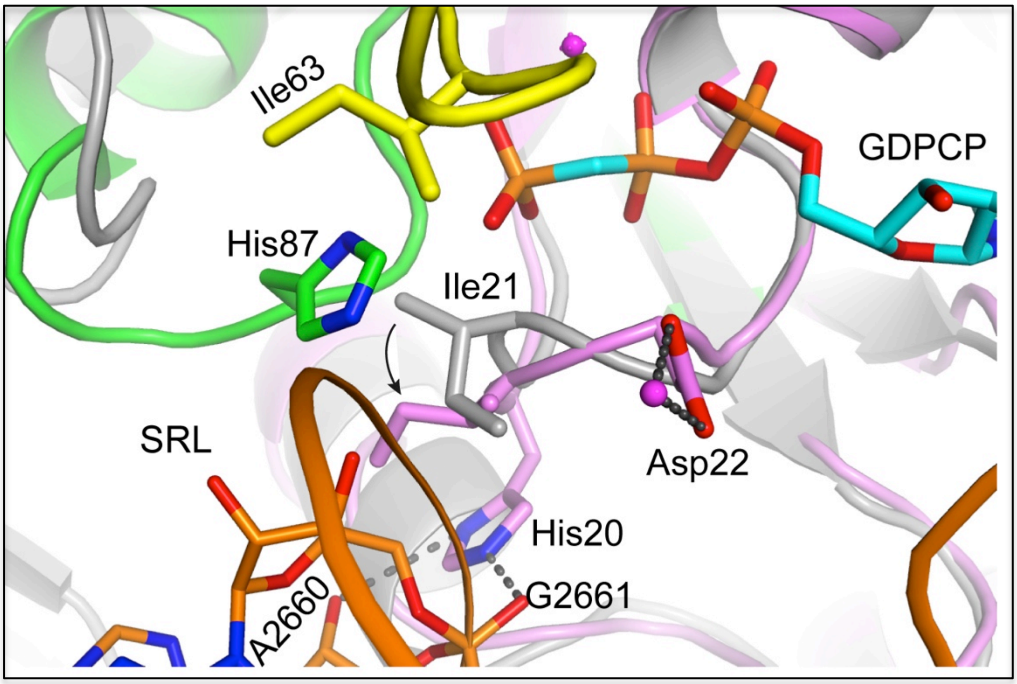

**Figure 21. "Hydrophobic gate" opening upon GTPase activation.** Superposition of the present EF-G structure with the structure of isolated EF-G bound to a GTP analogue (103). The two structures were superposed by aligning the G domain. In the present structure, compared to the isolated EF-G structure (gray), Ile21, referred to as one of the hydrophobic gate residues, avoids clashing with the catalytic His87 by undergoing a >2.0 Å shift of the side chain (~1.4 Å for the main chain) as well as a rotation of its side chain by almost 180°.

After GTP hydrolysis, the binding pocket of the inorganic γ-phosphate (Pi) appears to be retained, in line with the subsequent Pi release, which was shown to be a slow reaction (91). Pi must be released for the completion of translocation. Interestingly, a structural comparison of the pre- and post-translocational complexes reveals the diverse positioning of EF-G with respect to the CTD of L12, which could be relevant to the release of Pi (Figure 22). Indeed, mutations of the CTD of L12, which disrupt its interactions with the G' domain of EF-G, inhibit Pi release (91).

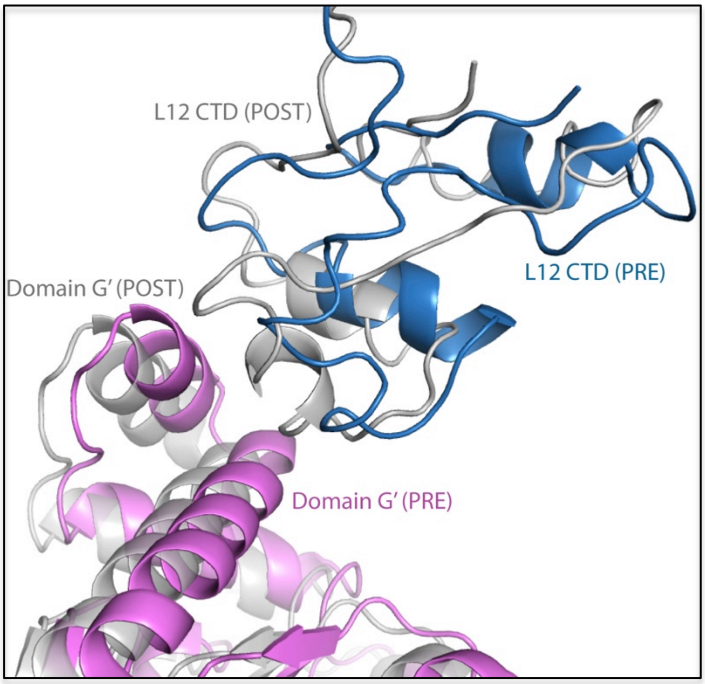

**Figure 22. EF-G G' domain rearrangement.** Comparison of the G' domain of EF-G with respect to C-terminal domain of L12 in pre- and post-translocational complexes is depicted. The G' domain of EF-G and the C-terminal of L12 in the current EF-G-ribosome complex are colored violet and blue, respectively. The corresponding domains in the post-translocational complex are colored gray. In both complexes, direct contacts of EF-G (G' domain) with the CTD of L12 were observed.

The exact mechanism of GTP hydrolysis by translational GTPase factors is still a matter of controversy. It was proposed that His84 of EF-Tu (equivalent to His87 in EF-G) acts as a general base to allow the nucleophilic water molecule to attack the γ-phosphate of GTP (74). In our structure, the active His87 appears to interact directly with the oxygen atom of the γ-phosphate, therefore the likely role of the positively charged His87 is to stabilize the transition state, rather than to activate a water molecule, which then attacks the γ-phosphate. In accordance with recent reports demonstrating that His84 in EF-Tu cannot act as general base (104, 105), as well as with the general mechanism introduced for GTPases (106), we propose the following mechanism. Ribosome-mediated GTPase activation of EF-G involves rearrangement of EF-G (domain III in particular) by the ratcheted ribosome. Domain III of EF-G functions as a signal "probe" to sense the precise extent of ribosome ratcheting and transmits the signal to activate the GTPase center. The SRL (particularly A2662) places His87 properly into the active site upon "hydrophobic gate" opening, which is regulated by the conserved His20 and Arg61 interacting with the SRL (particularly G2661 and A2660) and domain III. His87 activates the γ-phosphate, which then abstracts a proton from a water molecule, and the resultant hydroxide ion attacks the γ-phosphate leading to GTP hydrolysis. Thus, the positively charged His87 functions to initiate the reaction and to stabilize the transition state. Finally, the release of Pi is associated with the interactions between G' domain of EF-G and C-terminal of L12 protein.

Concurrent with the publication of our structure, three EF-G bound translocational intermediate state ribosome structures were published in Science by three different groups (107-109). Two of the complexes were trapped by using non-hydrolyzable GTP analogues (Tourigny *et al* and Pulk *et al*)(107, 108), the same strategy as used by us, while the third group (Zhou *et al*) (109) utilized fusidic acid to prevent Pi release as described earlier (67, 79). Interestingly, if we superimpose our structure with the first two structures, the catalytic His92 residue (*E. coli* numbering) is found to have exactly the same conformation, further consolidating our observation (Figure 23A). Thus, this orientation of histidine seems to represent the active state of the GTPase center. Moreover, computational studies reported by other groups also favor this notion (105, 110). On the other hand, in the structure reported by the third group (Zhou *et al*) (109), the His92 was in a considerably different orientation rotated away from the γ-phosphate (Figure 23B white). This histidine orientation is similar to what was observed in the post-translocational complex, indicating an inactive state of GTPase center. However, this is not surprising since, while this structure represents a translocation intermediate state, it is closer to the post-translocational complex, based on the body rotation and head swiveling of the small subunit. Meanwhile, in the structure of ribosome bound to RF3, the catalytic histidine demonstrates a position in between of the two orientations, reflecting its transition from "active" to "inactive" state.

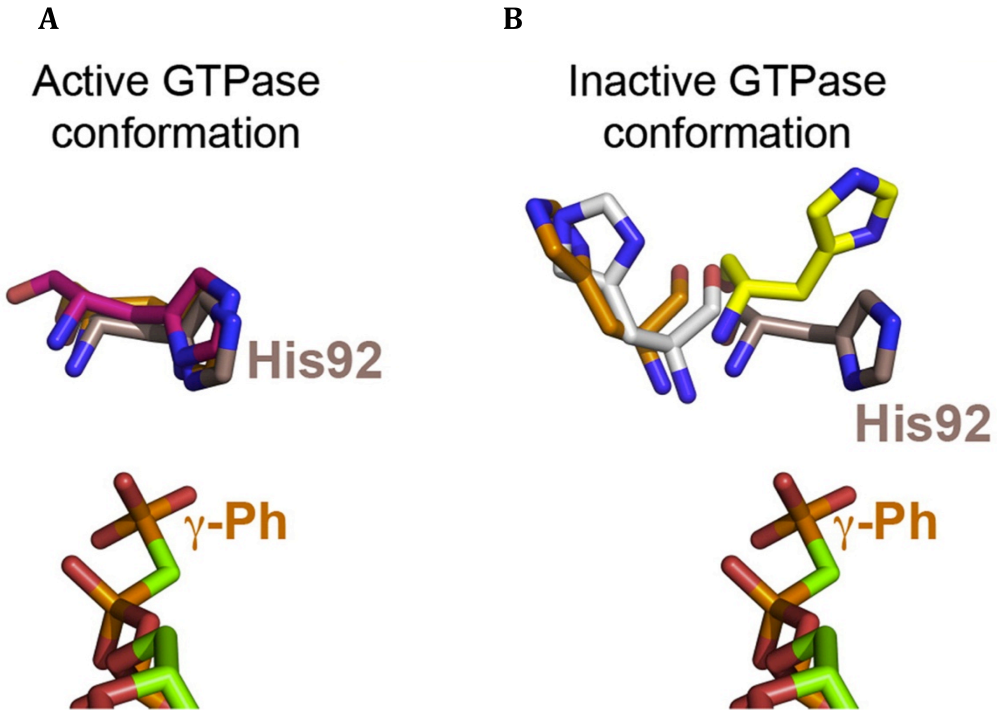

**Figure 23. Active and inactive orientations of the catalytic His92 residue. (A)** Active conformation of catalytic His92 residue. His92 from current structure (colored brown) and another two structures (PDB 4V9H colored orange and 4V9O colored magenta) of intermediate state ribosome complexes during translocation are aligned by the bound nucleotide (either GDPCP or GDPNP). This identical orientation of His92 within the interaction distance of γ-phosphate indicates an active conformation. **(B)** Inactive conformation of catalytic His92 residue. Similar alignment was conducted as in panel A by using the third intermediate state complex during translocation (PDB 4V9 colored white, Zhou et al), post-translocational complex (PDB 2WRI colored orange) and RF3 bound ribosome complex (PDB 3FSF colored yellow). For clarification, the active form histidine is shown in brown. (Adapted from John Achenbach *et al,* 2014)

The structure of ribosome bound to EF-Tu in a ternary complex with GDPCP and aminoacyl-tRNA reveals the structural basis for GTPase activation by EF-Tu (74). However, EF-Tu only binds to ribosome in the classical state, and GTP hydrolysis is triggered by the conformational change of switch I in response to the signal of codon-anticodon recognition at the decoding site (82). Unlike EF-Tu, GTPase activation of EF-G involves the movement of the SRL, which presumably occurs in response to the change in EF-G caused by intrinsic ratcheting of the ribosome. The favorable extent of ribosome ratcheting causes a proper positioning of EF-G with respect to the SRL, so as to establish a perfect coordination for "hydrophobic gate" opening and His87 repositioning leading to GTPase activation. In contrast, GTPase activation of EF-Tu does not seem to involve an opening of the gate. Given the conservation of the SRL and G domain, our results with an active EF-G on the ratcheted ribosome, provide wider implications of how the SRL and ribosome ratcheting is involved in GTPase activation in IF2 and RF3. Our findings also elucidate a molecular mechanism of GTPase activation and GTP hydrolysis for EF-G and RRF in ribosome recycling. Finally, this structure sheds light on GTPase activation of eukaryotic eEF2 due to the high degree of conservation with EF-G, including the universally conserved SRL.

## 4.2 Hybrid P/E tRNA formation and L1 stalk movement

The degree of 30S head swiveling and body rotation can vary greatly, namely 3°-18° and 4°-9°, respectively (51, 68, 90). Our structure shows a modest head swiveling (9.0°) and a nearly full body rotation (7.4°), while the three structures published in Science present different rotation states. However, Tourigny *et al* and Pulk *et al* reported similar head swiveling (5° and 6° respectively) and body rotation (7° and 4° respectively) as us, demonstrating that the different crystallization condition does not influence the ribosome ratcheting, while the structure reported by Zhou *et al* displayed dramatic different head swiveling (18°). These results imply that the ribosome can adopt varied intermediate states of ratcheting and that this dynamic feature of ribosome ratcheting is directly relevant to the formation of hybrid tRNA. The binding pocket of the ASL of P-site tRNA involves h32 and h42 in the 30S head, as well as h44 end and h24 in the 30S neck region. These ribosomal elements interact with tRNA from opposite sides. Superposition of the pre- and post-translocational complexes clearly shows that this binding pocket shifts toward E-site, following the direction of the 30S rotation. Notably, the ribosomal elements of this pocket at the 30S head and the neck region travel by 11-12 Å and 6-7 Å, respectively (Figure 18B). Such unequal bilateral displacement results in tRNA deformation, characterized by a divergence starting from C40 compared with the classical P-site tRNA, and stabilized by strong interactions between A1339-G1338 of 16S rRNA and C40-G42, ultimately orienting the tRNA in P/E hybrid state (Figure 18C). The newly observed interaction of the C-terminal tail of S13 with tRNA also facilitates its distortion (Figure 18C), thus promoting P/E tRNA formation.

Together with the body of S13 participating in an inter-subunit bridge, this structural feature is consistent with previous data demonstrating a critical role for S13 in maintaining a stable pre-translocational ribosome complex, and explains why S13-depleted ribosome exhibits an obvious deficiency in translocation (111).

The elbow region of the energetically unstable distorted P/E tRNA seems to be stabilized by direct interactions with L1 stalk (Figure 18B). Indeed, L1 stalk has been shown to be involved in the formation of hybrid P/E tRNA, and depleting L1 from the ribosome destabilizes the tRNA hybrid state (112). In addition to the role in hybrid tRNA formation, the L1 stalk has been implicated in further movement of the tRNA-mRNA complex. This notation is corroborated by translocation inhibition resulting from a P-site tRNA analogue consisting only of the anticodon arm (113). The reason for that is believed to be the lack of interactions with the L1 stalk. Superposition of the pre- and post-translocational structures clearly demonstrates the trajectory of tRNA movement from the P/E to the classical E-site coupled to the oscillation of the L1 stalk from closed to half-closed form in EF-G-GTP and EF-G-GDP structures (Figure 24), respectively. Interestingly, the tRNA 3'-CCA ends superposed well and appeared to be fixed by interactions with 50S E-site. During the aforementioned movement, the 3'-CCA end serves as an "anchor". In line with its function as an "anchor", modifications of the 3' end, which greatly decrease the affinity of E-site binding, result in lowering the translocation rate by up to 40-fold (114).

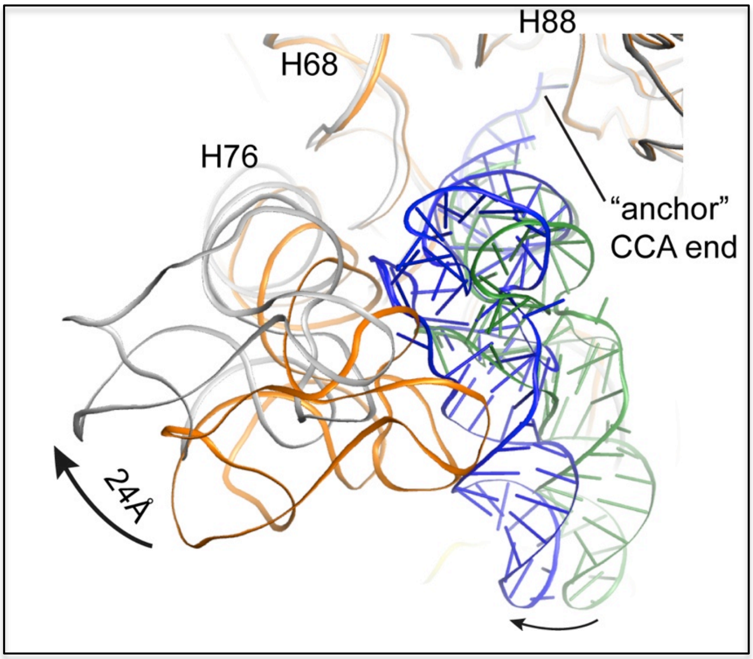

**Figure 24. P/E tRNA trajectory.** Superposition of the present complex L1 rRNA interacting with the hybrid P/E tRNA (blue) with that in the post-translocational complex based on 23S rRNA. Coupled to the migration of the L1 stalk, the P/E tRNA is likely to be placed into the classical E-site position, with the CCA end inclined to act as an "anchor" by retaining the interactions with the E-site. The classical E-site tRNA is colored blue. For clarity, only L1 rRNA is shown.

## 4.3 Implication for translocation

EF-G mediated ribosomal translocation involves a number of intermediate states. Recently, two intermediate states (TI$^{PRE}$ and TI$^{POST}$) for 70S and EF-G complex stalled by fusidic acid have been observed by cryo-EM, with 30S body rotation and head swiveling of 7°/5° and 4°/18°, respectively, further consolidating this notion. Our current result, together with structures reported by other groups, seems to be in good accordance with this cryo-EM study. Given the similar positioning of EF-G, full body rotation and minor head swiveling, our structure as well as those published by Venki Ramakrishnan's (107) and Jamie Cate's (108) groups are likely to be in an intermediate state closer to the cryo-EM TI$^{PRE}$ structure, while the one from Harry Noller's group (109) represents the TI$^{POST}$ structure characterized by minor body rotation and almost full head swiveling. All these structural data provide a wealth of information for our understanding of the translocation process. Particularly, in Noller's structure that is closer to

TI$^{POST}$, the barrier between the anticodon stems of P and E tRNAs preventing their movement, was found to be in an open state (Figure 25). This barrier, known as the A790 gate (20), is composed of four highly conserved bases G1338-A-N-U1341 from 30S head and the nucleotide A790 from 30S platform; and is for the first time observed in an open conformation that allows the tRNA movement. Opening of this gate is accompanied with, and thus believed to be induced by, the head swiveling of the 30S subunit. In the other three structures closer to TI$^{PRE}$ with a mild head swiveling as well as the post-translocational complex, the gates were observed to be closed (Figure 25). It is therefore reasonable to speculate that the TI$^{PRE}$ complex will advance to the TI$^{POST}$ complex. Coupled with further head swiveling, reverse body rotation and A790 gate opening, the ribosome finishes translocation. This is at the moment the most popular explanation of the acceleration of translocation mediated by EF-G-GTP. How exactly EF-G-GTP induces this intrinsic head rotation of the small subunit still remains the most important unsolved question.  After the translocation, the A790 gate is closed and, along with the positioning of EF-G domain IV at the decoding center, prevents the back-sliding of tRNA-mRNA complex.

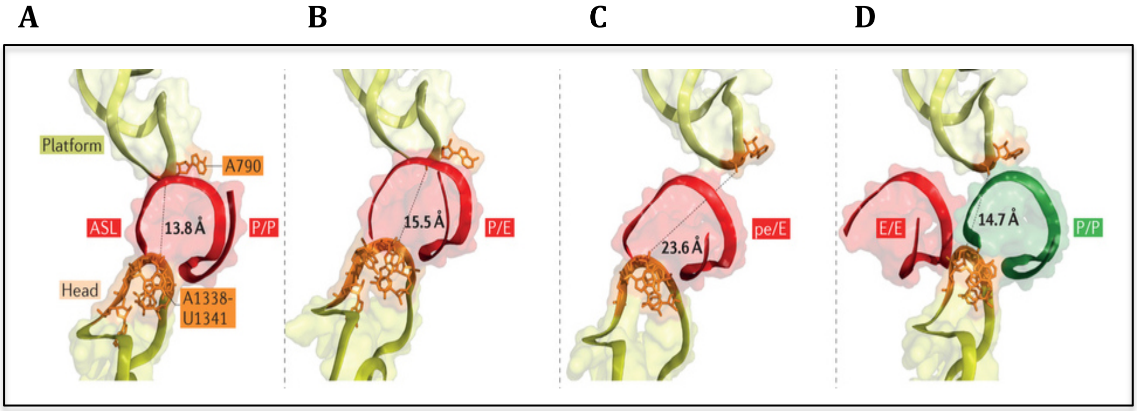

**Figure 25. A790 gate opening.** Positions of the 16S rRNA base A790, which is the essential component of the A790 gate that prevents the tRNA anticodon stem movement, are shown in four different ribosome complexes.  **(A)** Classical pre-translocation complex (PDB 3J0T). **(B)** Current structure closer to TI$^{PRE}$. **(C)** Structure reported by Harry Noller's group (PDB 4V9J). **(D)** Classical post-translocational complex (PDB 2WRI). (Adapted from Hiroshi Yamamoto *et al*, 2013)

## 4.4 Personal perspective

In this Chapter of the thesis, I described the structural study of ribosome complex bound with a P/E hybrid state tRNA and EF-G in a GTP state. From this structure, the clear observation of switch I and II regions of EF-G upon ribosome binding, in particular the positioning of catalytic residue His87 provides the first structural basis of EF-G GTP hydrolysis on the ribosome. This active state of His87 is coupled to hydrophobic-gate opening and involves the 23S rRNA sarcin-ricin loop and domain III of EF-G. Taken together this structure explains well all the previous biochemical data and based on this we proposed the mechanism how translational GTPases (IF2, EF-G and RF3) activation and GTP hydrolysis are achieved on the ribosome. This mechanism is favored by computational study (105, 110) and further consolidated by following up biochemical studies just published recently. In one of the study led by Norbert Polacek (202), they probed the interaction between the catalytic histidine (His87) and phosphate oxygen of A2662 of the SRL via atomic mutagenesis approach. Their data strongly corroborate that the non-bridging phosphate oxygen at the A2662 of the SRL is critically involved in the activation of GTP hydrolysis and support the notion that the electrostatic interactions between His87 and A2662 phosphate group and H-bond networks are key features of ribosome-triggered activation of translational GTPases. In another study by Wen Li *et al* (203), the authors found mutant EF-G (H91A) renders the factor impaired in GTP hydrolysis and the structure of this mutant EF-G bound to ribosome determined by cryo-EM argues in favor of a direct role of the conserved histidine in the switch II loop of EF-G in GTPase activation as well.

In addition, this structure displays a ratcheting state ribosome with small subunit head swiveling and body rotation as well as a P/E hybrid state tRNA. The extensive interactions observed between the hybrid P/E tRNA and the ribosomal elements including the entire L1 stalk and proteins S13 and S19, provide the structural basis of the stabilization of this P/E hybrid state tRNA. It in turn, also sheds light on how the formation and stabilization of the hybrid state tRNA is coupled to head swiveling and body rotation of the 30S subunit as well as the closure of the L1 stalk.

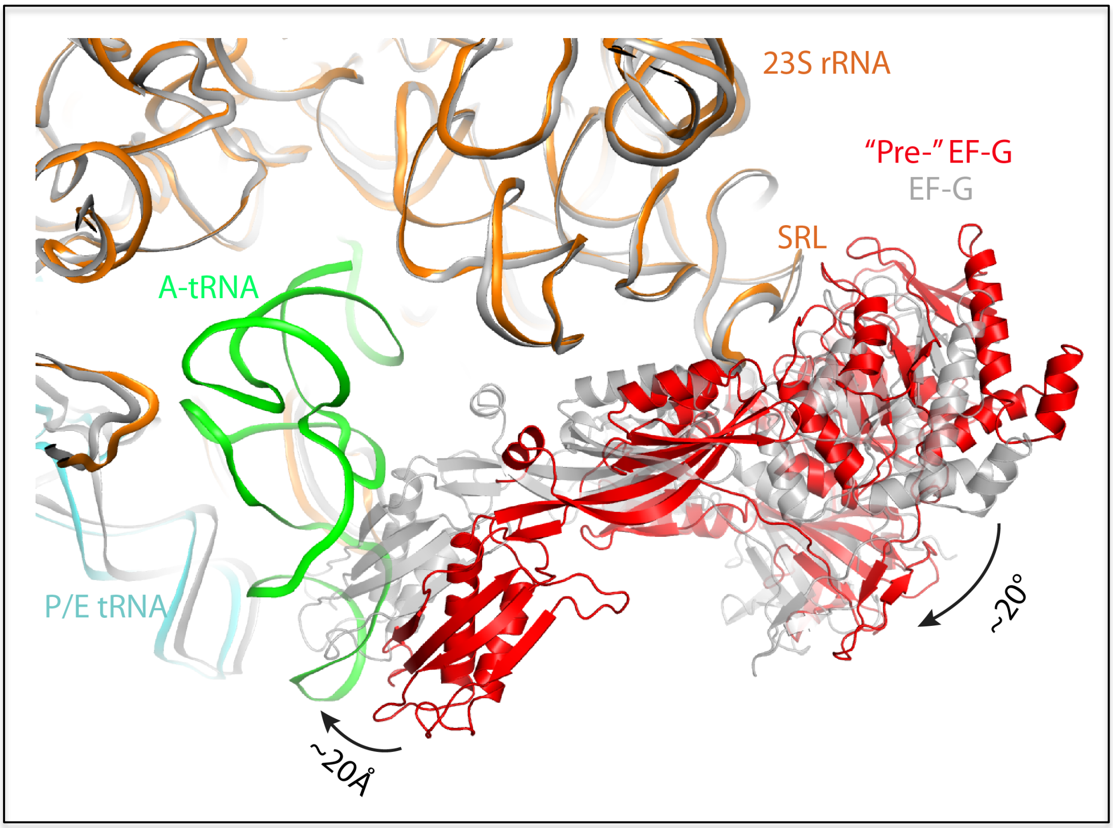

**Figure 26. EF-G conformation comparison.** Superposition of the present EF-G with that in the "pre-translocational" complex based on 23S rRNA. EF-G, A-tRNA, P-tRNA and 23S rRNA in the "pre-translocational" complex are colored red, green, cyan and orange respectively, while those in our current structure are colored gray.

However, this structure is far from perfect as much information is still missing, particularly when considering its limit in elucidating the mechanism of ribosome translocation. The biological substrate for EF-G facilitated translocation comprises the ribosome in complex with tRNAs in the A and P-sites, respectively. However, in this structure, only P/E tRNA is observed while the density for A-site or A/P state tRNA is missing, although A-site tRNA was added during the complex assembling. Actually, all of the four crystal structures described above (published at similar time) contain either only one tRNA or no tRNA. Cryo-EM analysis has revealed that, despite the fact that the two published ($TI^{PRE}$ and $TI^{POST}$) complexes contained only one tRNA, it was possible to dock a second tRNA into the $TI^{POST}$ complex, while for the $TI^{PRE}$ complex, there is even not enough space for docking a A-site tRNA. It is therefore speculated that the A-site tRNA in $TI^{PRE}$ is too transient to be captured by structural studies. This was soon verified by a cryo-EM study of the $TI^{POST}$ complex with two tRNAs (115), as well as the very recently published crystal structure of the similar complex (116). Both structures highlight similar structural features and shed light on the interactions of EF-G with the intermediate A-site tRNA, proposed by the author as ap/ap tRNA. However, in both studies, the authors used GTP and fusidic acid to trap the ribosome complex, resulting in a state closer to post-translocation, rather than pre-translocation. The authentic pre-translocational state ribosome complex still evades visualization. Actually, the only structure of the "pre-translocational" ribosome in complex with two tRNAs and EF-G was determined via cryo-EM in the presence of viomycin and fusidic acid (117). Without EF-G domain IV entering the A-site decoding center, the structure provides insights on the long-standing question of the early contacts between EF-G and ribosome that initially trigger the conformational change of EF-G and translocation. Comparing our structure with this "pre-translocational structure", the tip of domain IV is 20 Å closer to the A-site, causing a clash with the A-site tRNA (Figure 26). In addition, the EF-G rotates as a whole ~20° around from pre- state structure to our structure (Figure 26), demonstrating a trend of movement towards A-site tRNA. Despite all this, this structure is not sufficient answering all the questions regarding ribosome translocation. The question of what ribosomal contacts play the most significant role in this process is still to be determined. Moreover, even though the ribosome is in the "pre-translocational" state, the EF-G has already hydrolyzed GTP and is now in a GDP state. The structure is not in an authentic pre-translocational state before the GTP hydrolysis. It would be interesting to determine a similar structure with two tRNAs but EF-G in a GTP state and compare the conformational changes before and after GTP hydrolysis as well as with that of post-translocational state. Just recently, a compact conformation of EF-G bound to ribosome was determined for the first time by Thomas Steitz's group by using the antibiotic dityromycin (118). In this structure, the ribosome is in a non-ratcheting state with P and A-site tRNAs in classical states, while the domain arrangement of EF-G is significantly different from all the other ribosome bound EF-G structures determined. This new structure further expands our knowledge of translocation by demonstrating how the conformational transition of EF-G on the ribosome from the compact to the extended facilitates the translocation.

# Chapter II:

# Molecular mechanism of ribosome-dependent toxin YoeB in mRNA cleavage

# 1. Introduction

## 1.1. Bacterial toxin-antitoxin systems

### 1.1.1 Toxin-antitoxin systems

Toxin-antitoxin (TA) systems were originally identified on low-copy number plasmids, where their function is to maintain the plasmid by post-segregational killing of plasmid-free cells (119, 120). When the TA-encoding plasmids are lost from a cell, the growth of that cell is inhibited because it can no longer produce the unstable antitoxin, which can neutralize the stable toxin that is still present, eventually leading to cell death (121). To date, TA systems have been found to be highly abundant in chromosomes of both Eubacteria and Archaea (122-124). *E. coli* K-12 strain genomic DNA encodes for at least 36 putative TA systems (125, 126) (Figure 27), among which 12 are well-characterized: MazF-MazE (127, 128), RelE-RelB (129, 130), YoeB-YefM (131, 132), YafO-YafN (133, 134), YafQ-DinJ (135, 136), ChpBK-ChpBI (137), HipA-HipB (138), MqsR-MqsA (139, 140), HicA-HicB (141), YhaV-PrfF (142), HigB-HigA (143) and RnlA-RnlB (144).

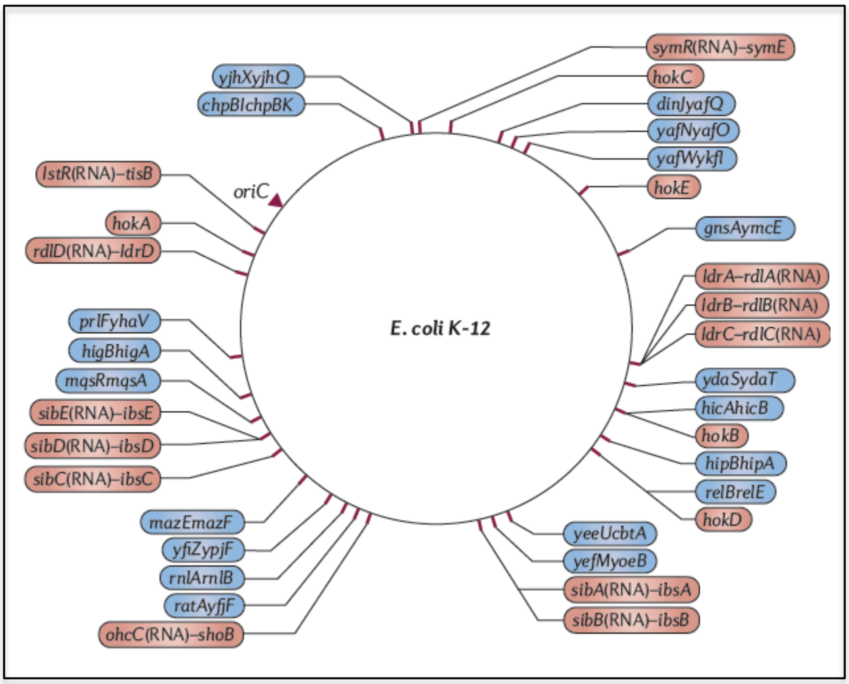
symR(RNA)–symE
yjhXyjhQ
hokC
chpBIchpBK
dinJyafQ
yafNyafO
yafWykfI
IstR(RNA)–tisB
oriC
hokE
hokA
rdlD(RNA)–ldrD
gnsAymcE
ldrA–rdlA(RNA)
ldrB–rdlB(RNA)
prlFyhaV
E. coli K-12
ldrC–rdlC(RNA)
higBhigA
ydaSydaT
mqsRmqsA
hicAhicB
sibE(RNA)–ibsE
hokB
sibD(RNA)–ibsD
hipBhipA
sibC(RNA)–ibsC
relBrelE
mazEmazF
hokD
yeeUcbtA
yfiZypjF
yefMyoeB
rnlArnlB
sibA(RNA)–ibsA
ratAyfjF
sibB(RNA)–ibsB
ohcC(RNA)–shoB

**Figure 27. Toxin-antitoxin systems in *E. coli* K-12 strain.** There are at least 36 TA modules in *E. coli*. Type I TA modules are shown in orange while type II TA modules are coloured blue. For clarification, RNA antitoxins are indicated in parantheses. (Adapted from Yoshihiro Yamaguchi *et al,* 2013)

Interestingly, while almost all the living Bacteria contain TA modules in their genomes, the number of TA systems varies greatly from species to species. It has been speculated that the number of TA systems might be correlated to the pathogenicity of the bacteria because *Mycobacterium tuberculosis* possesses over 60 TA modules while its nonpathogenic counterpart has only two (145). In addition, putative TA systems have been identified in yeast (146) and some other fungi by bioinformatics studies (121).

### 1.1.2 Classification of TA systems

#### 1.1.2.1 Types of TA systems

One TA system is composed of two genes organised into an operon that encodes a stable toxin and its cognate more labile antitoxin. Based on the chemical nature and the action mode of the antitoxin, TA systems are divided into five types (I-IV) (Table 5). While the toxins are always proteins, the antitoxins are either RNAs or proteins, adopting different mechanisms to neutralize the toxin. Type I TA: antitoxin RNA binds to the toxin-encoding mRNA to suppress its translation (147, 148); type II:  antitoxin protein binds to the toxin to cause its inactivation (149); type III:  antitoxin RNA binds to the toxin protein to interfere with its activity (150, 151); type IV: antitoxin protein competes with the toxin for the same binding target (152); type V: antitoxin protein directly cleaves the toxin-encoding mRNA (153).

**Table 5. Five (currently) known TA system types**

| Types | Chemical nature of toxin | Chemical nature of antitoxin | Action mode of antitoxin | Examples | References |
|---|---|---|---|---|---|
| Type I | Protein | RNA | RNA (AT)-mRNA (T) interaction | SymER | Kawano *et al.* 2007 |
| Type II | Protein | Protein | Protein (AT)-Protein (T) interaction | MazEF | Bernard *et al.* 1992 |
| Type III | Protein | RNA | RNA (AT)-Protein (T) interaction | ToxIN | Blower *et at.* 2011 |
| Type IV | Protein | Protein | Protein (AT)-Target interaction | CbtA | Masuda *et al.* 2012 |
| Type V | Protein | Protein | Cleavage of mRNA by Protein (AT) | GhoST | Wang *et al.* 2012 |

### 1.1.2.2 Type II TA systems

Of the five types of TA systems, type II was discovered first, and later revealed to be the most prevalent (121). In case of the type II TA system, antitoxin and toxin generally form a tight complex, which inhibits the activity of the toxin (Figure 28). In response to environmental stress, the labile antitoxins are prone to digestion by stress-induced proteases such as Lon (154) or other bacterial proteasome systems (155-157), enabling the free toxins to exert their functions, leading to cell growth inhibition and adaptation (Figure 28). There are at least eight well-characterized type II TA systems in *E. coli*, including RelE-RelB, YoeB-YefM, YafO-YafN, YafQ-DinJ, MazF-MazE, ChpBK-ChpBI, HipA-HipB, and MqsR-MqsA.

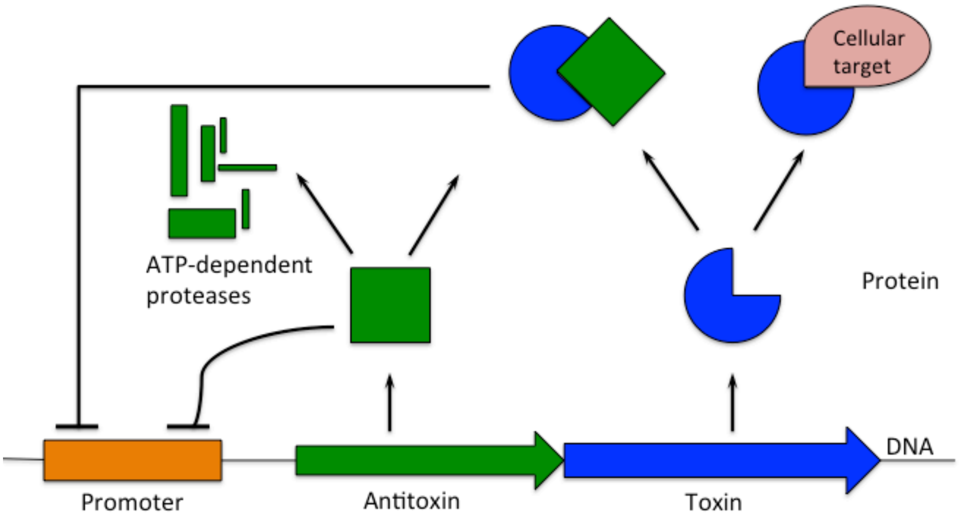

**Figure 28. Action mode of type II toxin-antitoxin systems.** Type II toxin and antitoxin are typically encoded in one operon controlled by the same promoter. Antitoxin gene is usually located upstream of toxin gene and highly expressed in order to ensure the neutralization of the toxicity. Antitoxin can auto-regulate the TA module, although the effect is weaker compared with the TA complex. Under stress conditions, antitoxin is subjected to degradation by ATP-dependent proteases, thereby freeing the toxin for binding to its cellular target.

## 1.2 Cellular targets and physiological functions of TA systems

### 1.2.1 Cellular targets of TA systems

The molecular targets of the TA systems are highly diverse and deciphering these targets is tremendously important for a better understanding of their functions. Known cellular targets of TA systems are summarized in Figure 29 and include: cell membrane (153), cell wall (158), mRNA (135), tRNA (159), 30S ribosome subunit (160), 50S ribosome subunit (161) and the DNA replication machinery (162). Many other targets likely remain to be characterized.

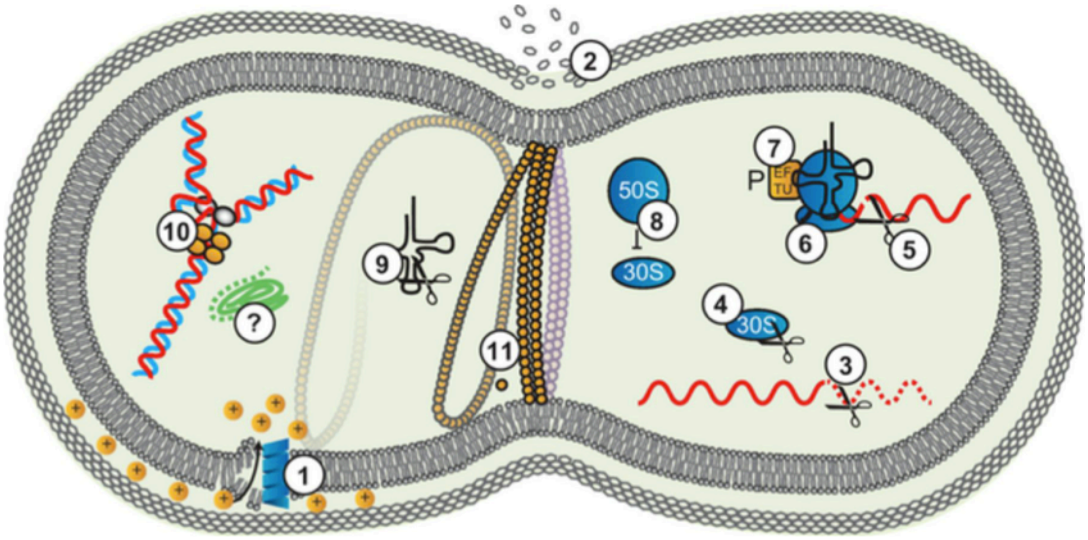

**Figure 29. Cellular targets of TA systems.** 1: Cell membrane can be targeted by type I and V toxins; 2: cell wall is targeted by ζ toxin; 3: free mRNA; 4: 16S rRNA; 5: ribosome dependent mRNA cleavage; 6: 30S ribosome subunit; 7: EF-Tu targeted by HipA; 8: 50S ribosome subunit; 9: tRNA; 10: DNA replication machinery; 11: cytoskeleton targeted by YeeV and CptA. (Adapted from Christopher *et al,* 2012)

Type I toxins are usually associated with cell membrane by disrupting the proton gradient across the inner membrane and thus inhibiting the ATP synthesis (123). Among all the cellular targets of type II TA toxins, mRNA proves to be one of the most frequent. Based on the requirement for ribosome in exerting their toxic function, these toxins are classified into to two classes, ribosome dependent and ribosome independent mRNA interferases. RelE family toxins such as YafO, YafQ and YoeB, cleave ribosome mRNA bound at A-site (131, 133)(135). The other family including MazF, Kid, and ChpK, targets free mRNA in a sequence dependent manner and does not involve ribosome binding (127)(137)(163). Other type II toxins can also inhibit protein translation by binding to either 30S (e.g. Doc) (160) or 50S subunit (e.g. RatA) (164). VapC cleaves tRNA$^{fMet}$ (159) while HipA phosphorylates EF-Tu and prevents its interaction with aminoacyl tRNA (138). Both result in translation suppression. However, CcdB and ParE exert their function by blocking DNA replication through disrupting the DNA gyrase activity of GyrA, which is essential for cell growth. Recently, it was discovered that type II ζ toxin can phosphorylate the peptidoglycan precursor UDP-N-acetylglucosamine (UNAG) and thus impair the bacterial cell wall synthesis (158). Type III toxin ToxIN, structurally similar to type II mRNA interferases, can also cleave RNA, although the exact mechanism remains unknown (150). Type IV toxins target the cytoskeleton by interacting with cytoskeleton protein FtsZ and MreB and disrupting their polymerization or GTPase activities. Type V toxins functions in a similar manner to type I (152).

### 1.2.2 Physiological function of TA systems

The physiological function of the plasmid encoded TA systems is maintaining the plasmid (165) as mentioned above. In addition, they also play important roles in excluding co-existent compatible plasmids (166).

However, bacterial chromosomes also encode a large number of TA systems and their functions are diverse and controversial. One of the most significant roles TA systems play, is the induction of bacterial persistence state, which leads to their insensitivity to antibiotics and causes multi-drug resistance (167). Several TA systems including MazE-MazF, MqsR-MqsA and HipA-HipB have been identified as important factors converting the bacteria to persisters (168). It has been well accepted that bacterial persistence is closely related to biofilm formation, in which MqsR has been reported to play a role (169). The deletion of mqsR gene inhibits biofilm formation while increased expression will enhance the cell mobility of *E. coli* (170). Another important function of the TA system is to cause cell growth arrest under stress conditions. Stress-induced MazF expression is reported to lead to growth arrest (171, 172) and even programmed cell death (173), although controversy still remains. MazF is also reported to have an essential role in fruiting body formation in Myxococcus by killing around 80% cell population whose lysis is a pre-request for fruiting body formation (174). Some TA systems, for example ToxI/ToxN, are proposed to serve as an anti-phage infection system. When infected, bacteria will expressed the ToxN toxin to kill the infected cells so as to protect the uninfected ones (150). To make matters more complicated, the possibility exists that there is a network of TA systems in the cell which will make their regulation much more complex (175).

## 1.3 Applications of TA systems

TA systems have considerable potential for a number of applications in biotechnology including pathogen control.

Due to plasmid instability, bacteria can lose the expression plasmids and these plasmids free cells grow faster than the construct containing cells as plasmids can significantly influence the growth of bacteria. TA systems can be utilized to enhance plasmid stability (176) by killing the host cells once the plasmid is lost, which will remove the plasmid free cells and increase the yield of recombinant protein. By making use of the toxicity of MazF, a single protein production (SSP) system has been established recently to overexpress one single protein in *E. coli,* by cleaving other mRNAs containing ACA specific cleavage site (177). This has proved to be highly useful in structural biology, particularly for NMR studies, due to the production of isotope-labelled proteins at reduced cost (178). Similarly, the toxicity of CcdB has been utilized in molecular cloning to improve the efficiency of positive colony growth. Only the colonies containing vector with correct insert can grow by counteracting with the chromosome toxin CcdB.

Considering their natural properties of repressing cell growth and even killing cells, TA systems have attracted intensive interest as potential targets for the development of novel antibiotics (179). Either the direct disruption of the TA complexes or preventing the complex formation, will release the free toxin to exert its function. Alternatively, activation of protease degrading the antitoxin or repression of transcription of the TA operon, leads to either more antitoxin degraded or less antitoxin expressed, both of which will activate the cognate toxin (180, 181). Recently, TA systems have been proposed to have anti viral activity. *E. coli* mazF gene was constructed into a retroviral vector under control of the TAR promoter from human immunodeficiency virus (HIV) (182). When CD4+ T-lymphoid cells containing this mazF construct are infected, MazF toxin is expressed and subsequently cleaves the HIV mRNA so that the cell is protected. Similarly, MazF toxicity was exploited to selectively eradicate the herpes C virus (HPC) infected cells in another study (183). In this strategy, the virus serine protease NS3 cleavage site was introduced between a fragment of mazE (antitoxin) gene and the full-length mazF gene. When infecting the host cells, HPC virus will express the protease NS3, which in turn cleaves the link between MazE and MazF, and releases the latter to digest the mRNA and kill the cell (Figure 30).

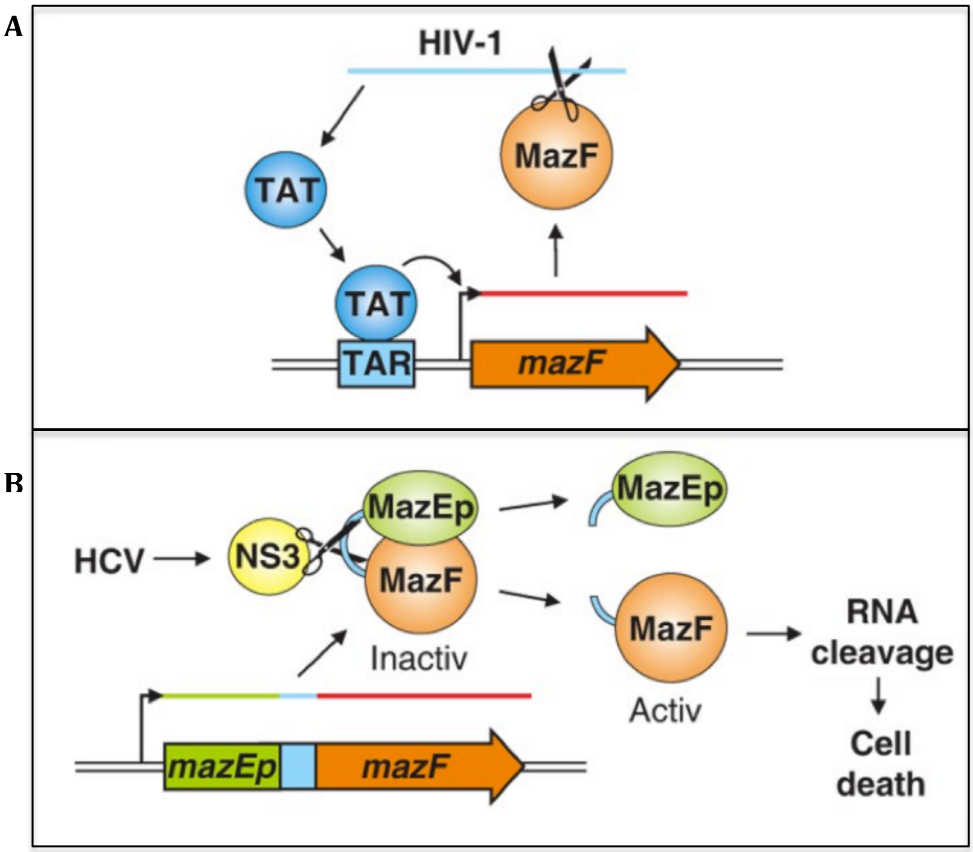

**Figure 30. Example applications of TA systems in virus control. (A)** The vector with the mazF gene under the control of TAR promoter (from HIV) is introduced into the CD4+ cells. Upon HIV infection, the HIV Tat protein is expressed and binds to the TAR promoter region, which will induce the expression of MazF. The expressed MazF cleaves the mRNA of HIV, inhibiting its replication. **(B)** Construct with partial mazE gene linked with full mazF gene is introduced into the HCV infected cells. HCV expressed NS3 cuts the linker between MazEp and MazF, thereby freeing the MazF for cleavage of RNA leading to cell death. (Adapted from Simon *et al,* 2013)

### 1.4 MazF and RelE TA systems

MazF and RelE have been extensively studied among the type II TA systems. MazF is a sequence-specific ribosome–independent single-stranded mRNA endoribonuclease (128). The homologues of MazF have been found in a large number of Bacteria and Archaea, and in some cases, more than one homologue has been characterized in one Bacterium (184). The specific sequences that MazF can recognize, vary between different species and consist of different number (3, 5 or 7) of nucleotide (185, 186). In addition, MazF can even cleave the 3' terminus of 16S rRNA removing the anti-SD sequence and resulting in a special subpopulation of ribosome (187). Interestingly, this ribosome population can specifically translate the leaderless mRNA resulting from MazF cleavage, without SD anti-SD sequence recognition (187).

RelE is an endoribonuclease, which cleaves mRNA in a ribosome–dependent manner (188). Homologues of RelE have been found in many Bacteria and Archeae, encoded both in chromosomes and on plasmids (188). RelE binds to the 30S subunit of ribosome and exerts its function by cleaving the mRNA at the ribosome A-site, between the second and third nucleotide (129). The cleavage leads to inhibition of translation elongation and thus the protein synthesis. Structures of RelE bound to ribosome before and after mRNA cleavage have been elucidated, shedding much light on the mechanism of mRNA recognition and cleavage (189). It should be noted that, RelE itself has no endoribonuclease activity.

### 1.5 YoeB and YefM

YoeB-YefM system is widespread among plasmids and genomes in Eubacteria and Archaea. Initially identified as Axe-Txe in a multidrug-resistant clinical isolate of *Enterococcus faecium* (190), YoeB-YefM has since been found in a large number of bacteria, including major pathogens such as *Staphylococcus aureus*, *Streptococcus pneumoniae*, *Mycobacterium tuberculosis*, and *Yersinia enterocolitica*. Recently, YoeB-YefM was identified as the first TA system in *Streptomyces* (191).

The toxin YoeB is a basic protein with a MW of 10 kDa while its cognate antitoxin YefM is acidic and slightly bigger (11 kDa). YefM is highly unstable and prone to degradation by Lon, an ATP dependent protease, and thus freeing YoeB to exert its function (192). Unlike RelE, YoeB associates with 50S ribosome subunit and specifically cleaves mRNA immediately downstream of the initiation codon so as to inhibit the formation of initiation complex. Although YoeB is classified as a ribosome dependent endoribonuclease, a weak activity was detected even in the absence of ribosome (193). In the presence of 70S ribosome, a partial cleavage of mRNA *in vitro* was observed using toeprinting assay even with a nuclease-negative mutant (H83Q) YoeB protein (132). Crystal structures of the *E. coli* YoeB-YefM$_2$ heterotrimeric complex and isolated YoeB dimer have been determined (131), revealing a microbial RNase fold of YoeB and an asymmetric disorder-to-order recognition strategy by YefM. YoeB structure is highly simiar to RNase Sa from *Streptomyces aureofaciens* (194) and Barnase (bacterial ribonuclease) from *Bacillus amyloliquefaciens* (195). Residues essential for YoeB RNase activity, including the general acid/base candidate His83/Glu46, have been identified. Neutralization of YoeB toxicity by YefM dimer involves the C-terminal region of one YefM monomer, This region undergoes a disorder-to-order transition upon YoeB binding and makes extensive interactions with the RNase fold of YoeB, leading to the conformation change that finally abolishes the RNase activity. The structural features and the mechanism of neutralization are demonstrated in Figure 31.

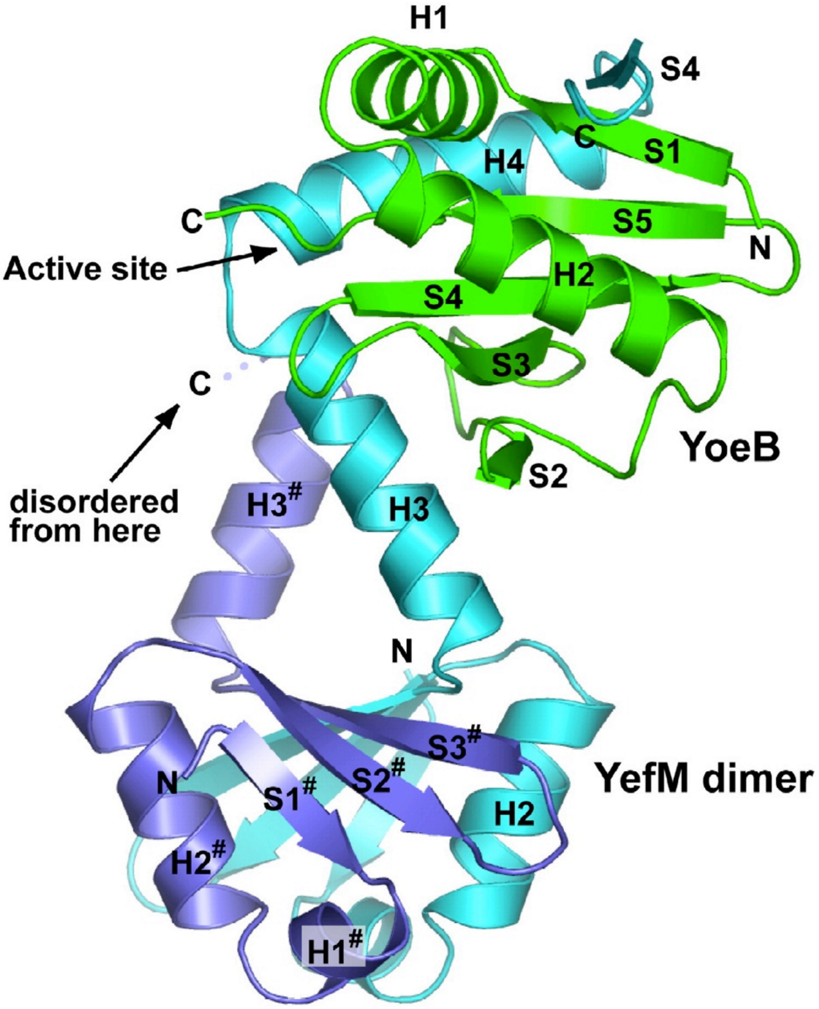

**Figure 31. Crystal structure of the YoeB-YefM complex.** YefM homodimer binds to YoeB monomer. One monomer (coloured lavender) of the YefM homodimer has a disordered C terminal end while the other monomer (coloured cyan) possesses an ordered C terminal interacting with the YoeB. YoeB is shown as cartoon in green. Secondary structure elements are labelled. (Adapted from Katsuhiko Kamada *et al,* 2013)

## 1.6 Aims and significance

YoeB appears to be a homologue of the well-characterized RelE toxin based on the structural similarity of the catalytic core. However, several major differences can be noted. First and foremost, the two toxins share only 15% amino acid sequence identity. Secondly, in contrast to RelE, YoeB shows only partial activity in some biochemical assays (131). Additionally, the two interact with ribosome in distinct ways. YoeB associates with the 50S subunit after ribosome dissociation (132), while RelE interacts with 16S rRNA of the 30S subunit (189).

Furthermore, YoeB and RelE inhibit translation by affecting initiation or elongation, respectively (121). Finally, YoeB contains general base/acid catalysis residues (Glu46 and His83) conserved in toxin YafQ and other RNases (131) (156), while RelE seems to lack these residues.

These differences suggest that YoeB is a more classical mRNA endoribonuclease than RelE that still requires the ribosome for its specific activity. Therefore, structural characterization on the YoeB bound to ribosome is of considerable interest for a better understanding of the function and catalytic mechanism of TA type II toxins. Thus, in this chapter we describe the structural information obtained from the determination of YoeB bound ribosome structure in a pre-cleavage state.

# 2. Materials and methods

## 2.1 Plasmid construction and protein purification

YoeB protein was obtained from our collaborator from Japan. *E. coli* YoeB was cloned, expressed, and purified using the same procedure as described previously (131). Briefly, YoeB and His-tagged YefM were co-expressed in *E. coli* BL21 (DE3) strain. The YefM-free YoeB was eluted from a $Ni^{2+}$ column to which YoeB-YefM complex was bound by a buffer containing 6M Guanidine-HCl. Denatured YoeB was then refolded by gradual dialysis against GF buffer (25 mM HEPES pH7.5, 200 mM NaCl, and 1 mM DTT). Subsequently, the refolded YoeB was purified further by Heparin-Sepharose column and gel filtration chromatography and finally concentrated to 350 μM in buffer G (50 mM KCl, 10 mM $NH_4Cl$, 10 mM MgOAc, 5 mM HEPES-KOH, pH7.5). All used buffer, except for $Ni^{2+}$ column chromatography, were prepared with RNase free chemicals. The protein preparation was finally checked with RNase Alert Lab Test Kit (Ambion) to confirm the absence of RNase contamination, flash frozen in liquid nitrogen and stored at -80 °C for further use.

## 2.2 Preparation of wild type ribosomes, tRNA, and mRNA

Ribosomes were purified as described above, except that *Thermus thermophilus* HB8 wild type strain cells were used. *E. coli* $tRNA^{fMet}$ was purchased from Sigma. The MOO4b mRNA with the sequence 5´ GGCAAGGAGGUAAAAAUG**UAA**AAAA 3´ was purchased from Dharmacon with 2′-O-methylation modifications in the three nucleotides at the A-site (shown in bold) to trap the ribosome-YoeB complex in a pre-cleavage state. The underlined AUG corresponds to the P-site codon. The unmodified MOO4 mRNA with same sequence was also synthesized.

## 2.3 Complex formation and crystallization

Complexes of YoeB with 70S ribosome, $tRNA^{fMet}$, and MOO4b mRNA, were formed as previously described (21). All complexes were formed in buffer G (5 mM HEPES pH 7.5, 50 mM KCl, 10 mM $NH_4Cl$, 10 mM Mg-acetate, and 6 mM 2-mercaptoethanol). 70S ribosomes at a final concentration of 4.4 μM were incubated with 8.8 μM mRNA for 6 min at 55 °C, following which, 13.2 μM tRNA$^{fMet}$ was added and incubated for another 30 min. The mixture was cooled down to 37°C prior to YoeB addition and incubated for additional 30 min. The complex was kept at room temperature for 30 min before crystallization.

The final concentration of all components during the complex formation is listed in Table 6.

**Table 6. Components and final concentration of YoeB bound ribosome complex**

| Component | Final concentration |
|---|---|
| Buffer G | 1x |
| *T. Th.* 70S ribosome (wild type) | 4.4 µM |
| MOO4b mRNA | 8.8 µM |
| tRNA$^{fMet}$ | 13.2 µM |
| YoeB | 44 µM |

Prior to crystallization, detergent Deoxy Big Chap (DOBC) was prepared as 14 mM in buffer G and added to the complexes with a final concentration of 2.8 mM. Crystals were grown and optimized via sitting-drop vapor diffusion method. 2.4 µl of complex sample plus 2 µl reservoir solution containing 0.1 M Tris-HAc pH 7.2, 0.2 M KSCN, 4.1%–4.3% (w/v) PEG 20K and 4.1%–4.3% (w/v) PEG 550MME, were mixed and left to equilibrate at 20°C. Crystals with stick morphology grew to a full size of ~1000 x 100 x 100 µm within one week. Crystals were equilibrated overnight with 10% increase of PEG to improve the diffraction and transferred stepwise into mother solution with 25% PEG 550MME as cryo-protectant before flash freezing by plunging into liquid nitrogen.

## 2.4 Data collection and structure determination

Crystals were screened on PX I beamline at the Swiss Light Source (SLS), and diffraction data were collected at 100K. All data were processed with XDS (80).

The empty 70S ribosome structure (189) was used as an initial model and refinement was carried out with CNS (81). All model building was done using COOT (82), and electron density map was generated with CNS (81). All figures were made with PyMOL (DeLano Scientific).

## 2.5 MALDI mass spectrometry

For MALDI mass spectrometry analysis, MOO4 mRNA without the 2′-O-methylation modifications was used so that YoeB can cleave the mRNA upon binding to the ribosome. Briefly, 3.5 μM unmodified MOO4 mRNA was incubated with 2.2 μM YoeB for 30 min at 37°C in the presence of programmed 70S ribosomes (4.4 μM) containing mRNA and tRNAs, which are formed in polymix buffer (20 mM HEPES pH 7.5, 95 mM K-glutamate, 5 mM Mg-acetate, 5 mM $NH_4Cl$, 0.5 mM $CaCl_2$, 1 mM spermindine, 8 mM putrescine, and 1mM DTT). For control, mRNA was incubated with YoeB in the absence of ribosomes. The reaction products were extracted with phenol-chloroform to remove proteins. Aqueous phase was collected and RNA (including rRNA, tRNA and mRNA) was ethanol precipitated. Samples were analyzed by 18% PAGE with 8 M urea, which can denature the secondary structure of RNAs. Separated RNA was visualized by staining with Sybr Gold (Life Technologies). ZR Small-RNA PAGE Recovery kit (Zymo Research) was used to improve the efficiency of RNA recovery from the gel. RNA fragments were precipitated by ethanol and dissolved in MilliQ water. All buffer used were prepared with RNase free chemicals. Prior to MALDI MS analysis, the samples were desalted and prepared with ZipTip C18 pipette tips (Millipore) according to manufacturers’ instructions. Mass spectrometry analysis was performed with MALDI TOF/TOF ABI4800 in a positive ion, linear mode.

# 3. Results

## 3.1 Ribosome-YoeB crystallization

Crystallization trials were carried out according to the previous reported method(68). DOBC was used as the detergent for crystallization of wild type ribosome. By varying the concentration of PEG 20K, crystals with stick morphology grew to a full size of ~1000 x 100 x 100 μm within one week. After several rounds of optimization, crystals with rod morphology were repeatedly obtained (Figure 32A). About 50 crystals were picked and analyzed at synchrotron (SLS, Switzerland), several of which diffracted to better than 3 Å.

Initially, YoeB was added to a final concentration of 22 μM during the complex formation. Preliminary analysis of X-ray diffraction data from these samples showed ambiguous electron density maps at the binding site of YoeB, indicating a low occupancy of YoeB. This prevented us from building a sound model of YoeB, although its binding was confirmed. Considering that YoeB has been known to form a homodimer in solution, the final concentration of YoeB was increased to 44 μM to ensure a molecular ratio of 1:5 between ribosome and YoeB. Although it was not known whether YoeB binds to the ribosome as a monomer or dimer.

As expected, higher YoeB concentration did not influence crystal packing and morphologically similar crystals were obtained (Figure 32B) that likewise diffracted to ~3 Å at synchrotron.

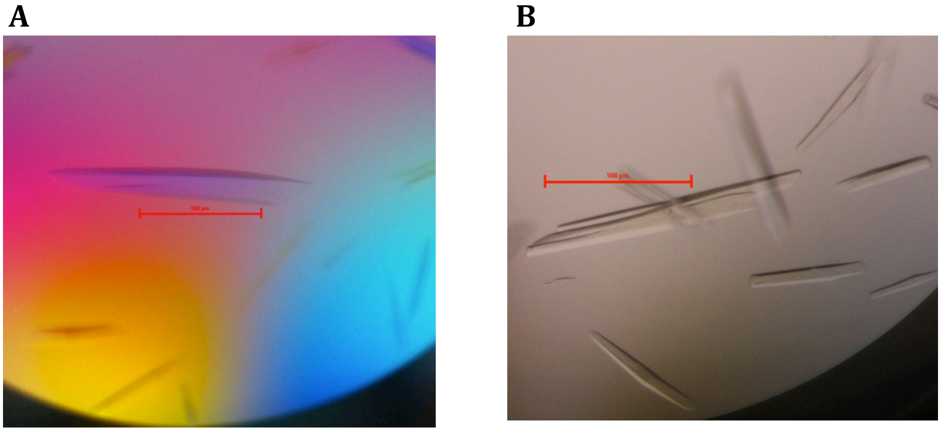

**Figure 32. Crystals of the YoeB-ribosome complex. (A)** Crystal obtained after optimization by varying the precipitant PEG 20K concentration. DOBC was used as detergent. **(B)** Crystals obtained after increasing YoeB concentration. 500 µm indicated in red bar for scale.

### 3.2 Structure determination

A full dataset for the YoeB-ribosome complex was collected at beamline PX I of the Swiss Light Source (SLS) on a Pilatus 6M (Dectris) detector at 100K. Diffraction data was processed with XDS and the statistics is summarized in Table 7. The complex crystallized in the spaces group $P2_12_12_1$, similar to other wild type 70S ribosome complexes, which was not unexpected because the conformational change upon YoeB binding should not influence crystal packing.

Empty 70S ribosome structure (21) was used to obtain an initial model, which was further refined with CNS (81). The difference density map clearly revealed the presence of YoeB and mRNA as well as P- and E- site tRNAs. Model was then manually built using COOT. The final structure was refined to 3.35 Å resolution ($I/\sigma(I)=1.6$), with a final $R/R_{free}$ of 0.221/0.261. Statistics of structure refinement is summarized in Table 7. The coordinates and structure factors have been deposited in Protein Data Bank (PDB) with accession code 4V8X.

## Table 7. Statistics of data collection and structure refinement of YoeB-ribosome complex

| | |
|---|---|
| **Data collection** | |
| Space group | $P2_12_12_1$ |
| Unit cell dimensions | |
| a,b,c (Å) | a=211.6, b=455.4, c=616.9 |
| $\alpha,\beta,\gamma$ (°) | $\alpha=\beta=\gamma=90$ |
| Resolution (Å) | 50-3.35 (3.4-3.35) |
| $R_{sym}$ (%) | 15.1 (106.2) |
| $I/\sigma I$ | 9.3 (1.6) |
| Completeness (%) | 99.7 (99.8) |
| Redundancy | 5.1 (4.7) |
| **Refinement** | |
| Resolution (Å) | 50-3.35 |
| No. of unique reflections | 842970 |
| $R_{work}/R_{free}$ (%) | 22.1/26.1 |
| No. of atoms | 298211 |
| RNA | 199460 |
| Protein | 98040 |
| Ions | 711 |
| Average B factor (Å$^2$) | |
| RNA | 111 |
| Protein | 125 |
| Ions | 92 |
| R.m.s. deviations | |
| Bond length (Å) | 0.006 |
| Bond angle (°) | 1.2 |

* Numbers in parenthesis refer to outer resolution shell

† I/s = 2.0 at 3.4 Å

## 3.3 Structural analysis

### 3.3.1 Overall structure of the ribosome-YoeB complex

The crystal structure of *T. thermophilus* 70S ribosome in complex with YoeB, tRNAs in the P- and E- sites, and mRNA, represents a pre-cleavage state (Figure 33A). The unbiased difference Fourier density shows both mRNA and YoeB with clearly distinguishable side chains (Figure 33B). The structure reveals that YoeB binds to the ribosome A-site as a homo-dimer and this consequently blocks the ribosome access of both A-site tRNA and translational factors, such as release and elongation factors (Figures 33A and 33C). This is not surprising because it has been reported that YefM-free YoeB would exist in the solution and crystallize as homo-dimers (131). The dimer interface does not interact directly with any ribosomal components. However, the entire dimer complements the shape of the ribosomal A-site, suggesting that the binding of YoeB to ribosome can stabilize the dimer. The YoeB monomer located in close proximity to the decoding centre, is referred to as monomer A, and the other monomer is referred to as B. Monomer A spans the head and body of the 30S subunit, with the RNase fold β-sheet contacting the A-site mRNA. Monomer B occupies the space between the head of 30S subunit and the A-site finger of 23S rRNA (Figure 33C). Upon binding to ribosome, a number of rearrangements occur in monomer A including various novel interactions. In particular, the C-terminal tail of monomer A swings towards mRNA by ~3 Å. In contrast, little conformational change is observed in monomer B.

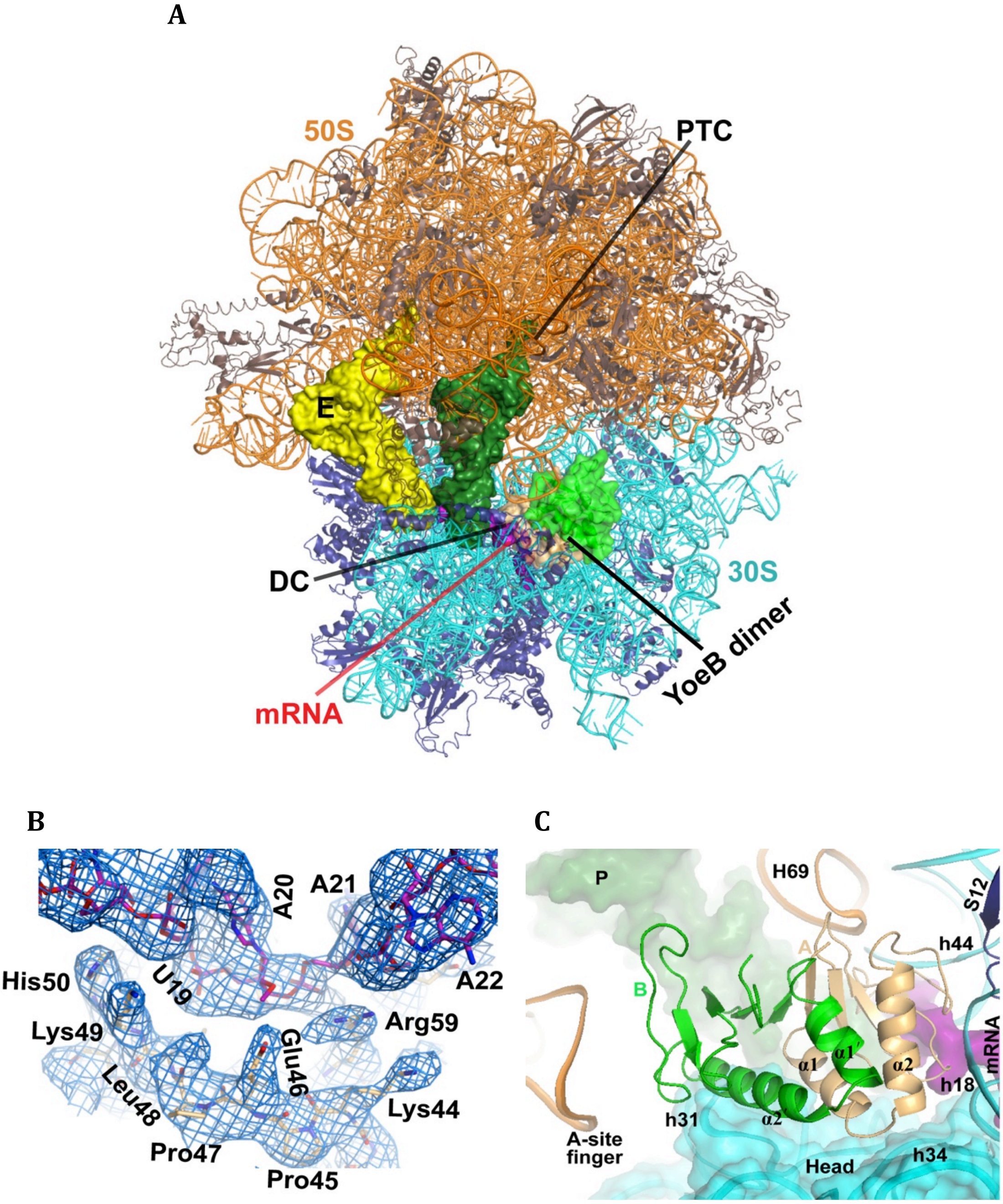
A
50S
PTC
E
DC
30S
YoeB dimer
mRNA
B
A20
A21
His50
U19
A22
Lys49
Arg59
Glu46
Leu48
Lys44
Pro47
Pro45
C
P
H69
S12
h44
A
B
α1
α1'
α2
mRNA
h18
h31
α2'
A-site finger
Head
h34

**Figure 33. Structure of YoeB bound to the 70S ribosome. (A)** Overall view of the ribosome in complex with YoeB dimer (colored light orange for monomer A and green for monomer B). The mRNA, P-site tRNA and E-site tRNA are shown as surface. The peptidyl transfer center (PTC) and the decoding center (DC) are indicated. **(B)** Unbiased difference Fourier electron density map corresponding to YoeB and mRNA interface displayed at 1.2 σ. **(C)** Close-up view of YoeB binding site on ribosome. The two N-terminal helices for both YoeB monomers are labeled. The 16S head is shown as cartoon with transparent surface.

### 3.3.2 Interactions between YoeB and ribosome

While it is uncertain whether or not YoeB functions as a dimer *in vivo*, both monomers are clearly visible in the current model, thus enabling us to describe the interactions between ribosome and both monomers. Monomer B, far apart from the ribosomal decoding center, contains a large number of basic residues (residues 21, 22, 25, 32, 35, and 36) in the helix $\alpha 2$ facing the 30S head (Figure 34A). Of these residues, Lys32, Arg35, and Arg36 are within hydrogen-bonding distance to h31 of 16S rRNA in the 30S head. Except for these interactions, monomer B does not make direct contacts with ribosomal components.

In contrast to monomer B, monomer A forms extensive contacts with rRNAs (both 16S and 23S), ribosomal protein S12, and mRNA (Figures 32C and 33B). The N-terminal $\alpha 1$ and $\alpha 2$ helices form a V-shaped arrangement wedging into the cleft between the head and body of 30S, where the basic residues Arg22 and Lys26 interact with U531 and C519 in the decoding region (Figures 32C and 33B). On the opposite side, monomer A forms strong interactions with the tip of H69 of 23S rRNA, A1492/A1493 in h44 of 16S rRNA, and S12 protein (Figure 34B). The Thr71 and Asp72 residues, located in the β-strand loop, establish hydrogen-bonding interactions with U1915 and C1914 in H69. Additionally, Phe39 enhances the interaction of YoeB with H69 via hydrophobic contact. H69 (1906-1924) is a highly conserved stem-loop involved in the formation of inter-subunit bridge B2a. H69 is known to interact with translational factors such as release factors RF1 and RF2 (196, 197), indicating a pivotal role in translation. YoeB tightly contacts H69, thereby likely interfering with its function. The neighbouring residue Glu40 of YoeB interacts with Thr44 located at the highly conserved β-loop of S12, which projects into the decoding center to participate in codon-anticodon recognition (5). In close proximity, Lys42 forms bilateral contacts with ribose O3 of C519 in h18 of 16S rRNA and Leu52 in the β-loop of S12, via hydrogen bond and side-chain hydrophobic interaction, respectively (Figure 34B). Moreover, the main chain N atom of Gly43 contacts phosphate oxygen of C519.

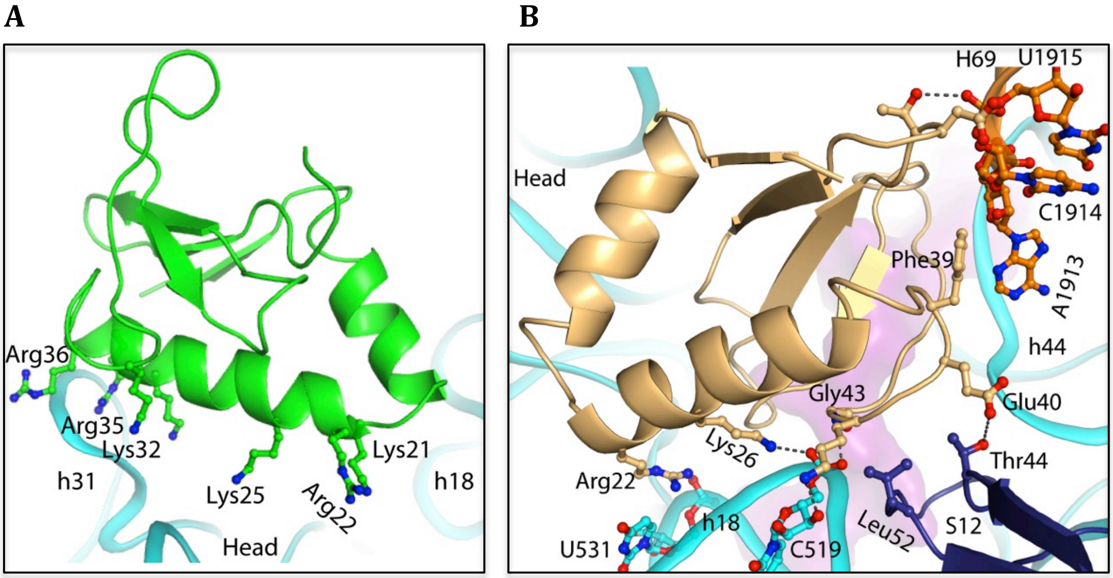

**Figure 34. Interactions between YoeB and ribosome. (A)** Interactions between monomer B of YoeB and helix 31 of the 16S rRNA in the 30S head. Monomer B, contains a large number of basic residues (shown as sticks) in helix α2 facing the 30S head. **(B)** Interactions of monomer A of YoeB with the body region of 30S (G519), ribosomal protein S12 and H69 (A1913) of 50S subunit 23S rRNA. The hydrogen-bonding interactions are indicated by dashed lines.

### 3.3.3 Active site interactions

Despite YoeB binding to the ribosome as a dimer under our experimental conditions, monomer B has no access to mRNA according to our model, demonstrating only one active site in YoeB dimer. At the decoding center, a network of interactions involving YoeB monomer A, G530 of 16S rRNA, S12, and mRNA is formed. In particular, Lys44 in YoeB interacts with the highly conserved Pro48 in S12 (Figure 35A). Pro48 is crucial for ribosome function, since mutation of the equivalent residue in *E. coli* S12 resulted in severe dominant growth defects (198). The loop linking α2 and β2 in YoeB also forms several tight interactions with the A1492 region of 30S, causing a significant conformational change in A1492 and A1493 (Figure 35A). The conformationally flexible decoding bases A1492 and A1493 are pulled completely out of h44 of 16S, which is complemented by a shift of the main chain toward the helical axis.

The ribose O2 of the first nucleotide (U19) of the A-site codon interacts with Asn51 of YoeB (Figure 35B), appearing to prevent it from rotating back to contact the P-site tRNA, in a similar way as observed in the RelE-bound state (189). The second and third nucleotide (A20 and A21) of the codon form direct interactions with a number of residues in YoeB, including Glu46, Arg59, Glu63, Arg65, His83 and Tyr 84, which are located in the β-sheet and the C-terminal loop (Figure 35B). These residues are highly conserved in the YoeB family and most of them have been demonstrated to be indispensable for the activity of YoeB (156). A conformational change in the YoeB C-terminal tail, resulting from ribosome binding, brings the two activity-required residues, His83 and Tyr84, into the reported position, where tight interactions with A20 and A21 are observed (Figure 35B). Interestingly, His83 and Glu63 stabilize the base of A21 by stacking to either side. The universally conserved A1493 and G530 residues orient the mRNA substrate for subsequent cleavage, which is supported by additional interactions mediated by YoeB residues. A1493 makes direct contacts with the second nucleotide (A20) of the codon, and G530 interacts with the guanidinium group of YoeB Arg59, which in turn contacts A21 residue at position 3 and the linked phosphate of A22.

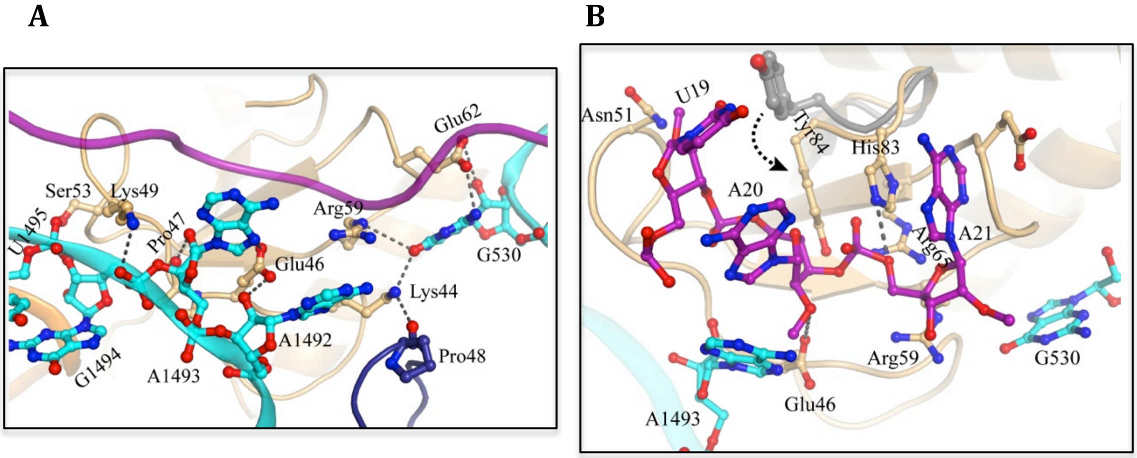

**Figure 35. Interactions at the mRNA cleavage site. (A)** YoeB interactions with ribosome at the decoding center. The mRNA is shown as ribbon magenta colored. The residues of YoeB within hydrogen-bonding distances (dashed lines) to ribosome are shown in sticks and labeled. **(B)** Active site of YoeB surrounding the codon at A-site. Catalytic residues Glu46 and His83 are within hydrogen-bonding distance to their reaction atoms. Compared with isolated YoeB colored gray, the conformational change of C-terminal tail of YoeB (particularly the Tyr84 residue) is shown by an arrow.

### 3.4 YoeB cleaves mRNA following the second position of the A-site codon

To determine the exact mRNA cleavage site of YoeB, analysis of the resulting RNA fragment was carried out by mass spectrometry. When mRNA was incubated with the YoeB in the absence of ribosome, a peak with a mass of 8189 Da corresponding to the full-length mRNA, was observed, whereas an RNA fragment with a mass of 6624 Da was detected in the presence of YoeB. In the absence of ribosome, the mRNA was hardly digested, while in the presence of the ribosome, the mRNA was fully digested. The mass of the fragment corresponds to cleavage occurring after the second position in the A-site codon (Figure 36). Moreover, cleavage by YoeB produces a RNA fragment with a 3′-phosphate at the newly formed 3′ end, unlike the RNA fragment with 2′–3′ cyclic phosphate at the 3′ end observed after RelE cleavage (189).

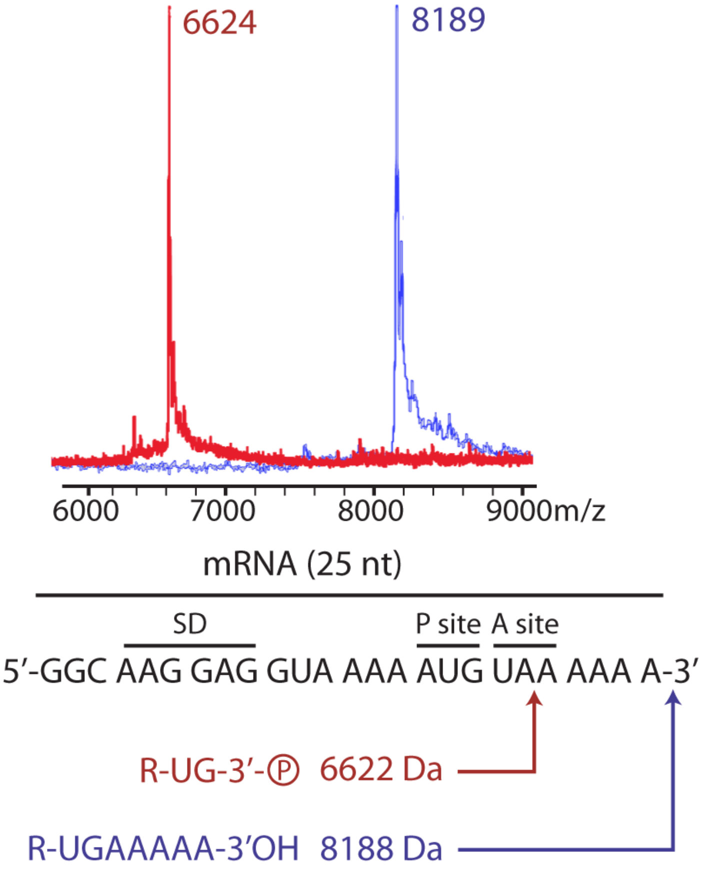

**Figure 36. MS analysis of YoeB cleaved mRNA fragments.** MALDI mass spectrometry profile. Corresponding RNA fragments and the position of cleavage deduced from MS results, are indicated.

# 4. Discussion

## 4.1 Comparison of RelE and YoeB bound ribosome structures

RelE represents a family of well-characterized ribosome-dependent mRNA interferases belonging to type II TA system. YoeB appears to be a homologue of RelE based on the structural similarity of the catalytic core, however, several major differences exist. For instance, the two share only 15% sequence identity, and YoeB shows only partial activity in some biochemical assays (131). Thus, it is of great interest to compare the structures of ribosome-YoeB and ribosome-RelE complexes to reveal their unique features.

While the YoeB monomer A and RelE occupy a similar position at the ribosome A-site, their interactions with the ribosome are notably different (Figure 37A). RelE contacts almost exclusively 16S rRNA and shows only moderate hydrogen–bonding interactions with the decoding center. In contrast, YoeB makes extensive contacts with 16S rRNA, 23S rRNA, and ribosomal protein S12. In particular, the region between residue 34 to 56 forms interactions with the decoding site involving the three universally conserved nucleotides G530, A1492, and A1493, which play a vital role in proper decoding by interacting with the codon–anticodon helix to construct the structural constraints necessary to inspect the accuracy of base pairing (5, 6). Moreover, YoeB tightly interacts with H69 of 23S rRNA, which is involved in the formation of an essential inter-subunit bridge B2a, as well as implicated in translation termination by interacting with release factors (6). Despite the fact that these interactions may change after mRNA cleavage or during ribosomal subunit dissociation, our observations provide support for two previously reported features of YoeB. First, YoeB effectively inhibits protein synthesis by binding to ribosome and blocking the A-site, and second, YoeB was found to associate with 50S subunit after 70S ribosome dissociation (132).

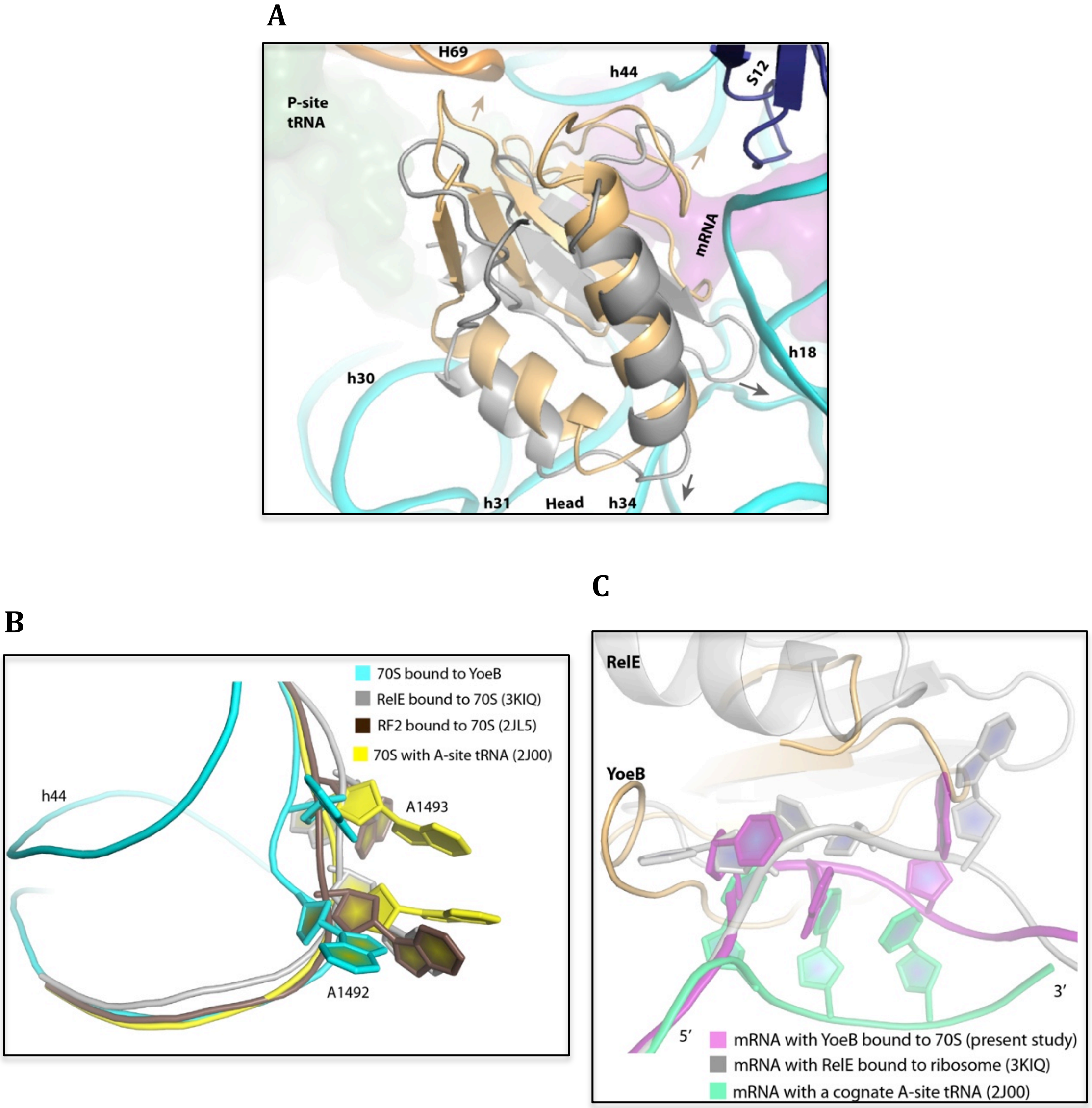
A
H69
h44
S12
P-site
tRNA
mRNA
h18
h30
h31
Head
h34
B
70S bound to YoeB
RelE bound to 70S (3KIQ)
RF2 bound to 70S (2JL5)
70S with A-site tRNA (2J00)
h44
A1493
A1492
C
RelE
YoeB
5′
3′
mRNA with YoeB bound to 70S (present study)
mRNA with RelE bound to ribosome (3KIQ)
mRNA with a cognate A-site tRNA (2J00)

**Figure 37. Differences between RelE and YoeB bound ribosomes. (A)** The positioning of YoeB (monomer A) and RelE in the ribosome. The ribosome-bound RelE in pre-cleavage state was superposed to YoeB in the present structure by aligning on 16S rRNA. YoeB (orange) and RelE (gray) are shown as cartoons. **(B)** Structural comparison of the two universally conserved decoding site nucleotides A1492 and A1493 residues in various ribosome complexes. YoeB bound to 70S (cyan), RelE bound to 70S (gray), RF2 bound to 70S (brown) and 70S with a cogntate A-site tRNA (yellow) complexes presented. **(C)** Comparison of the conformation of A-site mRNA codon residues in various ribosome complexes. mRNA in YoeB-ribosome complex (magenta), in RelE-ribosome complex (gray) and A-site tRNA-ribosome complex (aquamarine) were presented.

At the decoding center, the loop linking α2 and β2 in YoeB also forms several tight interactions with the A1492 region of 30S, causing a significant conformational change in A1492 and A1493. As a result, a unique conformation for the "decoding bases" is observed (Figure 37B). Such a conformation is distinct from that observed in ribosome bound to RelE (189). In the 70S-RelE complex (189), A1493 stacks with A1913 of 23S rRNA. Both A1493 and A1492 conformations observed in complex with RelE are incompatible with the binding of YoeB. In accordance, the deformed mRNA A-site codons are in notably different conformations in the YoeB- and RelE-bound structures as well (Figure 37C). The distances between the backbone phosphates of the three A-site nucleotides are 0.8, 6.5, and 4.6 Å, respectively. This is a consequence of the different interactions of YoeB and RelE with mRNA.

Based on our structure with YoeB, the position of the first A-site codon is compatible with accommodating any anti-codon base, whereas the second and third appear to favour adenine or, alternatively, guanine. This is different from RelE, which shows more strict sequence specificity toward A-site mRNA. Although cleavage by RelE was observed to be more frequent within the first ~100 codons *in vivo* (199), less strict requirements for the mRNA codon in case of YoeB is leading to its cleavage occurring immediately adjacent to the translational initiation site (132). Such a distinct specificity of these two toxins may account for their different inhibition mechanisms. Namely, as proposed previously, YoeB may act as an inhibitor for translation initiation, whereas RelE inhibits elongation (121).

## 4.2 Mechanism of YoeB dependent mRNA cleavage

In the present structure, which represents YoeB bound to ribosome in a pre-cleavage state, we observe a network of interactions at the decoding center involving the second and third nucleotides of A-site codon and a number of YoeB residues, including Glu46, Arg59, Glu63, Arg65, His83 and Tyr84. According to the mass spectrometry analysis, the mRNA substrate is cleaved exclusively between the second and the third nucleotides and a methylation of A-site mRNA nucleotides at 2′–O position completely abolishes mRNA cleavage by YoeB

(Figure 36). The fact that the aforementioned residues are highly conserved within the YoeB family (Figure 38A) indicates their potential roles in catalytic activity. This has also been confirmed by biochemical studies (156). Based on this, we propose a mechanism of mRNA cleavage by YoeB (Figure 38B) that resembles the mechanism accepted for RNase T1/RNase Sa (200, 201). Namely, Glu46 acts as a general base and its negatively charged side chain deprotonates the ribose 2′–O of A20, which is thereby activated for an inline nucleophilic attack on the adjacent 3′–phosphate. The negatively charged trigonal bipyramidal transition state is likely stabilized by His83, which is proposed to donate a proton leading to the formation of the leaving 5′OH group during the final stage of catalysis. His83 thus acts as a general acid. The positively charged side chain of Arg65 is in position to stabilize the transition state, consistent with its necessity for the enzymatic activity reported previously (131). Subsequent hydrolysis of the resulting 2′–3′ cyclic phosphate to the final RNA fragment with 3′–phosphate and 2′–OH group, involves an exogenous water molecule and His83, in a similar way as described for RNase T1 (200). The conserved Tyr84 residue in the proximity of the scissile phosphodiester bond is involved in catalysis by orienting mRNA via its benzene ring and forming a network of hydrogen-bonding interaction with Arg65 and phosphate-oxygen at the cleavage site in mRNA. This allows us to rationalize the mutagenesis data on Y84, namely that substitution with alanine results in completely abolishing the activity of YoeB, whereas substitution with another aromatic amino acid (Y84F) shows compromised activity (131).

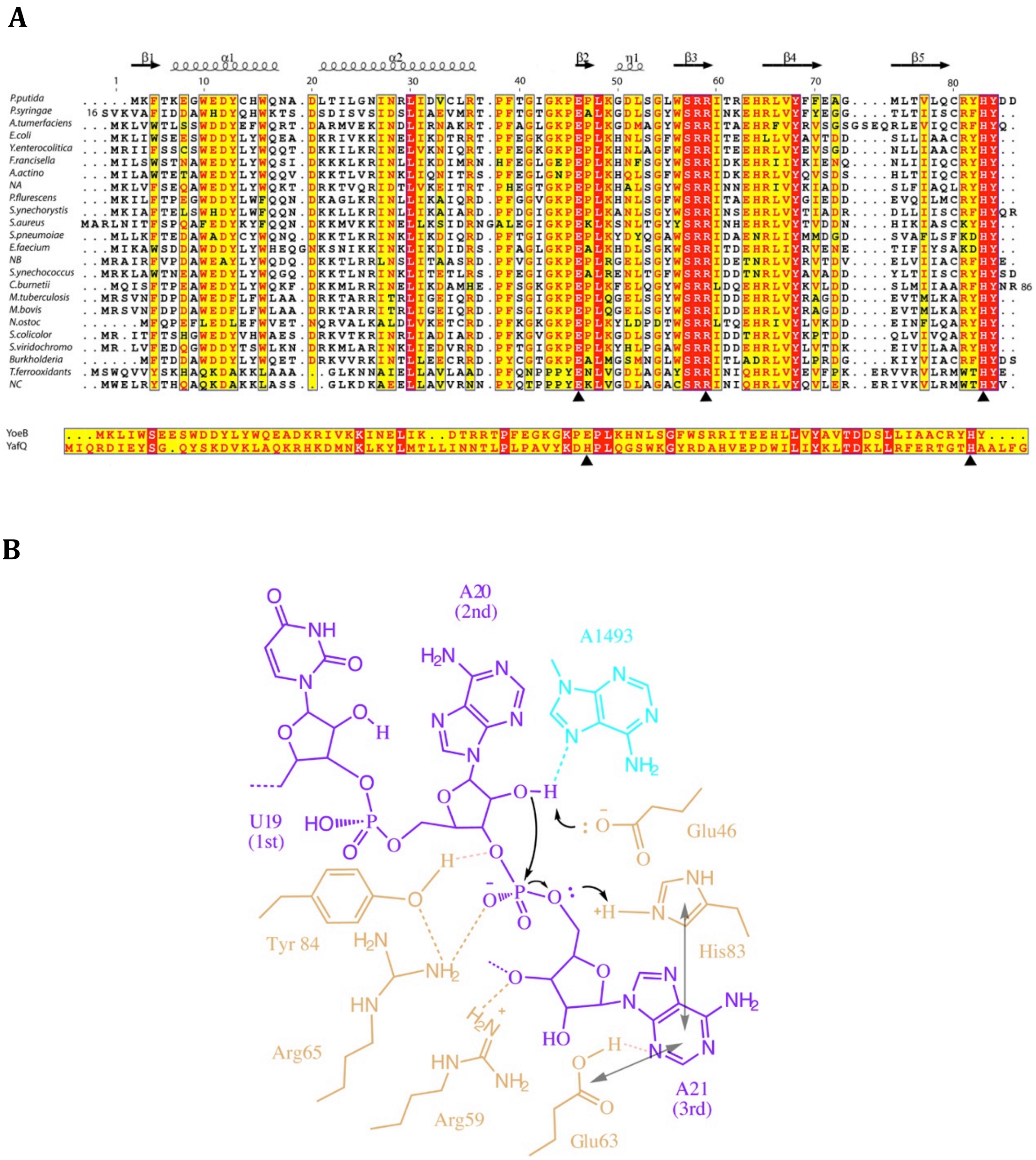
A
β1
α1
α2
β2
η1
β3
β4
β5
1
10
20
30
40
50
60
70
80
P.putida
P.syringae
A.tumerfaciens
E.coli
Y.enterocolitica
F.francisella
A.actino
NA
P.flurescens
S.ynechorystis
S.aureus
S.pneumoiae
E.faecium
NB
S.ynechococcus
C.burnetii
M.tuberculosis
M.bovis
N.ostoc
S.colicolor
S.viridochromo
Burkholderia
T.ferrooxidants
NC
YoeB
YafQ
B
A20
(2nd)
A1493
U19
(1st)
Glu46
Tyr 84
His83
Arg65
Arg59
A21
(3rd)
Glu63

**Figure 38. Amino acid sequence alignment of YoeB homologues and the proposed catalytic mechanism. (A)** Alignments of YoeB homologues, as well as YoeB and YafQ. Upper panel: alignment of YoeB homologues. All proteins are indicated by their strain names except for NA, NB, and NC, referring to the three predicted YoeB homologues in *N. europaea*. The secondary structure and sequence numbering are based on *E. coli* YoeB in this study. Three conserved residues Glu46 (general base), Arg59 (stabilization of transition state), and His83 (general acid), are marked by black triangle. Lower panel: alignment of YoeB and YafQ. YafQ is another family of bacterial ribosome-dependent endonuclease. The general base and general acid in YoeB are glutamic acid and histidine, respectively, and are indicated by black triangles. **(B)** Schematic presentation of the proposed mechanism of mRNA cleavage by YoeB. YoeB, mRNA, and A1493 of 16S rRNA colored light orange, magenta, and cyan, respectively.

*In vivo,* YoeB mediated mRNA cleavage occurs only within translated regions of the RNA in a ribosome–dependent manner (132). As described above, the universally conserved A1493 and G530 are involved in mediating YoeB interactions with the substrate mRNA. Particularly, the direct interaction of A1493 in the 16S rRNA with the base of mRNA A20, as well as the network of interactions amongst A1493, ribose O2 in A20 (site of hydrolysis), and carboxylic acid group of Glu46 (general base), rationalize the requirement for the ribosome for the activity of YoeB. Considering that the N7 atom of A1493 is in position to interact with ribose O2 in A20, and its potential for deprotonating, it is likely that A1493 might function as general base in the absence of Glu46, thereby explaining the compromised activity of Glu46 mutation (131). On the other hand, YoeB has a weak activity on naked mRNA, whereas RelE does not (188). As YoeB retains a complete RNase fold with catalytic residues glutamic acid and histidine with pKa values well suited for acting as general base/acid, it may be by itself capable of cleaving certain mRNA to some extent (131). The main contribution of the ribosome may therefore be the stabilization of mRNA in a conformation suitable for YoeB attack (131, 132, 191).

### 4.3 Personal perspective

Type II toxin-antitoxin systems are abundant in bacteria and have diverse functions. mRNA proves to be one of the most frequently used targets for these bacterial toxins, among which a large number belong to the family of ribosome-dependent endoribonucleases, including the well-characterized RelE. It has been proposed that the ribosome-dependent endoribonucleases in bacteria act as "adaptation enzymes", each responsible for a specific environmental condition. These enzymes are believed to degrade mRNA in response to a range of conditions, such as environmental stress, viral infections and ribosome stalling, thereby modulating protein translation to optimize the use of energy. The endoribonuclease YoeB belongs to the YoeB-YefM TA module and mediates cellular adaptation in diverse bacteria by degrading mRNAs upon its activation. Unlike structurally similar RelE, YoeB preserves the catalytic residues (Glu48 and His83) and presents a more classical endoribonuclease.

In this chapter, I described the determination of the structure of YoeB in complex with ribosome trapped in pre-cleavage state, which provides insights into the common features of ribosome-dependent nucleases as well as aspects unique to YoeB. Although YoeB seems to execute the classical acid-base catalysis mechanism common to many RNases, its activity intimately depends on the interactions with the ribosome and mRNA as visualized above. These results provide valuable implications in understanding the molecular mechanism of YoeB family members as well as many other bacterial toxins in translation regulation by degradation of mRNA. Nevertheless, many aspects of YoeB still remain unknown, such as the sequence specificity that needs to be identified. Complementary approaches will be required to further expand our knowledge of the intricate substrate requirement for this class of enzymes. Moreover, to determine the cleavage mechanism of ribosome-independent endoribonuclease like MazF and compare with that of YoeB or RelE would greatly deepen our understanding of both classes of endoribonucleases and type II toxins as a whole.

## Reference:

1. Benne, R. and Sloof, P. (1987) *Biosystems* **21**, 51-68
2. Kaltschmidt, E. and Wittmann, H. G. (1970) *Proc Natl Acad Sci* **67**, 1276-1282
3. Ramakrishnan, V. (2014) *Cell* **159**, 979-984
4. Noller, H. F., Hoffarth, V. and Zimniak, L. (1992) *Science* **256**, 1416-1419
5. Ogle, J. M., Brodersen, D. E., Clemons, W. M., Jr., Tarry, M. J., Carter, A. P. and Ramakrishnan, V. (2001) *Science* **292**, 897-902.
6. Demeshkina, N., Jenner, L., Westhof, E., Yusupov, M. and Yusupova, G. (2012) *Nature* **484**, 256-259
7. Nissen, P., Hansen, J., Ban, N., Moore, P. B. and Steitz, T. A. (2000) *Science* **289**, 920-930
8. Nierhaus, K. H. (1991) *Biochimie* **73**, 739-55.
9. Wower, I. K., Wower, J. and Zimmermann, R. A. (1998) *J Biol Chem* **273**, 19847-19852
10. Takyar, S., Hickerson, R. P. and Noller, H. F. (2005) *Cell* **120**, 49-58
11. Lake, J. A. (1976) *J Mol Biol* **105**, 131-139
12. Radermacher, M., Wagenknecht, T., Verschoor, A. and Frank, J. (1987) *EMBO J* **6**, 1107-1114
13. Byers, B. (1966) *J Cell Biol* **30**, C1-C6
14. Ban, N., Nissen, P., Hansen, J., Moore, P. B. and Steitz, T. A. (2000) *Science* **289**, 905-920
15. Wimberly, B. T., Brodersen, D. E., Clemons, W. M., Jr., Morgan-Warren, R. J., Carter, A. P., Vonrhein, C., Hartsch, T. and Ramakrishnan, V. (2000) *Nature* **407**, 327-339
16. Schluenzen, F., Tocilj, A., Zarivach, R., Harms, J., Gluehmann, M., Janell, D., Bashan, A., Bartels, H., Agmon, I., Franceschi, F. and Yonath, A. (2000) *Cell* **102**, 615-623
17. Agrawal, R. K., Penczek, P., Grassucci, R. A., Li, Y., Leith, A., Nierhaus, K. H. and Frank, J. (1996) *Science* **271**, 1000-1002
18. Stark, H., Orlova, E. V., Rinke-Appel, J., Junke, N., Mueller, F., Rodnina, M. V., Wintermeyer, W., Brimacombe, R. and van Heel, M. (1997) *Cell* **88**, 19-28
19. Yusupov, M. M., Yusupova, G. Z., Baucom, A., Lieberman, K., Earnest, T. N., Cate, J. H. and Noller, H. F. (2001) *Science* **292**, 883-896
20. Schuwirth, B. S., Borovinskaya, M. A., Hau, C. W., Zhang, W., Vila-Sanjurjo, A., Holton, J. M. and Cate, J. H. (2005) *Science* **310**, 827-834
21. Selmer, M., Dunham, C. M., Murphy, F. V. t., Weixlbaumer, A., Petry, S., Kelley, A. C., Weir, J. R. and Ramakrishnan, V. (2006) *Science* **313**, 1935-1942
22. Voorhees, R. M. and Ramakrishnan, V. (2013) *Annu Rev Biochem* **82**, 203-236
23. Ben-Shem, A., Garreau de Loubresse, N., Melnikov, S., Jenner, L., Yusupova, G. and Yusupov, M. (2011) *Science* **334**, 1524-1529

24. Rabl, J., Leibundgut, M., Ataide, S. F., Haag, A. and Ban, N. (2011) *Science* **331**, 730-736
25. Klinge, S., Voigts-Hoffmann, F., Leibundgut, M., Arpagaus, S. and Ban, N. (2011) *Science*
26. Bai, X. C., McMullan, G. and Scheres, S. H. (2015) *Trends Biochem Sci* **40**, 49-57
27. Amunts, A., Brown, A., Bai, X. C., Llacer, J. L., Hussain, T., Emsley, P., Long, F., Murshudov, G., Scheres, S. H. and Ramakrishnan, V. (2014) *Science* **343**, 1485-1489
28. Brown, A., Amunts, A., Bai, X. C., Sugimoto, Y., Edwards, P. C., Murshudov, G., Scheres, S. H. and Ramakrishnan, V. (2014) *Science* **346**, 718-722
29. Greber, B. J., Boehringer, D., Leitner, A., Bieri, P., Voigts-Hoffmann, F., Erzberger, J. P., Leibundgut, M., Aebersold, R. and Ban, N. (2014) *Nature* **505**, 515-519
30. Greber, B. J., Boehringer, D., Leibundgut, M., Bieri, P., Leitner, A., Schmitz, N., Aebersold, R. and Ban, N. (2014) *Nature* **515**, 283-286
31. Amunts, A., Brown, A., Toots, J., Scheres, S. H. and Ramakrishnan, V. (2015) *Science* **348**, 95-98
32. Khatter, H., Myasnikov, A. G., Natchiar, S. K. and Klaholz, B. P. (2015) *Nature* **520**, 640-645
33. Voorhees, R. M., Fernandez, I. S., Scheres, S. H. and Hegde, R. S. (2014) *Cell* **157**, 1632-1643
34. Peske, F., Rodnina, M. V. and Wintermeyer, W. (2005) *Mol Cell* **18**, 403-412
35. Grigoriadou, C., Marzi, S., Pan, D., Gualerzi, C. O. and Cooperman, B. S. (2007) *J Mol Biol* **373**, 551-561
36. Milon, P., Konevega, A. L., Gualerzi, C. O. and Rodnina, M. V. (2008) *Mol Cell* **30**, 712-720
37. Grigoriadou, C., Marzi, S., Kirillov, S., Gualerzi, C. O. and Cooperman, B. S. (2007) *J Mol Biol* **373**, 562-572
38. Ito, K., Uno, M. and Nakamura, Y. (2000) *Nature* **403**, 680-684
39. Frolova, L. Y., Tsivkovskii, R. Y., Sivolobova, G. F., Oparina, N. Y., Serpinsky, O. I., Blinov, V. M., Tatkov, S. I. and Kisselev, L. L. (1999) *RNA* **5**, 1014-1020
40. Song, H., Mugnier, P., Das, A. K., Webb, H. M., Evans, D. R., Tuite, M. F., Hemmings, B. A. and Barford, D. (2000) *Cell* **100**, 311-321
41. Zavialov, A. V., Buckingham, R. H. and Ehrenberg, M. (2001) *Cell* **107**, 115-124
42. Hirashima, A. and Kaji, A. (1973) *J Biol Chem* **248**, 7580-7587
43. Achenbach, J. and Nierhaus, K. H. (2014) *Biochimie*
44. Achenbach, J. and Nierhaus, K. H. (2013) *Nat Struct Mol Biol* **20**, 1019-1022
45. Villa, E., Sengupta, J., Trabuco, L. G., LeBarron, J., Baxter, W. T., Shaikh, T. R., Grassucci, R. A., Nissen, P., Ehrenberg, M., Schulten, K. and Frank, J. (2009) *Proc Natl Acad Sci U S A* **106**, 1063-1068
46. Schuette, J. C., Murphy, F. V. t., Kelley, A. C., Weir, J. R., Giesebrecht, J.,

Connell, S. R., Loerke, J., Mielke, T., Zhang, W., Penczek, P. A., Ramakrishnan, V. and Spahn, C. M. (2009) *Embo J* **28**, 755-765

47. Schmeing, T. M., Voorhees, R. M., Kelley, A. C., Gao, Y. G., Murphy, F. V., Weir, J. R. and Ramakrishnan, V. (2009) *Science* **326**, 688-694
48. Frank, J. and Agrawal, R. K. (2000) *Nature* **406**, 319-322
49. Valle, M., Zavialov, A., Sengupta, J., Rawat, U., Ehrenberg, M. and Frank, J. (2003) *Cell* **114**, 123-134
50. Fei, J., Kosuri, P., MacDougall, D. D. and Gonzalez, R. L., Jr. (2008) *Mol Cell* **30**, 348-359
51. Ratje, A. H., Loerke, J., Mikolajka, A., Brunner, M., Hildebrand, P. W., Starosta, A. L., Donhofer, A., Connell, S. R., Fucini, P., Mielke, T., Whitford, P. C., Onuchic, J. N., Yu, Y., Sanbonmatsu, K. Y., Hartmann, R. K., Penczek, P. A., Wilson, D. N. and Spahn, C. M. (2010) *Nature* **468**, 713-716
52. Blanchard, S. C., Kim, H. D., Gonzalez, R. L., Jr., Puglisi, J. D. and Chu, S. (2004) *Proc Natl Acad Sci U S A* **101**, 12893-12898
53. Cornish, P. V., Ermolenko, D. N., Noller, H. F. and Ha, T. (2008) *Mol Cell* **30**, 578-588
54. Rodnina, M. V., Savelsbergh, A., Katunin, V. I. and Wintermeyer, W. (1997) *Nature* **385**, 37-41
55. Uemura, S., Aitken, C. E., Korlach, J., Flusberg, B. A., Turner, S. W. and Puglisi, J. D. (2010) *Nature* **464**, 1012-1017
56. Robertson, J. M. and Wintermeyer, W. (1987) *J Mol Biol* **196**, 525-540
57. Dinos, G., Kalpaxis, D. L., Wilson, D. N. and Nierhaus, K. H. (2005) *Nucleic Acids Res* **33**, 5291-5296
58. Chen, C., Stevens, B., Kaur, J., Smilansky, Z., Cooperman, B. S. and Goldman, Y. E. (2011) *Proc Natl Acad Sci U S A* **108**, 16980-16985
59. Wilson, D. N. (2014) *Nat Rev Microbiol* **12**, 35-48
60. Vetter, I. R. and Wittinghofer, A. (2001) *Science* **294**, 1299-1304
61. Starosta, A. L., Lassak, J., Jung, K. and Wilson, D. N. (2014) *FEMS Microbiol Rev* **38**, 1172-1201
62. Bourne, H. R., Sanders, D. A. and McCormick, F. (1991) *Nature* **349**, 117-127
63. Marintchev, A. and Wagner, G. (2004) *Q Rev Biophys* **37**, 197-284
64. Kuhle, B. and Ficner, R. (2014) *EMBO J* **33**, 2547-2563
65. Connell, S. R., Takemoto, C., Wilson, D. N., Wang, H., Murayama, K., Terada, T., Shirouzu, M., Rost, M., Schuler, M., Giesebrecht, J., Dabrowski, M., Mielke, T., Fucini, P., Yokoyama, S. and Spahn, C. M. (2007) *Mol Cell* **25**, 751-764
66. Selmer, M., Gao, Y. G., Weixlbaumer, A. and Ramakrishnan, V. (2012) *Acta Crystallogr D Biol Crystallogr* **68**, 578-583
67. Gao, Y. G., Selmer, M., Dunham, C. M., Weixlbaumer, A., Kelley, A. C. and Ramakrishnan, V. (2009) *Science* **326**, 694-699
68. Jin, H., Kelley, A. C. and Ramakrishnan, V. (2011) *Proc Natl Acad Sci U S A* **108**, 15798-15803
69. Seo, H. S., Abedin, S., Kamp, D., Wilson, D. N., Nierhaus, K. H. and Cooperman,

B. S. (2006) *Biochemistry* **45**, 2504-2514

70. Aevarsson, A., Brazhnikov, E., Garber, M., Zheltonosova, J., Chirgadze, Y., al-Karadaghi, S., Svensson, L. A. and Liljas, A. (1994) *Embo J* **13**, 3669-3677
71. Hansson, S., Singh, R., Gudkov, A. T., Liljas, A. and Logan, D. T. (2005) *J Mol Biol* **348**, 939-949
72. Mohr, D., Wintermeyer, W. and Rodnina, M. V. (2002) *Biochemistry* **41**, 12520-12528
73. Diaconu, M., Kothe, U., Schlunzen, F., Fischer, N., Harms, J. M., Tonevitsky, A. G., Stark, H., Rodnina, M. V. and Wahl, M. C. (2005) *Cell* **121**, 991-1004
74. Voorhees, R. M., Schmeing, T. M., Kelley, A. C. and Ramakrishnan, V. (2010) *Science* **330**, 835-838
75. Zhou, J., Lancaster, L., Trakhanov, S. and Noller, H. F. (2012) *RNA* **18**, 230-240
76. Trabuco, L. G., Schreiner, E., Eargle, J., Cornish, P., Ha, T., Luthey-Schulten, Z. and Schulten, K. (2010) *J Mol Biol* **402**, 741-760
77. Fei, J., Bronson, J. E., Hofman, J. M., Srinivas, R. L., Wiggins, C. H. and Gonzalez, R. L. J. (2009) *Proc Natl Acad Sci U S A* **106**, 15702-15707
78. Yokoyama, T., Shaikh, T. R., Iwakura, N., Kaji, H., Kaji, A. and Agrawal, R. K. (2012) *EMBO J* **31**, 1836-1846
79. Feng, S., Chen, Y. and Gao, Y. G. (2013) *PLoS One* **8**, e58829
80. Kabsch, W. (1993) *J. Appl. Cryst.* **26**, 795-200
81. Brünger, A. T., Adams, P. D., Clore, G. M., DeLano, W. L., Gros, P., Grosse-Kunstleve, R. W., Jiang, J. S., Kuszewski, J., Nilges, M., Pannu, N. S., Read, R. J., Rice, L. M., Simonson, T. and Warren, G. L. (1998) *Acta Crystallogr D Biol Crystallogr* **54**, 905-921
82. Emsley, P. and Cowtan, K. (2004) *Acta Crystallogr D Biol Crystallogr* **60**, 2126-2132
83. Collaborative Computational Project Number 4 (1994) *Acta Cryst* **D50**, 760-763
84. Jenner, L., Demeshkina, N., Yusupova, G. and Yusupov, M. (2010) *Nat Struct Mol Biol* **17**, 1072-1078
85. Noller, H. F., Yusupov, M. M., Yusupova, G. Z., Baucom, A., Lieberman, K., Lancaster, L., Dallas, A., Fredrick, K., Earnest, T. N. and Cate, J. H. (2001) *Cold Spring Harb Symp Quant Biol* **66**, 57-66
86. Endo, Y. and Wool, I. G. (1982) *J Biol Chem* **257**, 9054-9060
87. Hausner, T. P., Atmadja, J. and Nierhaus, K. H. (1987) *Biochimie* **69**, 911-923
88. Brigotti, M., Rambelli, F., Zamboni, M., Montanaro, L. and Sperti, S. (1989) *Biochem J* **257**, 723-727
89. Rambelli, F., Brigotti, M., Zamboni, M., Denaro, M., Montanaro, L. and Sperti, S. (1989) *Biochem J* **259**, 307-310
90. Dunkle, J. A., Wang, L., Feldman, M. B., Pulk, A., Chen, V. B., Kapral, G. J., Noeske, J., Richardson, J. S., Blanchard, S. C. and Cate, J. H. (2011) *Science* **332**, 981-984

91. Savelsbergh, A., Mohr, D., Kothe, U., Wintermeyer, W. and Rodnina, M. V. (2005) *EMBO J* **24**, 4316-4323
92. Pan, D., Kirillov, S., Zhang, C. M., Hou, Y. M. and Cooperman, B. S. (2006) *Nat Struct Mol Biol* **13**, 354-359
93. Zavialov, A. V. and Ehrenberg, M. (2003) *Cell* **114**, 113-122
94. Pan, D., Kirillov, S. V. and Cooperman, B. S. (2007) *Mol Cell* **25**, 519-529
95. Shoji, S., Janssen, B. D., Hayes, C. S. and Fredrick, K. (2010) *Biochimie* **92**, 157-163
96. Peske, F., Savelsbergh, A., Katunin, V. I., Rodnina, M. V. and Wintermeyer, W. (2004) *J Mol Biol* **343**, 1183-1194
97. Martemyanov, K. A. and Gudkov, A. T. (2000) *J Biol Chem* **275**, 35820-35824
98. Garcia-Ortega, L., Alvarez-Garcia, E., Gavilanes, J. G., Martinez-Del-Pozo, A. and Joseph, S. (2010) *Nucleic Acids Res*
99. Shi, X., Khade, P. K., Sanbonmatsu, K. Y. and Joseph, S. (2012) *J Mol Biol* **419**, 125-138
100. Clementi, N., Chirkova, A., Puffer, B., Micura, R. and Polacek, N. (2010) *Nat Chem Biol* **6**, 344-351
101. Sprinzl, M., Brock, S., Huang, Y., Milovnik, P., Nanninga, M., Nesper-Brock, M., Rutthard, H. and Szkaradkiewicz, K. (2000) *Biol Chem* **381**, 367-375
102. Czworkowski, J., Wang, J., Steitz, T. A. and Moore, P. B. (1994) *Embo J* **13**, 3661-3668
103. Hansson, S., Singh, R., Gudkov, A. T., Liljas, A. and Logan, D. T. (2005) *FEBS Lett* **579**, 4492-4497
104. Liljas, A., Ehrenberg, M. and Aqvist, J. (2011) *Science* **333**, 37; author reply 37
105. Wallin, G., Kamerlin, S. C. and Aqvist, J. (2013) *Nat Commun* **4**, 1733
106. Schweins, T., Geyer, M., Scheffzek, K., Warshel, A., Kalbitzer, H. R. and Wittinghofer, A. (1995) *Nat Struct Biol* **2**, 36-44
107. Tourigny, D. S., Fernandez, I. S., Kelley, A. C. and Ramakrishnan, V. (2013) *Science* **340**, 1235490
108. Pulk, A. and Cate, J. H. (2013) *Science* **340**, 1235970
109. Zhou, J., Lancaster, L., Donohue, J. P. and Noller, H. F. (2013) *Science* **340**, 1236086
110. Aqvist, J. and Kamerlin, S. C. (2014) *Biochemistry*
111. Cukras, A. R., Southworth, D. R., Brunelle, J. L., Culver, G. M. and Green, R. (2003) *Mol Cell* **12**, 321-328
112. Munro, J. B., Altman, R. B., O'Connor, N. and Blanchard, S. C. (2007) *Mol Cell* **25**, 505-517
113. Joseph, S. and Noller, H. F. (1998) *Embo J* **17**, 3478-3483
114. Lill, R., Robertson, J. M. and Wintermeyer, W. (1989) *Embo J* **8**, 3933-3938
115. Ramrath, D. J., Lancaster, L., Sprink, T., Mielke, T., Loerke, J., Noller, H. F. and Spahn, C. M. (2013) *Proc Natl Acad Sci U S A* **110**, 20964-20969
116. Zhou, J., Lancaster, L., Donohue, J. P. and Noller, H. F. (2014) *Science* **345**,

1188-1191

117. Brilot, A. F., Korostelev, A. A., Ermolenko, D. N. and Grigorieff, N. (2013) *Proc Natl Acad Sci U S A* **110**, 20994-20999
118. Lin, J., Gagnon, M. G., Bulkley, D. and Steitz, T. A. (2015) *Cell* **160**, 219-227
119. Ogura, T. and Hiraga, S. (1983) *Proc Natl Acad Sci U S A* **80**, 4784-4788
120. Gerdes, K., Rasmussen, P. B. and Molin, S. (1986) *Proc Natl Acad Sci U S A* **83**, 3116-3120
121. Yamaguchi, Y. and Inouye, M. (2011) *Nat Rev Microbiol* **9**, 779-790
122. Blower, T. R., Short, F. L., Rao, F., Mizuguchi, K., Pei, X. Y., Fineran, P. C., Luisi, B. F. and Salmond, G. P. (2012) *Nucleic Acids Res* **40**, 6158-6173
123. Fozo, E. M., Makarova, K. S., Shabalina, S. A., Yutin, N., Koonin, E. V. and Storz, G. (2010) *Nucleic Acids Res* **38**, 3743-3759
124. Makarova, K. S., Wolf, Y. I. and Koonin, E. V. (2009) *Biol Direct* **4**, 19
125. Sevin, E. W. and Barloy-Hubler, F. (2007) *Genome Biol* **8**, R155
126. Shao, Y., Harrison, E. M., Bi, D., Tai, C., He, X., Ou, H. Y., Rajakumar, K. and Deng, Z. (2011) *Nucleic Acids Res* **39**, D606-D611
127. Zhang, Y., Zhang, J., Hara, H., Kato, I. and Inouye, M. (2005) *J Biol Chem* **280**, 3143-3150
128. Zhang, Y., Zhang, J., Hoeflich, K. P., Ikura, M., Qing, G. and Inouye, M. (2003) *Mol Cell* **12**, 913-923
129. Pedersen, K., Zavialov, A. V., Pavlov, M. Y., Elf, J., Gerdes, K. and Ehrenberg, M. (2003) *Cell* **112**, 131-140
130. Takagi, H., Kakuta, Y., Okada, T., Yao, M., Tanaka, I. and Kimura, M. (2005) *Nat Struct Mol Biol* **12**, 327-331
131. Kamada, K. and Hanaoka, F. (2005) *Mol Cell* **19**, 497-509
132. Zhang, Y. and Inouye, M. (2009) *J Biol Chem* **284**, 6627-6638
133. Brown, J. M. and Shaw, K. J. (2003) *J Bacteriol* **185**, 6600-6608
134. Zhang, Y., Yamaguchi, Y. and Inouye, M. (2009) *J Biol Chem* **284**, 25522-25531
135. Motiejunaite, R., Armalyte, J., Markuckas, A. and Suziedeliene, E. (2007) *FEMS Microbiol Lett* **268**, 112-119
136. Prysak, M. H., Mozdzierz, C. J., Cook, A. M., Zhu, L., Zhang, Y., Inouye, M. and Woychik, N. A. (2009) *Mol Microbiol* **71**, 1071-1087
137. Zhang, Y., Zhu, L., Zhang, J. and Inouye, M. (2005) *J Biol Chem* **280**, 26080-26088
138. Korch, S. B., Henderson, T. A. and Hill, T. M. (2003) *Mol Microbiol* **50**, 1199-1213
139. Yamaguchi, Y., Park, J. H. and Inouye, M. (2009) *J Biol Chem* **284**, 28746-28753
140. Brown, B. L., Grigoriu, S., Kim, Y., Arruda, J. M., Davenport, A., Wood, T. K., Peti, W. and Page, R. (2009) *PLoS Pathog* **5**, e1000706
141. Makarova, K. S., Grishin, N. V. and Koonin, E. V. (2006) *Bioinformatics* **22**, 2581-2584

142. Schmidt, O., Schuenemann, V. J., Hand, N. J., Silhavy, T. J., Martin, J., Lupas, A. N. and Djuranovic, S. (2007) *J Mol Biol* **372**, 894-905
143. Christensen-Dalsgaard, M., Jorgensen, M. G. and Gerdes, K. (2010) *Mol Microbiol* **75**, 333-348
144. Koga, M., Otsuka, Y., Lemire, S. and Yonesaki, T. (2011) *Genetics* **187**, 123-130
145. Pandey, D. P. and Gerdes, K. (2005) *Nucleic Acids Res* **33**, 966-976
146. Satwika, D., Klassen, R. and Meinhardt, F. (2012) *Appl Microbiol Biotechnol* **96**, 345-356
147. Gerdes, K., Gultyaev, A. P., Franch, T., Pedersen, K. and Mikkelsen, N. D. (1997) *Annu Rev Genet* **31**, 1-31
148. Gerdes, K. and Wagner, E. G. (2007) *Curr Opin Microbiol* **10**, 117-124
149. Wang, X. and Wood, T. K. (2011) *Appl Environ Microbiol* **77**, 5577-5583
150. Fineran, P. C., Blower, T. R., Foulds, I. J., Humphreys, D. P., Lilley, K. S. and Salmond, G. P. (2009) *Proc Natl Acad Sci U S A* **106**, 894-899
151. Blower, T. R., Evans, T. J., Przybilski, R., Fineran, P. C. and Salmond, G. P. (2012) *PLoS Genet* **8**, e1003023
152. Masuda, H., Tan, Q., Awano, N., Wu, K. P. and Inouye, M. (2012) *Mol Microbiol* **84**, 979-989
153. Wang, X., Lord, D. M., Cheng, H. Y., Osbourne, D. O., Hong, S. H., Sanchez-Torres, V., Quiroga, C., Zheng, K., Herrmann, T., Peti, W., Benedik, M. J., Page, R. and Wood, T. K. (2012) *Nat Chem Biol* **8**, 855-861
154. Smith, A. S. and Rawlings, D. E. (1998) *J Bacteriol* **180**, 5458-5462
155. Aizenman, E., Engelberg-Kulka, H. and Glaser, G. (1996) *Proc Natl Acad Sci U S A* **93**, 6059-6063
156. Cherny, I. and Gazit, E. (2004) *J Biol Chem* **279**, 8252-8261
157. Donegan, N. P., Thompson, E. T., Fu, Z. and Cheung, A. L. (2010) *J Bacteriol* **192**, 1416-1422
158. Mutschler, H., Gebhardt, M., Shoeman, R. L. and Meinhart, A. (2011) *PLoS Biol* **9**, e1001033
159. Winther, K. S. and Gerdes, K. (2011) *Proc Natl Acad Sci U S A* **108**, 7403-7407
160. Liu, M., Zhang, Y., Inouye, M. and Woychik, N. A. (2008) *Proc Natl Acad Sci U S A* **105**, 5885-5890
161. Schifano, J. M., Edifor, R., Sharp, J. D., Ouyang, M., Konkimalla, A., Husson, R. N. and Woychik, N. A. (2013) *Proc Natl Acad Sci U S A* **110**, 8501-8506
162. Bernard, P. and Couturier, M. (1992) *J Mol Biol* **226**, 735-745
163. Munoz-Gomez, A. J., Lemonnier, M., Santos-Sierra, S., Berzal-Herranz, A. and Diaz-Orejas, R. (2005) *J Bacteriol* **187**, 3151-3157
164. Zhang, Y. and Inouye, M. (2011) *Mol Microbiol* **79**, 1418-1429
165. Gerdes, K., Larsen, J. E. and Molin, S. (1985) *J Bacteriol* **161**, 292-298
166. Cooper, T. F. and Heinemann, J. A. (2000) *Proc Natl Acad Sci U S A* **97**, 12643-12648

167. Gerdes, K. and Maisonneuve, E. (2012) *Annu Rev Microbiol* **66**, 103-123
168. Shah, D., Zhang, Z., Khodursky, A., Kaldalu, N., Kurg, K. and Lewis, K. (2006) *BMC Microbiol* **6**, 53
169. Gonzalez Barrios, A. F., Zuo, R., Hashimoto, Y., Yang, L., Bentley, W. E. and Wood, T. K. (2006) *J Bacteriol* **188**, 305-316
170. Kim, Y. and Wood, T. K. (2010) *Biochem Biophys Res Commun* **391**, 209-213
171. Pedersen, K., Christensen, S. K. and Gerdes, K. (2002) *Mol Microbiol* **45**, 501-510
172. Christensen, S. K., Pedersen, K., Hansen, F. G. and Gerdes, K. (2003) *J Mol Biol* **332**, 809-819
173. Kolodkin-Gal, I. and Engelberg-Kulka, H. (2008) *J Bacteriol* **190**, 3169-3175
174. Nariya, H. and Inouye, M. (2008) *Cell* **132**, 55-66
175. Zhu, L., Sharp, J. D., Kobayashi, H., Woychik, N. A. and Inouye, M. (2010) *J Biol Chem* **285**, 39732-39738
176. Stieber, D., Gabant, P. and Szpirer, C. (2008) *Biotechniques* **45**, 344-346
177. Suzuki, M., Zhang, J., Liu, M., Woychik, N. A. and Inouye, M. (2005) *Mol Cell* **18**, 253-261
178. Suzuki, M., Mao, L. and Inouye, M. (2007) *Nat Protoc* **2**, 1802-1810
179. Williams, J. J. and Hergenrother, P. J. (2012) *Trends Microbiol* **20**, 291-298
180. Erental, A., Sharon, I. and Engelberg-Kulka, H. (2012) *PLoS Biol* **10**, e1001281
181. Kumar, S., Kolodkin-Gal, I. and Engelberg-Kulka, H. (2013) *MBio* **4**, e00314-e00313
182. Chono, H., Matsumoto, K., Tsuda, H., Saito, N., Lee, K., Kim, S., Shibata, H., Ageyama, N., Terao, K., Yasutomi, Y., Mineno, J., Kim, S., Inouye, M. and Kato, I. (2011) *Hum Gene Ther* **22**, 35-43
183. Shapira, A., Shapira, S., Gal-Tanamy, M., Zemel, R., Tur-Kaspa, R. and Benhar, I. (2012) *PLoS One* **7**, e32320
184. Zhu, L., Zhang, Y., Teh, J. S., Zhang, J., Connell, N., Rubin, H. and Inouye, M. (2006) *J Biol Chem* **281**, 18638-18643
185. Park, J. H., Yamaguchi, Y. and Inouye, M. (2011) *FEBS Lett* **585**, 2526-2532
186. Zhu, L., Inoue, K., Yoshizumi, S., Kobayashi, H., Zhang, Y., Ouyang, M., Kato, F., Sugai, M. and Inouye, M. (2009) *J Bacteriol* **191**, 3248-3255
187. Vesper, O., Amitai, S., Belitsky, M., Byrgazov, K., Kaberdina, A. C., Engelberg-Kulka, H. and Moll, I. (2011) *Cell* **147**, 147-157
188. Christensen, S. K. and Gerdes, K. (2003) *Mol Microbiol* **48**, 1389-1400
189. Neubauer, C., Gao, Y. G., Andersen, K. R., Dunham, C. M., Kelley, A. C., Hentschel, J., Gerdes, K., Ramakrishnan, V. and Brodersen, D. E. (2009) *Cell* **139**, 1084-1095
190. Grady, R. and Hayes, F. (2003) *Mol Microbiol* **47**, 1419-1432
191. Sevillano, L., Diaz, M., Yamaguchi, Y., Inouye, M. and Santamaria, R. I. (2012) *PLoS One* **7**, e32977
192. Christensen, S. K., Maenhaut-Michel, G., Mine, N., Gottesman, S., Gerdes, K.

and Van Melderen, L. (2004) *Mol Microbiol* **51**, 1705-1717

193. Christensen-Dalsgaard, M., Overgaard, M., Winther, K. S. and Gerdes, K. (2008) *Methods Enzymol* **447**, 521-535
194. Sevcik, J., Dodson, E. J. and Dodson, G. G. (1991) *Acta Crystallogr B* **47**, 240-253
195. Buckle, A. M., Henrick, K. and Fersht, A. R. (1993) *J Mol Biol* **234**, 847-860
196. Laurberg, M., Asahara, H., Korostelev, A., Zhu, J., Trakhanov, S. and Noller, H. F. (2008) *Nature* **454**, 852-857
197. Weixlbaumer, A., Jin, H., Neubauer, C., Voorhees, R. M., Petry, S., Kelley, A. C. and Ramakrishnan, V. (2008) *Science* **322**, 953-956
198. Sharma, D., Cukras, A. R., Rogers, E. J., Southworth, D. R. and Green, R. (2007) *J Mol Biol* **374**, 1065-1076
199. Hurley, J. M., Cruz, J. W., Ouyang, M. and Woychik, N. A. (2011) *J Biol Chem* **286**, 14770-14778
200. Loverix, S. and Steyaert, J. (2001) *Methods Enzymol* **341**, 305-323
201. Sevcik, J., Zegers, I., Wyns, L., Dauter, Z. and Wilson, K. S. (1993) *Eur J Biochem* **216**, 301-305
202. Koch, M., Flur, S., Kreutz, C., Ennifar, E., Micura, R. and Polacek, N. (2015) *Proc Natl Acad Sci U S A* **112**, E2561-E2568
203. Li, W., Liu, Z., Koripella, R. K., Langlois, R., Sanyal, S. and Frank, J. (2015) *Sci Adv* **1**,

## Publication

1. **Chen Y**, Feng S, Kumar V, Ero R, Gao YG. "Structure of EF-G-Ribosome complex in a pretranslocation state", Nature Structural & Molecular Biology, 2013, 20: 1077-1084. Highlighted under News and Views in Nature Structural & Molecular Biology, 2013, 20: 1019-1022.

2. Feng S*, **Chen Y***, Kamada K, Wang H, Tang K, Wang M, Gao YG. "YoeB–ribosome structure: A canonical RNase that requires the ribosome for its specific activity", Nucleic Acids Research, 2013, 41(20): 9549-9556

3. Feng S*, **Chen Y***, Gao YG. "Crystal structure of 70S ribosome with both cognate tRNAs in the E and P sites representing an authentic elongation complex", 2013, PLOS ONE, 2013, 8(3): e58829.

4. Toh DW*, Sun L*, Lau ZM, Tan J, Low JA, Tang WQ, Cheong JY, Tan JH, **Chen Y**, Hong W, Gao YG†, Woon ECY†. "A Strategy Based on Nucleotide Specificity Leads to Subfamily-Selective and Cell-Active Probe of N6-Methyladenosine Demethylase FTO", Chemical Science (Cover Image), 2015, 6: 112-122.

5. Ero R, Dimitrova V T, **Chen Y**, Bu W, Feng S, Liu T, Wang P, Xue C, Tan S M and Gao YG "Crystal structure of Gib2, a signal-transducing protein scaffold associated with ribosomes in Cryptococcus neoformans", Scientific Reports, 2015, 5, 8688.

6. Kumar V, **Chen Y***, Ero R*, Ahmed T*, Tan J, Li Z, Wong AS, Bhushan S, Gao YG. "Structure of BipA in GTP form bound to the ratcheted ribosome", PNAS, 2015, 112(35):10944-9.

### Notes:

* These authors contribute equally.

† Co-corresponding author.

The scope of this thesis is based on publications 1 and 2.

## Author contribution

In the first study described in Chapter I in this thesis, I carried out all the way in EF-G protein purification, ribosome complex assembling, ribosome complex crystallization and optimization, data collection and structure determination, as well as the manuscript preparation.

In the second study described in Chapter II in this thesis, I worked closely with Dr. Feng Shu from our lab as well as other collaborators from both Japan and Singapore. YoeB was purified and provided by our collaborator in Japan. Dr. Feng and I worked together in ribosome complex crystal optimization and data collection, as much endeavor is required to obtain a good-diffracting ribosome crystal. On the other hand, I did most of the job in MALDI-Mass spectrometry assay together with our collaborator in Singapore and was involved in manuscript preparation as well.